Flying-V Design Optimisation for the Global Warming Impact and Operating Cost

Rowan de Voogt

Delft University of Technology

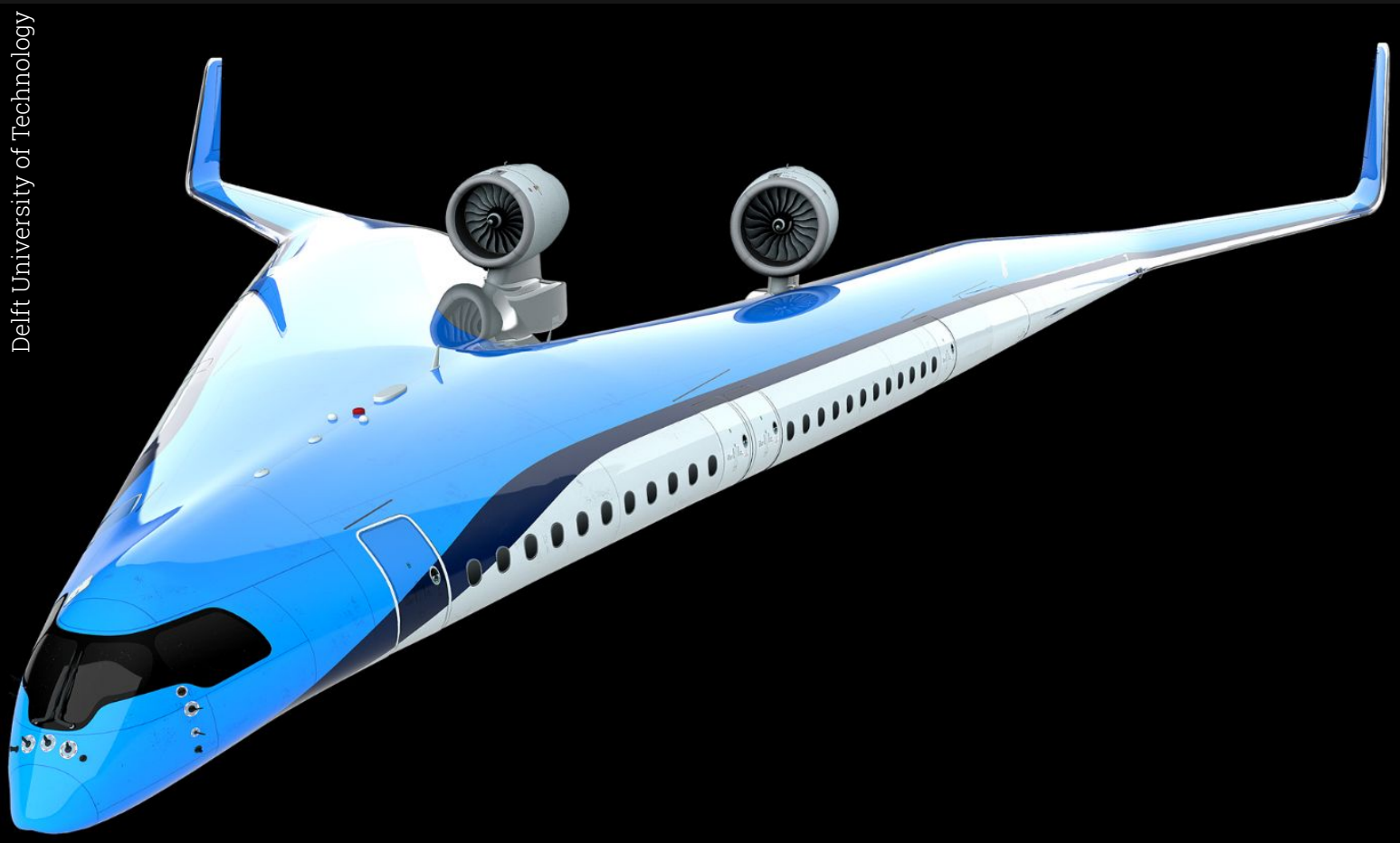

TU Delft

Flying-V Design Optimisation for the Global Warming Impact and Operating Cost

by

Rowan de Voogt

to obtain the degree of Master of Science

at the Delft University of Technology,

to be defended publicly on Thursday June 6, 2024 at 9:00 AM.

Student number:	4544064	
Project duration:	March , 2023 – June , 2024	
Thesis committee:	Dr. ir. R. Vos,	TU Delft, supervisor
	Ir. P. Proesmans,	TU Delft, supervisor
	Dr. C. Varriale,	TU Delft, Chair
	Dr. F. Yin	Tu Delft, Examiner

Cover:	Flying-V, retrieved from `https://www.tudelft.nl/en/ae/flying-v` on May 27 2024
Style:	TU Delft Report Style, with modifications by Daan Zwaneveld

An electronic version of this thesis is available at `http://repository.tudelft.nl/`.

TU Delft

Acknowledgments

This thesis represents the culmination of academic carreer in aerospace engineering, focusing on the climate impact and operational costs of the innovative Flying-V aircraft. Studying the balance among economic feasibility, environmental sustainability, and aircraft design is the main goal.

Pieter-Jan Proesmans and Roelof Vos have my sincere appreciation for their invaluable advice, assistance, and knowledge during this project. This research has been significantly shaped by their support and ideas.

My parents deserve my sincere gratitude as well for their constant encouragement and support, without which this achievement would not have been feasible.

It gives me great pleasure to offer this thesis as a thorough and insightful investigation of the Flying-V aircraft's potential for a more sustainable aviation industry. My sincere hope is that this work will advance our knowledge of sustainable aviation and motivate more investigation.

Rowan de Voogt
Delft, May 2024

Contents

List of Figures

List of Tables

Nomenclature

Abbreviations

BPR	Bypass Ratio
CG	Centre of gravity
CH_4	Methane
CO_2	Carbon dioxide
COC	Cash operating cost
DOE	Design of Experiments
DRF	Distributed Random Forest
FV	Flying-V
g	Gravitational acceleration
H_2O	Water
ICAO	International Civil Aviation Organization
LCDP	Lateral Control Departure Parameter
MAC	Mean aerodynamic chord
MDAO	Multi-disciplinary design analysis and optimisation
MOO	Multi objective optimisation
MTOM	Maximum take-off mass
NO_x	Nitrogen Oxides
O_3	Ozone
OEM	Operational empty weight
OPR	Overall engine pressure ratio
PCE	Polynimonal Chaos Expansion
RANS	Reynolds-averaged Navier Stokes equations
RPK	Revenue passenger kilometres
SM	Static margin
SO_4	Sulfate
SOO	Single objective optimisation
TIT	Turbine inlet temperature
TLAR	Top level aircraft requirement
TOM	Take-off mass
TSFC	Thrust specific fuel consumption
ULH	Uniforma latin hypercube
USD	United States Dollars
XDSM	extended design matrix

Greek Symbols

α	Angle of attack [°]
β	Side slip angle [°]
Δ	Difference
δ	Deflection angle [°]
Λ	Sweep angle [°]
λ	Taper ratio
ϕ	Bank angle [°]
Π	Pressure ratio

Latin Symbols

$\dot{m}$	Mass flow rate
b	Wing span [m]
c	Chord [m]
c'	Normalised chord [m]
C_D	Drag coefficient
C_L	Lift coefficient coefficient
C_l	Roll moment coefficient
C_m	Pitching moment coefficient
C_n	Yaw moment coefficient
C_y	Side force coefficient
$C_{D,w}$	Wave drag coefficient
C_{D_0}	Zero lift drag coefficient
C_{D_i}	Induced drag coefficient
D	Drag [N]
e	Oswald factor
f	Objective function
H	Height, m
h	Altitude, m
L	Length [m]
L	Lift [N]
L/D	Lift-to-drag Ratio
M	Mach number
m	Mass [kg]
N	Number
r	Range [km]
RF	Radiative forcing [W/m^2]
RF^*	Normalized radiative forcing
S	Area [m^2]
T	Thrust [N], Temperature [K]
t	time [s]
V	Velocity [m/s], Volume [m^3]
W	Weight [N]
w	Width [m]

Subscripts

1	Section 1
100	100 year period
3	Section 3
a	Aileron
AC	Aircraft
ann	Annual
app	Approach
c	Crown
cr	Cruise
dd	Drag divergence
DYN	Dynamic
e	Elevator
fan	Fan
fin	Fin
fwd	Forward
hpc	High pressure compressor
in	Inner section
k	Keel
lpc	Low pressure compressor

max	Maximum	pax	Passengers
mech	Mechanical	pol	Polytropic
min	Minimum	R	Take-off rotation
mis	Reference mission	r	Rudder
out	Outer section	TO	Take-off
outer	Outer section	yr	Year

Introduction

As evidenced by the increasingly stringent regulations put forth in the Paris agreement during UN climate change conferences aimed at keeping global warming below 2°C, the issue of climate change has gained significant prominence in the field of engineering [9] The aviation sector, which contributes significantly to global warming, has not been spared from this trend. In fact, the aviation sector alone is estimated to account for 3.5% of the net effective anthropogenic radiative forcing by 2018, and as the fastest growing transport sector with an expected annual growth of 4.3%, neglecting the effects of the COVID pandemic, its influence on global warming is increasing [3][6]. Although carbon-neutral solutions and electrical propulsion are becoming more common in sectors such as land-based transportation, the adoption of electric flight for long-range commercial aircraft remains a distant possibility due to strict weight and power constraints. As a result, alternative solutions for reducing aircraft's climate effect must be investigated.

These solutions could take the form of novel aircraft configurations that combine multiple functionalities into a single component, reducing the number of components required. The goal is to improve the overall efficiency of the concept by reducing the weight and drag associated with additional components. The Flying-V by [1] is one of these concepts, which improves aerodynamic efficiency by removing the fuselage of the aircraft and integrating it with the wings. This innovative design has the potential to reduce fuel consumption and emissions, making it a promising candidate for future aircraft development.

Changing the operating conditions could lead to further advancements. Nowadays, aircraft are optimised for minimal operating costs, which results in flying high and fast. However, research by [4] has shown that flying at a lower altitude and speed can significantly reduce the impact of an aircraft on global warming. The Flying-V-900, despite the fact that it is optimised for minimum fuel consumption and thereby minimising CO_2 emissions even faces challenges for minimising the climate impact of aircraft. The Flying-V-900 does have a higher global warming impact than the comparative conventional tube-and-wing aircraft the Airbus A350-900, as it flies at a higher altitude [7]. This is due to non-CO_2 effects such as NO_x emissions and contrail formation, which tend to increase with altitude. As a result, it is worthwhile to investigate the Flying-V's climate performance at lower altitudes. However, flying at this lower altitude increases the cash operating cost, as optimal performance at low altitudes is obtained at slower velocities, resulting in longer flights, which necessitates more flights.

Therefore, is it of interest to examine how the geometry, turbofan engine, and mission parameters of the Flying-V-900 can be enhanced to achieve better climate performance or operational cost efficiency, and to compare these designs with those of a conventional aircraft. This study aims to address the following research questions: What is the Pareto-optimal trade-off between the Flying-V aircraft's global warming impact measured by ATR_{100} and its cash operating costs in U.S. Dollars? Additionally, how does this trade-off compare with conventional long range aircraft? The goal of this project is to analyse and optimise the Flying-V-900 design for multiple objectives, including global warming impact and cash operating costs, and then compare the findings to those of a conventional long range wide-bodied aircraft. By addressing these issues, we can help advance sustainable aviation and propel the industry towards a more environmentally friendly and economically viable future. This will be achieved through the creation and implementation of a model that considers various design factors such as Flying-V geometry, engine type, and mission, as well as the use of appropriate optimisation algorithms.

The structure of this thesis report is as follows: Part I presents the scientific paper. The scientific paper describes the methodology applied for the multidisciplinary analysis and multi objective optimisation of the Flying-V-900, which was verified and validated. Moreover, the results are explained and an answer is provided to the research question. Part II consists of a comprehensive literature study that provides support for the research. This section was previously evaluated as part of the TU Delft master

course ’AE4020’. Finally, Part III offers supplementary material. This part consists of an explanation of ModeFrontier, which was the optimisation software applied. Moreover, does it consist of additional verification of assumptions and additional results.

Part I

Scientific Paper

Flying-V Design Optimisation for the Global Warming Impact and Operating Cost

R. de Voogt *, R. Vos†, P. Proesmans‡

A. Abstract

This study investigates the optimisation of design variables for the unconventional Flying-V-900 aircraft to minimise its climate impact, taking into account operational costs. The study examines the compromises between operational costs and climate factors. A multidisciplinary analysis and optimisation framework is developed in order to minimise the Flying-V-900's impact on global warming, cash operating costs, and fuel efficiency. This study investigates the influence of geometry, turbofan engine, and mission design variables on these objectives. The findings indicated that fuel- and cost-optimised designs demonstrated nearly identical performance, whereas a climate-optimised design exhibited contradictory performance. These results indicate that adopting a climate-optimised Flying-V-900 could potentially reduce the impact of global warming compared to a conventional aircraft, as measured by the average temperature response over a 100-year period, by approximately 60%. However, it is important to note that this transition would come with a significant increase in cash operating costs, specifically by 32%. This analysis considers the impacts of both CO_2 and non-CO_2 factors, including contrail formation and NO_x emissions. It demonstrates that the climate-optimised Flying-V aircraft gives priority to flying at a low altitude of 6km and a velocity of Mach 0.60 in order to minimise contrail formation and NO_x emissions. However, achieving this requires a 20% increase in fleet size to maintain productivity.

I. Introduction

As evidenced by the increasingly stringent regulations put forth in the Paris agreement during UN climate change conferences aimed at keeping global warming below 2°C, the issue of climate change has gained significant prominence in the field of engineering [1] The aviation sector, which contributes significantly to global warming, has not been spared from this trend. In fact, the aviation sector alone is estimated to account for 3.5% of the net effective anthropogenic radiative forcing by 2018, and as the fastest growing transport sector with an expected annual growth of 4.3%, neglecting the effects of the COVID pandemic, its influence on global warming is increasing [2][3]. Although carbon-neutral solutions and electrical propulsion are becoming more common in sectors such as land-based transportation, the adoption of electric flight for long-range commercial aircraft remains a distant possibility due to strict weight and power constraints. As a result, alternative solutions for reducing aircraft's climate effect must be investigated.

These solutions could take the form of novel aircraft configurations that combine multiple functionalities into a single component, reducing the number of components required. The goal is to improve the overall efficiency of the concept by reducing the weight and drag associated with additional components. The Flying-V by [4] is one of these concepts, which improves aerodynamic efficiency by removing the fuselage of the aircraft and integrating it with the wings. This innovative design has the potential to reduce fuel consumption and emissions, making it a promising candidate for future aircraft development.

Changing the operating conditions could lead to further advancements. Nowadays, aircraft are optimised for minimal operating costs, which results in flying high and fast. However, research by [5] has shown that flying at a lower altitude and speed can significantly reduce the impact of an aircraft on global warming. The Flying-V-900, despite the fact that it is optimised for minimum fuel consumption and thereby minimising CO_2 emissions even faces challenges for minimising the climate impact of aircraft. The Flying-V-900 does have a higher global warming impact than the comparative conventional tube-and-wing aircraft the Airbus A350-900, as it flies at a higher altitude [6]. This is due to non-CO_2 effects such as NO_x emissions and contrail formation, which tend to increase with altitude. As a result, it is

*Student, Faculty of Aerospace Engineering,

†Associate Professor, Faculty of Aerospace Engineering, AIAA Associate Fellow ‡PhD Candidate,

Faculty of Aerospace Engineering, AIAA Student Member

worthwhile to investigate the Flying-V's climate performance at lower altitudes. However, flying at this lower altitude increases the cash operating cost, as optimal performance at low altitudes is obtained at slower velocities, resulting in longer flights, which necessitates more flights.

Therefore, is it of interest to examine how the geometry, turbofan engine, and mission parameters of the Flying-V-900 can be enhanced to achieve better climate performance or operational cost efficiency, and to compare these designs with those of a conventional aircraft. This study aims to address the following research questions: What is the Pareto-optimal trade-off between the Flying-V aircraft's global warming impact measured by ATR_{100} and its cash operating costs in U.S. Dollars? Additionally, how does this trade-off compare with conventional long range aircraft? The goal of this project is to analyse and optimise the Flying-V-900 design for multiple objectives, including global warming impact and cash operating costs, and then compare the findings to those of a conventional long range wide-bodied aircraft. By addressing these issues, we can help advance sustainable aviation and propel the industry towards a more environmentally friendly and economically viable future. This will be achieved through the creation and implementation of a model that considers various design factors such as Flying-V geometry, engine type, and mission, as well as the use of appropriate optimisation algorithms.

The ideal outcome of this project would be to identify a Pareto-optimal solution and create a reusable model to assess the Flying-V's global warming impact and cash operating costs. The model will include a multidisciplinary analysis and optimisation (MDAO) workflow and design guidelines that will allow future Flying-V iterations to be optimised for the global warming effect and cash operating costs.

The paper is structured in the following way. The optimisation problem and the methodologies involved will be described in section II. The approach involves the combinations of models by previous research on the Flying-V and global warming impact by Oosterom, van der Toorn and Proesmans [7][8][9]. The integration of these models and the added extensions will then be verified in section III. The results from the optimisation studies will be described in section IV. A comprehensive summary of the findings with recommendations will be given in section V.

II. Optimisation setup and Methods

In order to answer the research question presented in section I, a thorough and multidisciplinary design and optimisation process is developed. This section outlines the structure of the implemented framework, which has been specifically designed to meet the current research objective. subsection II.A offers a comprehensive analysis of how the optimisation problem is formulated and presents the overall strategy. In the following section, specifically in subsection II.C, the methodologies related to the individual analyses and design disciplines are explored. This methodical approach seeks to clarify the systematic procedure employed to enhance the Flying-V aircraft for the two main goals of minimising global warming impact measured in average temperature response over 100 years (ATR_{100}) and decreasing cash operating costs (COC) measured in U.S. dollars (USD). The Flying-V design method is implemented in the knowledge based engineering environment ParaPy* programmed in Python. This framework was applied as it was used by previous studies on the Flying-V, hence a fully specific knowledge based engineering environment for the conceptual design of the Flying-V was already available [10][7] [8]. Moreover, the implementation of ParaPy ensured dependency tracking, runtime caching and demand driven evaluation, which ensured that values only were determined and updated when required, such that no computational resources were wasted.

A. Optimisation Problem Definition

The optimisation problem consists of two objectives: a minimum ATR_{100} and a minimum COC. Firstly, both optimisations are performed separately as single-objective optimisations with an additional single-objective optimisation of the fuel mass. Afterwards, a multi-objective optimisation is performed for both objectives, resulting in a Pareto-optimal solution. The objective functions are normalised to the values of the baseline aircraft, which was the family-optimised Flying-V-900, from the research by Oosterom [7]. The optimisation problem is formulated as follows:

$$\begin{aligned} \underset{\mathbf{X}}{\text{minimize}} \quad & f(\mathbf{x}) = \frac{\text{ATR}_{100}(\mathbf{x})}{\text{ATR}_{100_0}} \text{ or } \frac{\text{COC}(\mathbf{x})}{\text{COC}_0} \text{ or } \frac{m_{\text{fuel}}(\mathbf{x})}{m_{\text{fuel}_0}} \\ \text{subject to} \quad & g_i(\mathbf{x}) \geq 0 \quad \text{for } i = 1, 2, \ldots, 26 \\ & x_i^L \leq x_i \leq x_i^U \quad \text{for } i = 1, 2, \ldots, 14 \end{aligned} \tag{1}$$

*ParaPy. Retrieved on July 2th, 2023, from `https://www.parapy.nl/`

The optimisation is carried out using the PilOPT function of ESTECO's modeFrontier programme[†]. This is a multi-strategy self-adapting algorithm that combines the benefits of local and global search and is capable of efficiently identifying the dominated set of solutions to a multi-objective optimisation. Furthermore, it is capable of solving a complex single-objective optimisation problem.

The design vector, represented by **x**, consists of 21 design variables, each clearly described along with their corresponding limits in Table 1. The design variables are categorised into three distinct groups: 14 variables related to the airframe, 5 variables related to the engine, and 2 variables that govern the mission considerations. However, this design vector was considered too large for the optimisation at hand and would result in excessive evaluation time for the multi-objective optimisation.

Therefore, a sensitivity analysis is performed for both main objectives. This is performed by initially performing a design-of-experiments with a uniform Latin hypercube algorithm of 1000 evaluations in modeFrontier. The sensitivity analysis is performed with a polynomial chaos expansion in modeFrontier, as this provided the highest accuracy and indicated with a performance measured in R-squared of 0.98 that several design variables could be kept as constants. Table 1 gives the sensitivities for all design variables. The sensitivities computed by the polynomial chaos expansion are the variance-based sensitivity indices called Sobol' indices, which are normalised. They indicate the contribution of input variables to each output variable, in which the two outputs of the the multi objective optimisation are applied. It is decided that variables with both sensitivities lower than 0.016 would be set as constant, resulting in the omission of all heights of the keel and crown, w_1/w_3, Λ_{out} and $\Pi_{lpc_{cr}}$.

Table 1 Design variables with description, their bounds and their sensitivity w.r.t. both objectives, where the design variables with * will be constants

Variables	Description [Unit]	Lower bound ($\mathbf{x}^L$)	Upper bound ($\mathbf{x}^U$)	Sensitivity ATR	Sensitivity COC
b_{outer}	Wing span of the outer wing [m]	13	20	0.031	0.041
c'_1	Normalised chord at section 1[-]	1.00	1.25	0.023	0.038
c'_3	Normalised chord at section 3[-]	1.017	1.25	0.032	0.038
H_{c_1}*	Height of crown at section 1 [m]	0.5	0.8	0.001	0.001
H_{c_3}*	Height of crown at section 3 [m]	0.5	0.8	0.002	0.002
H_{k_1}*	Height of keel at section 1 [m]	0.4	0.7	0.002	0.002
H_{k_3}*	Height of keel at section 3 [m]	0.4	0.8	0.002	0.002
L_1	Length of the first section of the main wing [m]	19.2	28.8	0.019	0.025
L_3	Length of the third section of the main wing [m]	8.8	15.4	0.008	0.019
L_{fin}	Length of the fin [m]	5.6	10.5	0.087	0.118
w_1/w_3*	Ratio of width at section 1 over width at section 3 [-]	0.85	1.07	0.007	0.008
λ	Taper of the outer wing [-]	0.07	0.15	0.020	0.018
Λ_{in}	Sweep of the inner wing section [°]	55	70	0.046	0.073
Λ_{out}*	Sweep of the outer wing section [°]	35	45	0.010	0.010
BPR_{cr}	Bypass ratio at cruise [-]	6	13.5	0.027	0.029
$\Pi_{\text{fan}_{\text{cr}}}$	Pressure ratio of the fan at cruise [-]	1.28	1.8	0.070	0.063
$\Pi_{\text{hpc}_{\text{cr}}}$	Pressure ratio of the hpc at cruise [-]	15	27.6	0.021	0.011
$\Pi_{\text{lpc}_{\text{cr}}}$*	Pressure ratio of the lpc at cruise[-]	1.3	1.7	0.015	0.008
TIT_{cr}	Turbine inlet temperature at cruise[K]	1350	1700	0.054	0.033
h_{cr}	Initial cruise altitude [m]	6000	13000	0.327	0.267
M_{cr}	Cruise Mach number [-]	0.6	0.9	0.202	0.211

The optimisation process is additionally regulated by 26 constraints. Constraints can be divided into three types: geometric constraints, stability & control constraints, and engine constraints. The five geometric constraints ensure that

[†]modeFrontier. Retrieved on April 9th 2024 ,https://engineering.esteco.com/modefrontier/

the necessary fuel capacity can be accommodated within the allocated area specifically designated for fuel storage, that all passengers fit in the cabin, and there is sufficient floor area to accommodate the cargo and payload. The maximum total wingspan and total tail height should not exceed the 65m and 20.1m, respectively, to comply to ICAO code 4E hangar size requirements.

Stability and control constraints are incorporated to ensure compliance with federal regulations as dictated by EASA's CS-25 Certification Specifications and Acceptable Means of Compliance for Large Aeroplane Subpart B - Flight. There are four stability constraints to ensure longitudinal, lateral and directional control. Longitudinal stability is ensured by a nose-down pitching moment through the enforcement of a positive static margin and enforcing a maximum restriction on the displacement of the centre of gravity (CG) during extreme flight conditions, as specified by the regulations of CS25.27. Lateral stability is ensured by maintaining the rolling moment derivative with respect to the sideslip angle negative. Directional stability is ensured by having a sufficiently high yawing moment derivative with respect to sideslip angle, where the target value ($C_{n_{\beta,\text{target}}}$) depends on the surface area.

The control constraints ensure the controllability of the aircraft according to the regulations, and the selected requirements, the evaluation method, and conversion to design constraints are described in more detail in the previous research by Van der Toorn. However, a short description of the 15 control constraints is provided. The maximum deflection of the control surfaces is set to 25°. The first control constraint requires compliance with regulations during the landing process, specifying that the Flying-V must not exceed a maximum approach velocity of 140 knots. The aircraft should be able to perform steady level 1-g trimmed flight at all speeds and altitudes, this is satisfied when the elevator angle (δ_e) is below the maximum deflection of 25° and the angle of attack (α) is below the angle at which pitch break occurs which was at 20°. From a trimmed 1-g flight, the aircraft should be able to pull a load factor of 1.3 either within the acceptable elevator deflection and angle of attack range. The aircraft is required to fly steadily under maximum crosswind conditions, which corresponds to a side-slip angle of 11°. This steady sideslip trim is achieved using the aileron deflection (δ_a), rudder deflection (δ_r) and a bank angle (ϕ), which should all fall within the maximum range of 25°, 25° and 5° respectively. Three similar constraints are placed on the one engine-out trim condition, in which an aircraft is required to perform straight flight with one engine inoperative at minimum control speed and MTOM. Furthermore, there is a constraint on the time to bank in which the aircraft is required to roll from a 30° banked turn to a 30° banked turn in the opposite direction in 7 seconds. The aircraft should either be able to rotate for pitch up at take-off at a velocity (V_R) lower than the minimum take-off safety speed ($V_{2_{min}}$). Finally, two constraints are set on the susceptibility to loss of control at high angles of attack. The dynamic yawing derivative with respect to sideslip angle ($C_{n_{\beta_\text{DYN}}}$) ensures yaw departure tendency. To assess the spin resistance and susceptibility to roll departure due to the ailerons, the Lateral Control Departure Parameter (LCDP) is used.

The engine constraints are set to ensure the feasibility and manufacturability of the turbofan engine. The first limitations include a restriction on the highest achievable TIT during take-off, which is set at a maximum of 2000 K. This limitation is imposed to comply with cooling and material limitations. The second limitation is set on the overall pressure ratio (OPR) which should not exceed 60, as most modern engines do not operate at pressure ratios higher.

All the constraints were normalised and written as inequality constraints larger than zero. The full list of constraints is given in Table 2, with separation between the geometric, stability & control and engine constraints.

The multidisciplinary design optimisation setup is presented in the form of an extended design structure matrix, as introduced by Lambe and Martins in Figure 9 [11]. This shows that there is first a convergence of inner design that guarantees consistency among all aircraft in terms of weight, shape, and operational performance. In this inner loop the airframe model consists of the geometry definition and the weight estimation. Subsequently, the impact of climate change and costs are calculated, resulting in objective function values for the optimise module. Finally, the optimise module modifies the design vector, taking into account the constraint violations identified in step 9.

B. Top Level Aircraft Requirements and Fleet Scenario

The Flying-V aircraft must ensure its competitiveness in the current aircraft market. The focus of this research is on the Flying-V-900, a long-range aircraft model. Hence, the Flying-V-900 will be evaluated in comparison to a conventional long-range wide-bodied aircraft, specifically the long-range wide-bodied kerosene aircraft studied by Proesmans, which is based on the A350 model [12]. The top level aircraft requirements (TLAR) are similar to the conventional long range aircraft A350. This corresponds to a design range, which is the maximum range with maximum amount of passengers without cargo of 14800km at a payload weight of 31000kg. Additionally, the passengers and cargo should fit the pressurised oval fuselage section. This is taken into account with constraints were the dimensions of all the cabin components are taken from the research by Benad [4]. A summary of the most important requirements is given in

Table 2 Overview of the constraints ordered by category

Number	Description	Constraint
1	Fuel capacity	$V_{\text{fuel}} < V_{\text{tank}}$
2	Cabin capacity	$S_{\text{pax}} < S_{\text{cabin}}$
3	Floor capacity	$S_{\text{cargo}} + S_{\text{pax}} < S_{\text{floor}}$
4	Maximum span	b<65m
5	Maximum tail height	h_{tail}<20.1m
6	Static margin	SM>0.06·MAC
7	CG shift	Δx_{cg}<3.2m
8	Lateral stability	C_{l_β}<0
9	Directional stability	$C_{n_\beta} > C_{n_{\beta,\text{target}}}$
10	Approach speed	V_{app}<140kts
11	Longitudinal trim: alpha	$\alpha < 19°$
12	Longitudinal trim: elevon	$\delta_{\text{e}} < 25°$
13	Pull up: alpha	$\Delta_\alpha < 10°$
14	Pull up: elevon	$\Delta_{\delta_{\text{e}}} < 25°$
15	Steady sideslip: δ_{r}	$\delta_{\text{r}} < 25°$
16	Steady sideslip: δ_{a}	$\delta_{\text{a}} < 25°$
17	Steady sideslip: ϕ	$\phi < 5°$
18	Engine-out trim: δ_{r}	$\delta_{\text{r}} < 25°$
19	Engine-out trim: δ_{a}	$\delta_{\text{a}} < 25°$
20	Engine-out trim: ϕ	$\phi < 5°$
21	Time to bank	$t_{\text{bank}} < 7$s
22	Take-off rotation	$V_{\text{R}} < V_{2_{\text{min}}}$ - 5m/s
23	Departure: dynamic	$C_{n_{\beta_{\text{DYN}}}} > 0$
24	Departure: LCDP	LCDP > 0
25	Maximum TIT_{TO}	TIT_{TO} <2000K
26	Maximum OPR_{cr}	OPR_{cr}<60

Table 3 Top level aircraft requirements

Requirement, unit	Value
Design range [km]	14800
Approach speed V_{app} [m/s]	72.0
Maximum span b_{max} [m]	65.0
Landing mass factor	0.76
RPK-2050	$1.21 \cdot 10^{12}$
Number of first class passengers	48
Number of economy class passengers	280

Table 4 Top level aircraft assumptions

Assumption, unit	Value
Reference block range r_{block} [km]	6060
Reference load factor, passengers	253
Annual utilisation [hrs/year]	4300
Takeoff thrust to weight ratio T/W	0.278
Takeoff lift coefficient $C_{L_{\text{TO}}}$	0.55

Table 3 and the most important assumptions are given in Table 4.

Studies have demonstrated that reducing both altitude and velocity during flight has a positive effect on minimising the impact of global warming [9][12]. Nevertheless, reducing the speed of the aircraft leads to longer block time and reduced productivity. To maintain constant productivity, it is necessary to increase the number of passengers on board or the number of flights. In this study, the productivity and the number of passengers are held constant, thus the impact of additional flights needed to be considered. This was accomplished by assessing ATR_{100} and COC across the entire fleet. The study conducted by Proesmans will serve as a basis for our fleet composition and productivity [12]. The aircraft will be launched in 2020, operated for a period of 35 years, and then retired. The annual aircraft production remains consistent and concludes in the year 2050. The fleet size exhibits a linear growth from 2020 to 2050, remains constant between 2050 and 2055, and then decreases linearly until the entire fleet is retired in 2085. The maximum fleet size needed will be determined based on the constant maximum productivity measured in Revenue Passenger Kilometres (RPK) required in 2050, which will remain consistent for all analyses. The ATR_{100} is measured between the years 2020 and 2120.

C. Design and Analysis Models

This section offers a comprehensive overview of the various disciplines integrated into this multidisciplinary optimisation. The models with respect to the Flying-V are the culmination of various previous studies on the Flying-V. As the geometry definition is generated by van Hillen [10]. The mission analysis and part of the weight estimation are analysed by

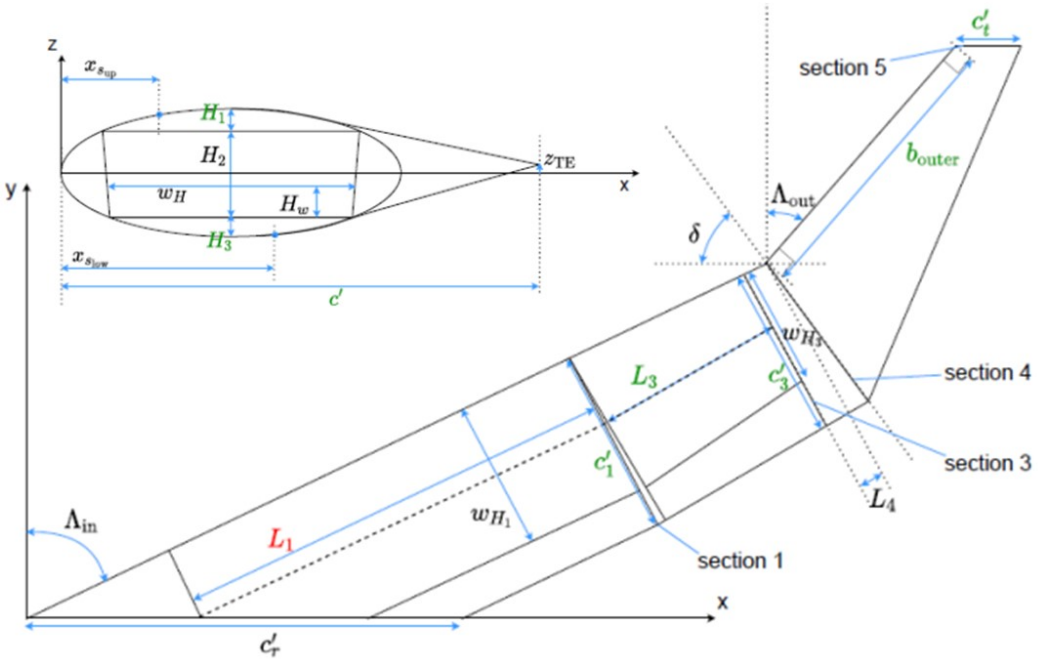

Fig. 1 Planform and Cross sectional of the inner wing of the Flying-V[7]

Oosterom [7]. The aerodynamic, mass, and stability analysis is modelled by van der Toorn [8]. The propulsion, climate, and cost models are added to the Flying-V code and are based on code developed by Proesmans [9]. Since these models have been thoroughly documented in their respective research papers, our discussion here will provide a brief representation of the methodologies, focussing on important assumptions and justifications for their use. Specifically, this section will provide in-depth explanations for the recently introduced components.

1. Geometry Definition

The parameterisation developed by Hillen [10] defines the geometric characteristics of the Flying-V. The primary wing is made up of five segments and a vertical winglet. The initial three sections of the aircraft comprise a pressurised oval fuselage section that accommodates both passengers and cargo. The final two sections serve as the connection between the outer wing and the control surfaces, with the purpose of facilitating the aircraft's manoeuvrability. The oval fuselage section is determined by the width at the arm height (w_H) and the height of the crown, cabin, and keel at section 1 and the end of tapered section 3. The remaining planform of the inner wing is characterised by the inner sweep angle, length, and normalised chord of the untapered section, as well as the length and normalised chord of the tapered section. The chord is normalised using the Equation 2.

$$c' = \frac{c}{w_H + H_2} \tag{2}$$

The transition to the outer wing is determined by two fixed parameters: the length (L_4) and the orientation (δ) of the starting point of the outer wing. The outer wing's cross-sectional shape is characterised by CST coefficients, while the planform is determined by the outer sweep angle, outer span, and the tip chord, which is adjusted using the outer taper ratio [13]. Horwitz developed a parameterisation method for the fins to which the rudders are attached, which includes the bend radius, cant angle, sweep angle, length, tip twist, and taper ratio [14]. Ultimately, the twist and dihedral angles at each section could be modified, but they are fixed at constant values that matched those of the baseline aircraft design. This is condensed into Figure 1.

2. Weight Estimation

The mass estimation method used for the MDO of the flying-V family design employed a semi-analytical approach that combined structural analysis with empirical relationships [7]. The mass of components that resemble those found in a typical aircraft, such as systems, payload items, landing gear, engine, operational items and cabin provisions, was estimated using methods described by Torenbeek [15]. The mass of the fuselage and the outer wing was determined using a simplified method in which the weight is scaled with the volume of these sections relative to the baseline aircraft, as the use of EMWET was not possible due to VORLAX not providing a lift distribution [8].

Finally, the mass of the oval fuselage of the inner wings was determined using a semi-analytical method developed by Schmidt and Vos [16]. This approach offers a higher level of specificity compared to the original technique to estimate the weight of an oval. It enables the determination of the dimensions of all main structural components and provides significant adaptability to adjust the loads on these components. In addition, this method has undergone thorough verification and validation [17][16]. The mass estimations derived from this model were validated through a comparison with previous studies and the results obtained from the Finite Element Method analysis conducted by Claeys [7][18]. The simplified method for the fuselage and outer wing made by van de Toorn was validated by comparison with the Oosterom model and showed a maximum difference of 1.6%[8]. These slight deviations indicate that the model is capable of producing satisfactory results for optimisation and comparative analysis.

3. Aerodynamic Analysis

The aerodynamic model calculates the aerodynamic properties such as lift, drag, moments, and stability derivatives of the Flying-V geometry. The aerodynamic model for this optimisation problem had to have a low computational cost to allow for optimisation and to provide accurate lift, drag and moment coefficients, lift and moment distributions, and stability derivatives in the transonic regime. Therefore, the VORLAX2020 analysis model was applied, which is the in 2020 Souders and Takahashi revised version of the VORLAX model of Lockheed-California Company from 1970, and is a vortex lattice solver[19][20].

However, the VORLAX solver provided unrealistic results for drag, as it gave negative induced drag at several sections of the wing. The application of another aerodynamic solver Athena Vortex Lattice was investigated, but this resulted in worse performance at the low lift coefficient regime in which the Flying-V operates and was computationally more extensive. Therefore, it was decided to compute the induced drag using the drag polar equation, utilising the Oswald factor (e) of the baseline aircraft as determined by Oosterom. This decision was confirmed in subsection III.A. The drag coefficient was determined using equation Equation 3, where the first term represents the zero lift drag coefficient (C_{D_0}), the second term represents the lift-induced drag (C_{D_i}), and the third term represents the wave drag ($C_{D,w}$). Nevertheless, the VORLAX solver was utilised to calculate stability and control estimations.

Since, the drag polar equation only calculates the induced drag a complementary viscous model was required to calculate the zero lift viscous drag forces on the Flying-V. The analytical viscous model of the Flying-V was developed by Faggiano and accounts for the skin friction and pressure drag, while neglecting the lift-related profile drag, which was a validated assumption [21].The viscous model relies on the idea of flat plates with skin friction coefficients and form factors, and it is assessed for the main wing, nacelles, and pylons. The skin friction coefficients are determined using Raymer's method, while the form factors are assessed using Torenbeek's method, which yielded the most accurate alignment with experimental data [22][15].

As Flying-V is flying in the transonic regime, wave drag is important. The wave drag effects are accounted for by the third term given in Equation 3 developed by Pinho based on Mason's method, where M_{cr} is the cruise mach number [23].The drag divergence Mach number (M_{dd}) is fixed at a constant value of 0.925, which corresponds to the drag divergence Mach number obtained in the research conducted by Laar [24].The validation of this model is provided in subsection III.C.

$$C_D = C_{D_0} + C_{D_i} + C_{D,w} = C_{D_0} + \frac{C_L^2}{\pi A e} + 20\left[M_{\text{cr}} - M_{\text{dd}} + \left(\frac{0.1}{80}\right)^{1/3}\right]^4 \tag{3}$$

Extended landing gear and flaps during take-off and landing phases result in additional drag. Therefore, it was crucial to establish the drag polar specifically for these phases. To achieve this, the supplementary drag coefficients were derived from the research conducted by de Zoeten and subsequently modified to consider the relevant reference area for the present design [25].

Finally, the decision was made to apply VORLAX2020 for the stability and control computations, despite its shortcomings, because the longitudinal stability is mostly affected by the lift and moment coefficient and would have a

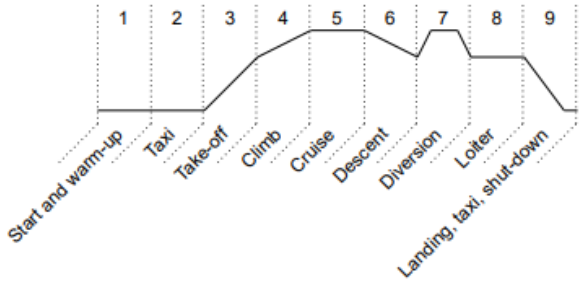

Fig. 2 The standard mission design [7]

negligible affect of the inaccurate induced drag. Lateral stability is affected more by drag, so these results will have a lower accuracy, but since they are not limiting the design, were they evaluated for completeness. The VORLAX2020 solver calculates stability and control derivatives under different conditions, such as varying Mach numbers, angles of attack, sideslip angles, and control surface deflections. The stability and control considerations are in accordance with EASA's CS-25 Certification Specifications and Acceptable Means of Compliance for Large Aeroplane Subpart B - Flight. The evaluation employs methodologies established by Roskam, Kay, and Lee [26][27]. The model, attributed to van der Toorn, was created based on the principles and assumptions outlined in his research [8].

4. Propulsion

The engines in this study feature two turbofan engines with a two-spool architecture without additional features such as bleed air and cooling flows. The propulsion model developed by Proesmans is applied, which is based on the one-dimensional thermodynamic sizing process from Mattingly et al. while accounting for a variable specific heat with the gas model of Walsh and Fletcher [9][28][29]. The model performs thermodynamic on-design and off-design analyses from the engine design variables, polytropic coefficients, mechanical efficiencies, inlet and combustor pressure losses, cruise drag polar and cruise and takeoff conditions. The thrust at takeoff (T_{TO}) is calculated from a constant thrust-to-weight ratio of 0.278 taken from the research by de Zoeten [25]. The component efficiencies are constant to decrease compuational cost by eliminating the need for component maps. This analysis evaluates the thrust specific fuel consumption (TSFC) and emissions in both cruise and take-off. Afterwards, the propulsion model calculates the dimensions and weight of the engine based on the findings of the thermodynamic analysis. Proesmans used TASOPT appendix H to model the engine mass, but the model was based on outdated materials [30]. However, when compared to the GEnx-1B-70, which the propulsion model had been based on, it was found that the new materials option proposed provided a better match. The nacelle and systems weight of the engine that make up the remainder of the engine weight are computed with a method proposed by Torenbeek [15]. The drag of the nacelle and pylon was incorporated in the viscous drag model, where the viscous drag of the nacelle was computed with a method proposed by Raymar and a constant drag of the pylon of 3 drag counts was assumed according to research by Bourget [22][31].

5. Mission

The aircraft is designed in the convergence loop for the standard mission shown in Figure 2. This mission profile is similar to the mission profiles applied by previous studies on the Flying-V-900 and corresponds to the design mission profile of a conventional long range aircraft as the A350-900, which has a range of 14800km with 48 first class passengers and 280 economy class passengers, with a diversion distance of 200nm and 30 minutes loiter time. The cruise phase of the mission profile involves a continuous climb in altitude, enabling the aircraft to consistently operate at its optimal lift coefficient. As the fuel is combusted, the weight of the aircraft decreases progressively, normally reducing the lift coefficient. For this mission, the required fuel mass is evaluated using the Roskam fuel fraction method, where the fuel fraction of the cruise phase is estimated using the Breguet range equation. The fuel of the diversion and loiter phase is taken into account by implementing the reserve fuel of 5%. The fuel fractions for the other phases are assumed similar to the values applied by Roskam [32]. Finally, the maximum takeoff mass (MTOM) is calculated from the operational empty mass (OEM) and the payload mass.

Proesmans used a comprehensive mission analysis that incorporated fundamental principles of flight mechanics,

engine off-design performance, and multiple drag polars. This analysis was used to simulate the burn and emissions of the mission fuel in specific time intervals [12]. This method was exclusively utilised for the analysis of the impact of global warming outside of the convergence loop, as it required significantly more time compared to Roskam's fuel fraction method.

The evaluation of the impacts of global warming was carried out utilising a widely employed reference mission formulated by Proesmans, which relies on transport data from preceding decades [12]. The reference mission was specifically designed with a reduced cruise range of 6060km, and it could only accommodate a total of 253 passengers. The aircraft experiences a slight increase in altitude as it becomes lighter during the mission. However, it is interesting to note that, in its maximum range, the aircraft would experience a significant cruise climb, which could increase the impact of global warming by flying to altitudes that have an increased impact on global warming. The capacity to loiter and diverge was still upheld by incorporating an additional 5% of fuel as a contingency. These reference missions fall comfortably within the payload range limits and are not the missions that impose design constraints.

6. Climate

The climate analysis model is of paramount importance in the study, serving as the main optimisation objective. Placed outside the convergence loop, it forms the cornerstone for evaluating the impact of the Flying-V aircraft on global warming. In the evaluation of the global warming impact, it is of importance to choose the climate metric wisely. The Average Temperature Response over a hundred-year horizon was regarded the best climate metric for this study, as it takes into account the location of the emission, is climate-relevant by giving a temperature change, and it takes into account the short and long term effects of both CO_2 and non-CO_2 climate agents. The ATR_{100} is defined as the integral of the expected temperature response ΔT over a 100-year period, providing a comprehensive assessment of long-term impacts (CO_2 emission, methane, and ozone depletion) and short-term radiative effects (ozone creation, contrails, and water vapor at low altitudes). The assessment period begins with the introduction of the aircraft model into the market in 2020, as this makes it possible to compare it to results obtained by previous studies of Proesmans [12].

$$\mathrm{ATR}_{100} = \frac{1}{100}\int_0^{100} \Delta T(t)\mathrm{d}t \tag{4}$$

The temperature response for each flight has been obtained with a model similar to the model utilised in the research of Proesmans. A short description of the modelling and uncertainties of the various climate forcers will be presented here, but more details are provided in the research by Proesmans [9]. The model determines ΔT from a linearised temperature response model. CO_2 emission is directly related to carbohydrate-containing fuel burning and has a long life, making the effects independent of the location of emission, which is the case for shorter-lived species, and will therefore be determined with a convolution integral with a response function from research by Sausen and Schumann [33].

NO_x emission has only an indirect effect of the global warming impact, by means of long term methane and ozone depletion, which has a cooling effect, but also a short term warming effect due to ozone formation. The long term effects are again implemented by means of a convolution integral, but for short lived species that is emitted a simpler method directly related to the emission is applied. However, the effects of NO_x is heavily dependent on the altitude at which it is emitted, hence an additional altitude forcing term, which is determined from research by Dallara and Kroo [34]. Furthermore, NO_x emissions consist of multiple species, and those are formed under different circumstances, keeping the emission index constant but dependent on engine and combustion conditions. Hence, the emission index for the various operating conditions and engines must be determined by means of fuel flow methods or analytical expressions. In this study, the P3-T3 method of Dallara is applied [35]. This NO_x model has several uncertainties from the emission index calculated with the P3-T3 model, the omission of geographical location, and the change in methane lifetime due to depletion.

Water, soot, and sulphate are other short-lived greenhouse gases and are computed without a convolutional integral and a constant emission index. The altitude dependencies of these species are neglected, as they are negligible at transonic cruise altitude [5].

The condensation trails that form due to the hot and humid exhaust are calculated from the accumulated contrail length and an altitude-dependent forcing factor. The accumulated contrail length is only evaluated when persistent contrails form, which is the case if the Schmidt-Appleman criterion is met, the static ambient temperature lies below the threshold, and the partial pressure of the mixed exhaust that reached ambient temperature lies between thresholds for saturation above liquid water and the saturation level above ice [36]. However, the effect of soot and sulphate on the

nucleation mechanism to generate ice crystals and droplet formation is not taken into account, which has an impact on the lifetime and radiative forcing of contrails [37]. Furthermore, only linear contrails are taken into account, and not the spread of contrail-cirrus, as the effect of contrail-cirrus on radiative forcing is highly uncertain [35]. Finally, the effects of day and night and geographical location are not taken into account [38].

Climate response modelling involves integrating non-linear relationships between emissions and the Earth's climate system. However, it is imperative to recognise the prevailing deficiencies in climate modelling, which frequently depend on substantial assumptions, resulting in uncertainties within these models. Dallara performed uncertainty quantification investigations, employing Monte Carlo analysis. The results indicated a range of 66% likelihood for reductions in ATR compared to the reference aircraft. These findings indicate that, when conducting comparative studies, it is reliable to consider decreases in ATR, as long as the same model is consistently applied and the associated uncertainties are taken into account. Furthermore, the analysis revealed a higher likelihood of attaining significant rather than minor reductions in ATR [35].

7. Cost

The cost model calculates the cash operating cost in USD, which is the second objective of the optimisation. In this analysis, the costs of fuel, oil, maintenance, and salaries are taken into account. This is different from direct operating cost, which also takes into account depreciation, financing costs, and fees. These costs are omitted because they introduce significant uncertainties. Proesmans developed the cost model, which is based on the Roskam method [9][39]. Similar cost values as Proesmans are applied. Proesmans determines all costs at a value of 2030 USD, which is based on the values from 2020 and 2021 and adjusted for an annual inflation rate of 2%. The fuel and oil expenses amount to 2.71 USD per US gallon and 73 USD per US gallon, respectively. The crew costs are calculated based on the average salaries of the respective personnel in the United States for 2020 and 2021, adjusted for inflation to reflect the levels projected for 2030.

Since the climate impact is calculated for a fleet that is in operation for an extended period of time, it is important to express the costs either for a fleet. The total fleet cash operating costs ($\mathrm{COC}_{\mathrm{fleet}}$) can be calculated from the operating cost of one aircraft per year ($\mathrm{COC}_{\mathrm{AC}}$) with Equation 5, where $\mathrm{RPK}_{\mathrm{AC,ann}}$ represents the total revenue passenger kilometres flown by a single aircraft within a year. N_{yr} refers to the operational lifespan of an aircraft, while N_{AC} represents the total number of aircraft in the fleet. For the analysis, a constant productivity is assumed; therefore, N_{AC} depends on the block time, so longer flights are likely to result in additional aircraft and higher costs.

$$\mathrm{COC}_{\mathrm{fleet}} = \mathrm{COC}_{\mathrm{AC}} \cdot \mathrm{RPK}_{\mathrm{AC,ann}} \cdot N_{\mathrm{yr}} \cdot N_{\mathrm{AC}} \tag{5}$$

III. Verification

The models used in this study depend significantly on previous research efforts, particularly those conducted by Oosterom, van der Toorn and Proesmans, as described in subsection II.C [7] [8][9][12]. More precisely, the propulsion model closely corresponds to the one that Proesmans had previously verified to be accurate using GSP [9].Likewise, the mission and part of the weight model are similar to Oosterom's extensively verified model [7]. The other parts of the weight model and the stability and control model are similar to the models of van der Toorn and have already been verified in his research [8].

While utilising the strong framework established by these existing models, our attention is directed towards the integration of the propulsion and climate models in the Flying-V model of Oosterom and van der Toorn and the newly integrated aerodynamic model, in which the lift-induced drag is obtained with the drag polar function and a wave drag model is added. In order to guarantee that the integration still works properly, a verification is performed between the aircraft model and the results of Oosterom. Additionally, validation is carried out for the climate, wave drag, propulsion, and cost models to validate that the generated values are rational.

A. Aircraft Model

The convergence loop of the Flying-V models is validated by comparing the results of the baseline aircraft with the values obtained by Oosterom. The baseline aircraft used in this comparison is the FV-900, which has been optimised for the family. However, with the implementation of a new, more straightforward aerodynamic model, a decision had to be made regarding which variables should be utilised for the oswald factor and zero lift drag coefficient. Firstly, the values obtained from Oosterom's model can be utilised, as this model has been validated and employed in other studies on

Table 5 Aircraft model verification parameters, where three models with the standard viscous model, one with the corrected model, and two oswald factors, are compared to the FV-900 by Oosterom. The third column with * is applied in this research.

Parameter	FV-900 Oosterom[7]	$C_{D_0} = 0.0055, e = 0.78$	$C_{D_0} = 0.0055, e = 0.62$*	$C_{D_0} = 0.0072, e = 0.78$
MTOM	$234{\cdot}10^3$ kg	$220{\cdot}10^3$ kg	$234{\cdot}10^3$ kg	$237{\cdot}10^3$ kg
OEM	$115{\cdot}10^3$ kg	$113{\cdot}10^3$ kg	$115{\cdot}10^3$ kg	$116{\cdot}10^3$ kg
m_{fuel}	$87.5{\cdot}10^3$ kg	$76.3{\cdot}10^3$ kg	$88.4{\cdot}10^3$ kg	$90.7{\cdot}10^3$ kg
L/D	21.6	24.4	21.5	21.0
m_{engine}	7277 kg	5805 kg	6488 kg	6613 kg
TSFC_{cr}	$1.428{\cdot}10^{-5}$kg/N/s	$1.443{\cdot}10^{-5}$kg/N/s	$1.443{\cdot}10^{-5}$kg/N/s	$1.443{\cdot}10^{-5}$kg/N/s

the Flying-V. Nevertheless, the values by Laar were obtained using a highly accurate computational fluid dynamics (CFD) analysis. Initially, the oswald factor obtained by Laar of 0.78 and the viscous model of Faggiano implmented by Oosterom was applied, but this resulted in a significantly higher lift-to-drag ratio (L/D) and thereby greatly improved performance, as shown in Table 5, which was considered to be incorrect [21]. This discrepancy arose from the fact that the Laar viscous model had a zero-lift drag coefficient of 72 drag counts, whereas the standard viscous model used by Oosterom yielded a value of 55 drag counts. Two alternative options were suggested: one utilising the standard Flying-V viscous model developed by Faggiano, combined with the Oswald factor of 0.62 determined by Oosterom; or modifying the standard viscous model to align with the drag coefficient determined by Laar, along with the Oswald factor of 0.78 proposed by Laar. The outcomes of both alternatives are presented in Table 5 and demonstrate the most optimal alignment with the Oosterom baseline model, which utilises the standard viscous model and a low Oswald factor of 0.62. Consequently, this approach was adopted for the purposes of this study.

Table 5 demonstrates a small rise in fuel mass, which can be attributed to the 0.1 decrease in L/D and the higher TSFC. The decrease in L/D is attributed to the implementation of a new aerodynamic model that considers the effective aspect ratio of the wing and one winglet was used instead of the aspect ratio of the wing and both winglets. This leads to a marginally reduced aspect ratio, resulting in a slightly diminished aerodynamic performance, due to the higher induced drag. The higher thrust coefficient was a result of the engine efficiencies taken, which were loosely modelled after the GEnx-1B70. Nevertheless, the Oosterom model utilised a constant coefficient derived from the Trent-XWB-84, resulting in a small deviation. The decrease in engine mass is attributed to the use of the smaller and lighter GEnx-1B70 engine. The results remain within acceptable limits, validating the successful integration and dependability of the propulsion model and the new aerodynamic model into the aircraft model.

B. Climate Model Verification

The integration of the climate model developed by Proesmans into the Flying-V model is validated by comparing it to research by Proesmans, Reekers and Lee[9][6][2]. Table 6 gives the ATR and radiative forcing (RF) in the year 2050 of all the species followed by their percentage relative to the total of the baseline Flying-V. The ATR of the a conventional long range aircraft optimised for cost computed by Proesmans, the ATR of Flying-V researched by Reekers and relative radiative forcing by Lee are either presented as a comparison.

The ATR analysis shows that there is an almost similar relation between the relative ATR of all the species for the FV-900 with respect to the conventional aircraft. Only the contrail formation is higher; this might be due to the Flying-V flying at a higher altitude. However, the NO_x emission is lower, but a higher NO_x would also be expected at a higher altitude and a lower CO_2, which is not the case. However, all these changes are significantly influenced by engine parameters, which are different for both aircraft and are considered to be in an acceptable range. The ATR due to CO_2 emissions are approximately 24% lower than for the conventional aircraft and because CO_2 emissions are directly related to burning fuel does this closely corresponds to the 20% lower fuel consumption of the Flying-V-900 as found by Oosterom [7], hence the implementation of the climate model into the Flying-V framework is verified.

Initially, it was anticipated that contrails would have a greater impact on the ATR compared to CO_2 emissions, based on Lee's research, which stated that 57% of the effective radiative forcing for aircraft is from contrails, while 34% from CO_2 [2]. However, Lee's research was based on radiative forcing, while the ATR is the integral over time of the change in temperature, which is the convolution integral of radiative forcing. Hence, species with a long perturbation time as CO_2 keep increasing the temperature and thereby the ATR even when the fleet is retired, while for short lived species

Table 6 ATR of the baseline FV-900, FV-900 by Reekers, conventional long range aircraft by Proesmans, and RF of the baseline and relative RF by Lee with relative to total in brackets.

Species	ATR FV-900	ATR FV-900 Reekers[6]	ATR conventional	RF FV-900, mW/m^2	RF Lee[2]
Total	3.60mK (100%)	2.31mK(100%)	4.73mK (100%)	16.1 (100%)	100%
CO_2	2.10mK (58.3%)	0.44 mK(19%)	2.75mK (58.1%)	4.97 (30.9%)	34%
NO_x	0.62mK (17.2%)	0.78mK(34%)	0.98mK (20.7%)	2.90 (18.0%)	17%
Soot	0.045mK (1.3%)	-	0.059mK (1.2%)	0.36 (2.2%)	1%
SO_4	-0.058mK (1.6%)	-	-0.076mK (1.6%)	-0.36 (-2.2%)	-7%
H_2O	0.035mK (0.97%)	0.03mK (1%)	0.045mK (0.95%)	0.17(1.1%)	2%
Contrail	0.85mK (23.6%)	1.16mK (50%)	0.96mK (20.2%)	8.04(50.0%)	57%

such as contrails it decreases. Therefore, the ATR of CO_2 is much higher than for contrails.

In contrast, Reekers' study, employing AirClim and a distinct fleet analysis, offers an alternative viewpoint on the comparative makeup of ATR contributions. Although both studies do not consider contrail cirrus due to uncertainties in the transition from linear contrails to contrail cirrus, Reekers' findings demonstrate a notably greater contrail contribution. Reekers' research assumes a fleet that operates consistently from 2050 to 2150. In contrast, our research model predicts a peak fleet in 2050, with aircraft gradually being retired until the entire fleet is phased out by 2085. This makes it difficult to directly compare the two studies.

In order to validate the climate model, the relative radiative forcing of all species in the year 2050 was utilised and compared to Lee's radiative forcing data as a benchmark. The choice of the year 2050 is strategic because it corresponds to a time when emissions reach their highest point. This allows for a clear understanding of the effects of short-lived species, while long-lived climate forcers are not yet saturated with aged particles. This validation showcases significant agreement despite inherent uncertainties in climate modelling, making our model appropriate for comparative climate analyses using consistent methodologies. Nevertheless, the accuracy of absolute values is still susceptible to a certain degree of uncertainty.

C. Verification of Wave Drag Model

The validation of the initial wave drag model demonstrated that the drag of these highly swept wings did not exhibit any increase as a result of wave drag. These findings are consistent with Laar's results, which indicated that there was minimal change in drag until the aircraft reached a Mach number of 0.85, which was the speed at which the baseline aircraft was flying [24]. Nevertheless, there was a notable rise in drag at a Mach number of 0.90. However, the wave drag model by Chiozotto still did not account for wave drag, as the calculated drag divergence Mach number from the wave drag model was 0.965, whereas Laar obtained a value of 0.925.

Laar acknowledged that there were uncertainties in the computation of the wave drag using the RANS code. However, he also pointed out that the baseline design exhibited excessive wave drag on the outboard wing, which suggests that wave drag would be anticipated. Thus, the decision was made to fix the drag divergence Mach number at 0.925. As a result, the derivative of drag over Mach was found to be 0.107 at $M = 0.925$, which is slightly greater than the value of 0.10 suggested by Airbus and Douglas [40]. Therefore, this modification to the wave drag model is dependable. Furthermore, it is interesting to note that the higher zero lift drag coefficient obtained by Laar could be caused by the excessive wave drag on the outboard wing, as this increases the form factor and thus increases the viscous drag [22].

IV. Results and Discussions

This section presents a comprehensive analysis of the resulting design variables for the single objective optimisation ATR_{100}, COC and fuel, and multiobjective optimisation of the ATR_{100} and COC of the Flying-V aircraft. Through computational simulations of the methodology described in section II and data analysis, this section aims to provide insights into the trade-offs and synergies inherent in optimising these critical design parameters. By exploring the Pareto-optimal front and evaluating the change in design variables, the findings shed light on the potential benefits and challenges associated with different design configurations. Additionally, the discussion delves into the implications of these results for the future of aircraft design, highlighting opportunities for enhancing performance, sustainability, and operational efficiency.

A. Single Objective Optimisation Results

Optimised values for the three single-objective optimisations are provided in Table 7. This table displays the absolute values and the values relative to the minimum achievable values. There are two options available for the conventional long range aircraft. One option provides a cost optimal design, while the other option provides a climate optimal design. It reveals that flying at the minimum ATR_{100} leads to a decrease in ATR of approximately 60% with respect to the other objectives and to costs that are 36% higher than flying at the minimum for COC, and a fuel burn that is 24% higher than the minimum achievable. Moreover, does it suggest that a design focused on fuel efficiency and cost efficiency leads to designs that has quite similar performance for the objectives, due to flying at approximately the same altitude and velocity. The research results confirm that optimising ATR_{100} leads to significantly better ATR performance than focusing on minimising fuel mass, as indicated in prior research by Reekers [6]. More precisely, the design that is optimised for ATR_{100} demonstrates a notably different mission design, which reinforces the notion that the Flying-V could achieve superior results in terms of its contribution to global warming when specifically tailored for this purpose. In contrast to Reekers' analysis, which specifically examined the effect of fuel-optimised designs on global warming, this study emphasises the significance of targeted optimisation strategies in improving the climate performance of aircraft design.[6].

The top view of the three optimised aircraft are depicted in Figure 3. The top view shows a marginally extended root chord and shorter wingspan for the climate-optimised design, which is depicted with red.The cost-optimised design, depicted in blue, and the fuel-optimised design, depicted in green, have a similar wingspan at the maximum limit. The fuel-optimised design features a greater sweep angle and a design that is more loaded towards the rear. The extended design of the fuel-optimised configuration is also evident in Figure 4, which depicts the side view of the rear section of all three wings. Additionally, does the side view indicate that the climate-optimised design features a reduced fin length.

Table 7 Optimised objective values for the FV-900 and a conventional aircraft from Proesmans research [12]

	Absolute values			Relative to minimum value		
Objective	m_{fuel} $[10^3 kg]$	COC_{fleet}, 10^{12}USD	ATR_{100}, mK	m_{fuel} %	COC_{fleet} %	ATR_{100}%
Conventional Cost	77	1.45	5.0	13%	3%	150%
Conventional Climate	84	1.80	2.8	23%	29%	40%
FV-900 Fuel	68*	1.41	3.3	-	1%	60%
FV-900 Cost	69	1.40*	3.2	1%	-	60%
FV-900 Climate	84	1.91	2.0*	24%	36%	-

The objective values demonstrate that the Flying-V is able to outperform the conventional aircraft optimised for

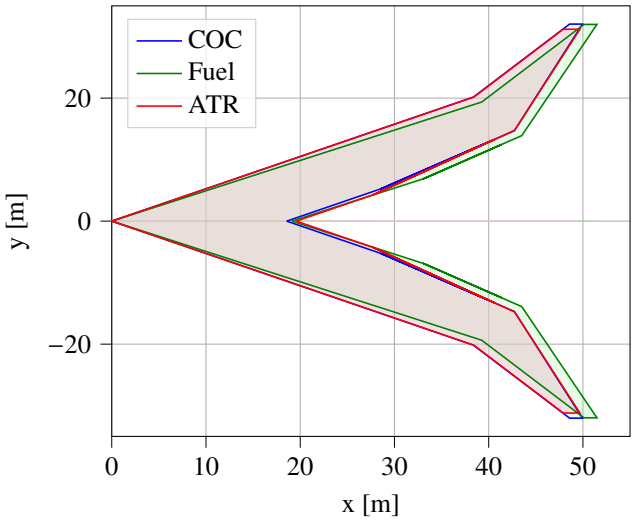

Fig. 3 Top view of the three optimised Flying-V

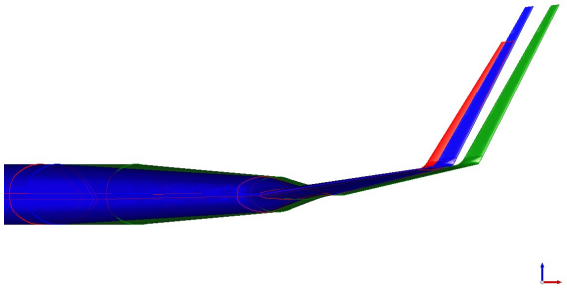

Fig. 4 Side view of the rear part of the wing for the climate (red), cost (blue) and fuel (green) optimised Flying-V-900

both objectives, with the most significant improvement of 40% observed in terms of the global warming impact. The optimised values for the conventional aircraft are derived from the model developed by Proesmans [12].

The climate-optimised Flying-V has a similar fuel consumption as the climate-optimised conventional aircraft, however it has a 40% lower ATR, but a 6% higher operational cost. The climate-optimised FV-900 has the potential to lower the ATR with 60% with respect to the cost optimised conventional aircraft, which is nowadays the most driving design requirement in the aviation industry. This comes however with 9% increase in fuel mass and a significant increase of 31% in costs.

The potential viability of developing and introducing the climate-optimised FV-900 design into the market could be at risk due to a 31% increase in operational costs. Nevertheless, this highlights the considerable market opportunity for a competitive FV-900 model that is specifically designed to maximise either fuel efficiency or COC. This design has the potential to achieve a 13% decrease in fuel consumption and a 56% reduction in ATR with a 3% reduction in operational expenses. Nevertheless, it would demonstrate a 14% greater ATR, but a decrease of 23% in fuel consumption and 24% in COC in comparison to a conventional aircraft specifically designed for ATR. However, this enhanced aircraft is not currently accessible in the market. The introduction of such an aircraft would require a fundamental change in the design philosophy of the aviation industry. This would also involve a lengthy development period.

The optimised design variables for these three designs are provided in Table 8, while additional performance indicators can be found in Table 9. The design to achieve the lowest possible cost is influenced by two factors: minimising fuel mass to reduce fuel expenses, and minimising block time (t_{block}) to decrease labour costs, which is based on flight hours. The requirement for a reduced fuel mass led to a nearly identical performance and mission design compared to the aircraft optimised for fuel mass. This effect is due to the fact that fuel and oil cost make up approximately 50% of all cash operating costs, while labour costs only amount to 30%, hence the dominance of minimising fuel mass.

Both designs operate at a cruising altitude of around 11.5 km and a velocity of approximately 0.85, which is similar to the baseline aircraft that is optimised for minimal fuel consumption by Oosterom, as indicated in Table 8. Nevertheless, the cost-optimised design functions at a slightly higher velocity of Mach 0.02 faster, with the intention of minimising block time. However, once the aircraft reaches a velocity of Mach 0.85, wave drag begins to have an impact. This means that any further increase in velocity would result in a penalty in terms of drag. As a result, the fuel-optimised design does not allow for this increase in velocity. This altitude of 11.5 km and Mach of 0.85 are significantly higher than the 6 km and Mach of 0.60 at which the climate-optimised design operates. Operating at a higher altitude reduces air resistance due to the decreased air density. In addition, the decrease in air density allows faster flying speeds, resulting in shorter block times, which is advantageous for cost-optimised aircraft. Moreover, it decreases the lift-induced drag.

Furthermore, all three aircraft utilise a higher effective aspect ratio than the baseline aircraft, which had a value of 5.2, to minimise lift-induced drag. This is achieved by maximising the wingspan, lengthening the fin, and minimising the chords, as shown in Table 8. However, the disparities between the fuel-optimised and cost-optimised designs arise from the maintenance expenses of the aircraft, which depend on the OEM, asTable 9 gives a lower OEM for the cost-optimised aircraft. In addition, decreasing the OEM also decreases MTOM, resulting in a further reduction in block time. This is because the duration of ground manoeuvres is affected by the MTOM. Hence, the cost-optimised Flying-V incorporates a decreased sweep angle and reduced L_1, while simultaneously increasing L_3 to maintain the wide wingspan, thereby leading to a decrease in the structural mass of the wing. An increase in L_3 led to a decrease in L_1, resulting in a higher aspect ratio due to the shorter chord of the third section. Therefore, it is anticipated that the Flying-V optimised for fuel would have a shorter L_1. However, reducing the length of the first section, which contains the most fuel, would result in a fuel tank volume that is too low for the fuel-optimised aircraft. This is because the fuel tank volume decreases with sweep angle, as the engine section takes over more of the space normally used for the fuel tank. The climate-optimised has a slightly shorter wingspan and longer root chord, as depicted in Figure 1, and an the shortest L_1 further decreasing the structural mass

The cost-optimised Flying-V's engine operates at an Overall Pressure Ratio (OPR) of 54.9, which is lower than the fuel-optimised design's OPR of 59.5. The purpose of reducing OPR is to alleviate the costs related to engine maintenance caused by higher pressure ratios. However, a higher OPR reduces the fuel consumption as more compressed air enters the combustion chamber, hence reducing the TFSC of the fuel-optimised design, as shown in Table 9. The climate-optimised design has an even lower OPR of 49.9, as this decreases NO_x emissions. None of the designs are at the maximum OPR permissible of 60, however the fuel-optimised Flying-V is close as expected.

The BPR of the climate-optimised aircraft is higher than for the cost- and fuel-optimised aircraft. A higher BPR results in decreased fuel consumption due to an enhanced propulsive efficiency. However, this advantage is counterbalanced by an increase in drag and weight, which may outweigh the benefits of improved propulsive efficiency. Furthermore, this could result in an increase in NO_x emissions and contrails, as it requires higher pressure ratios and TIT

Table 8 Optimised design variables for the three objectives along with the baseline aircraft from research by oosterom

Variables, unit	Baseline[7]	ATR_{100}	COC_{fleet}	Fuel
b_{outer} [m]	14.75	16.2	16.3	17.2
c_1 [m]	9.38	9.11	8.63	8.46
c_3 [m]	7.93	7.14	7.14	7.14
L_1 [m]	24.0	19.2	20.4	24.9
L_3 [m]	11.0	15.4	14.2	9.6
L_{fin} [m]	7.0	8.5	10.5	10.5
λ [-]	0.10	0.091	0.074	0.072
Λ_{in} [°]	64.5	62.3	62.3	63.7
BPR_{cr}[-]	9.3	11.5	10.8	10.5
$\Pi_{fan_{cr}}$[-]	1.51	1.37	1.66	1.59
$\Pi_{hpc_{cr}}$[-]	23.0	23.8	21.6	24.4
TIT_{cr} [K]	1450	1432	1555	1501
h_{cr} [km]	11.50	5.98	11.51	11.46
M_{cr} [-]	0.85	0.60	0.87	0.85

Table 9 Performance indicators for the three objectives

Variables, unit	ATR_{100}	COC_{fleet}	Fuel
MTOM [10^3kg]	220	204	204
OEM [kg]	105.7	104.5	105.5
S [m^2]	734	721	727
A [-]	6.6	7.4	7.3
W/S [N/m^2]	2946	2773	2753
L/D_{cr}	23.7	24.5	25.0
T_{TO} [kN]	301	278	278
$TFSC_{cr}$ [10^{-5}kg/N/s]	1.224	1.421	1.383
t_{block} [hh:mm]	10:13	7:54	8:05
$N_{AC_{yr}}$	1446	1119	1143

to generate the power needed for the larger fan. Furthermore, enhanced engine efficiency leads to a steeper slope of the mixing line according to the Schmidt-Appleman criteria, increasing the likelihood of persistent contrail formation[36]. Nevertheless, the heightened likelihood of contrail formation does not impact the climate-optimised Flying-V since it operates at an altitude so low that contrails do not form, as indicated in Table 10.

The cost- and fuel-optimised aircraft has a lower BPR because increasing the BPR of a turbofan operating at their cruise altitude would require a significantly larger engine to generate the required thrust at takeoff, such that the increased weight and drag has more impact than the increased propulsive efficiency. The cost-optimised engine has a higher Bypass Ratio compared to the fuel-optimised design. This is because a higher BPR leads to lower engine maintenance costs. The higher BPR in the cost-optimised design correlates with a higher Fan Pressure Ratio because more bypass air needs to be compressed to enhance engine efficiency with a higher BPR. In contrast, the climate-optimised design achieves a higher BPR with a lower fan pressure due to the denser air at lower altitudes, eliminating the need for excessive compression to generate thrust efficiently, making it possible to keep the TIT low, which reduces NO_x emissions. It is interesting to note that the climate optimised Flying-V is close to the highest permissible TIT at take-off, which is 2000K. This enabled achieving the optimal engine performance for a specific cruise objective while also providing the necessary power during take-off.

The higher TIT in the cost-optimised design, as shown in Table 8 requires a reduced mass flow rate through the engine to achieve the desired thrust, as a greater amount of energy is introduced into the flow within the combustor. As a consequence, there is a reduction in the size of the turbofan engine, leading to a decrease in weight. This, in turn, contributes to a further reduction in both OEM and maintenance costs. The smaller engine enhances aerodynamic efficiency by reducing viscous drag. Nevertheless, the smaller engine experiences a reduced mass flow through both the core and bypass, leading to a diminished propulsive efficiency despite its higher thermal efficiency. Therefore, the fuel-optimised design incorporates a lower TIT. This is done to enhance the propulsive efficiency by utilising a larger turbofan, which compensates for the decrease in TIT. As a result, the fuel-optimised design achieves an optimal lower thrust specific fuel consumption than the cost-optimised design by balancing the size and TIT. The TIT for the climate-optimised Flying-V is lowered, in order to decrease the emission of NO_x, This reduction in TIT helps to minimise the formation of thermal NO_x. NO_x emissions could be further reduced by implementing an improved combustion architecture. However, these aspects are not within the scope of this research.

The data in Table Table 9 demonstrates that the TSFC of the climate-optimised aircraft is lower than that of the fuel-optimised aircraft, even though the engine efficiency is lower. Although seemingly contradictory, this pattern has also been observed in previous studies conducted by Proesmans and Torenbeek [9][41]. According to Proesmans, this is due to the decreased cruise velocity of the aircraft, resulting in lower ram pressure and drag. As a result, there is a favourable decrease in TSFC, but an unfavourable a reduction in the propulsive efficiency of the turbofan engine.

Furthermore, is the TSFC a function of the Mach number hence, the increased TFSC at a lower Mach number.

The Flying-V optimised for climate operates at the lowest possible altitude and velocity, as opposed to the fuel and cost-optimised Flying-V, which operates at a significantly higher altitude and velocity. These findings suggest that the ATR_{100} of the Flying-V is influenced by both carbohydrate fuel combustion and the short-term effects of contrail formation and NO_x emissions. In fact, the likelihood of contrail formation decreases to the extent that contrails may not form at all when the ambient temperature exceeds 235K. In the case of NO_x, the emission of NO_x has three effects. One of these effects is the creation of ozone, which has a short-lived warming effect. This phenomenon decreases at lower altitudes, resulting in a reduction in radiative forcing [42]. The radiative impacts of water, soot, and sulphate also decrease as altitude decreases [5]. However, this research does not consider an altitude forcing for these species and only focusses on the effects caused by fuel combustion for these species, due to the small overall contribution to the ATR.

Figure 5 display the variation in surface temperature resulting from all climate forcers. This demonstrates, as previously discussed in section subsection III.B, that CO_2 emissions have the most significant influence on both temperature change and ATR. The ATR refers to the integral of the surface temperature change over time represented by the area under the curves in the graph. The significant impact of CO_2 arises from its long perturbation time, which causes the surface temperature to continue increasing even after the fleet size declines from 2055 and fully retires in 2085. The contrails are not observable, as the climate-optimised designs do not produce any contrails. Water vapour and soot particles have a minor heating impact on the Earth's atmosphere , while sulphate particles have a cooling effect on the ATR. The NO_x emissions initially exhibit the short-term warming impact of ozone formation. Nevertheless, once the fleet diminishes in size, the long-term cooling impact caused by the reduction of Methane (CH_4) and ozone becomes dominant, leading to a net cooling effect starting from the year 2075. As a result, there is almost no contribution of NO_x to the ATR, as shown in Table 10.

The ATR of all climate drivers for the three optimised FV-900 designs is displayed in Table 10. This demonstrates that the climate-optimised design has reached an optimal state where the impact of short-lived climate drivers, such as NO_x and contrails, is minimised to the extent that they account for 0.0% of the overall ATR. Therefore, the global warming impact of this design is solely derived from the combustion of carbohydrate-based fuels, with nearly all of the warming effects originating from the release of CO_2. Hence, the utilisation of alternative fuel could exert a substantial influence on this design. The cost- and fuel-optimised approach has a combined climate impact of approximately 45% due to NO_x emissions and contrail formation. Therefore, using alternative fuels may result in a lesser impact on the climate.

The cost-optimised design was anticipated to have a greater climate impact compared to the fuel-optimised design due to its operation at a higher altitude and increased fuel consumption. However, the influence of contrails diminishes at an altitude of 11km, and the impact of short-term ozone depletion shows a slight decrease between 11km and 12km, as reported by Köhler [42]. Consequently, the ATR of the cost-optimised design is lower. The climate-optimised design exhibits an ATR that is 16% to 20% higher for CO_2, soot, SO_4, and H_2O. This increase in ATR is closely associated with the combustion of 24% more fuel. However, it should be noted that the ATR values for soot, SO_4, and H_2O has some uncertainties, as the altitude effect of these species, as suggested by Matthes, has not been taken into consideration [5].

Table 10 ATR for all forcers and ATR relative to the total for the climate, cost and fuel-optimised FV-900

Climate forcer	Climate ATR, mK	Cost ATR, mK	Fuel ATR, mK
Total	2.03 (100%)	3.25 (100%)	3.26 (100%)
CO_2	2.01 (99.0%)	1.75 (53.9%)	1.70 (52.2%)
NO_x	0.004 (0.0%)	0.62 (19.1%)	0.65 (20.0%)
Soot	0.043 (2.1%)	0.038 (1.2%)	0.037 (1.1%)
SO_4	-0.055 (-2.7%)	-0.048 (-1.5%)	-0.047 (-1.4%)
H_2O	0.033 (1.6%)	0.029 (0.89%)	0.028 (0.86%)
Contrail	0.0 (0.0%)	0.86 (26.5%)	0.89 (27.3%)

The most violated design constraints were determined by geometric factors, specifically the available floor area, fuel tank volume, and wing span. From an aerodynamic point of view, this is a rational conclusion, as the wing naturally seeks to expand its span while decreasing its surface area. This results in an increased aspect ratio and a reduction in the lift-induced drag. Reducing the area will decrease the parasite drag by minimising the exposed surface, which in turn improves the aerodynamic efficiency. The design was influenced by several stability and control constraints, with the

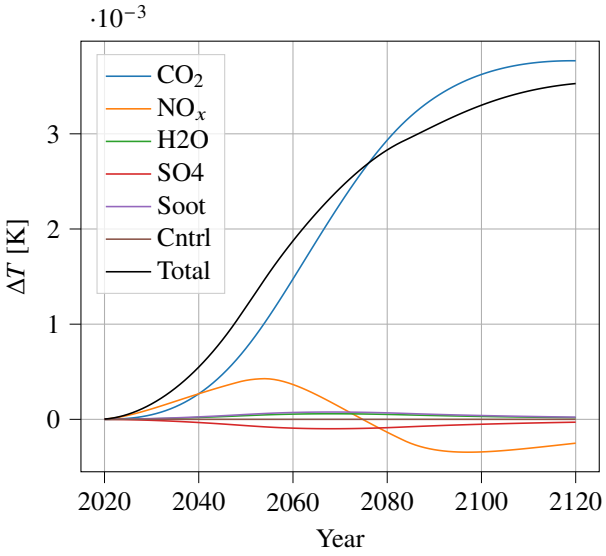

Fig. 5 Surface temperature change of every climate forcer for the climate-optimised design

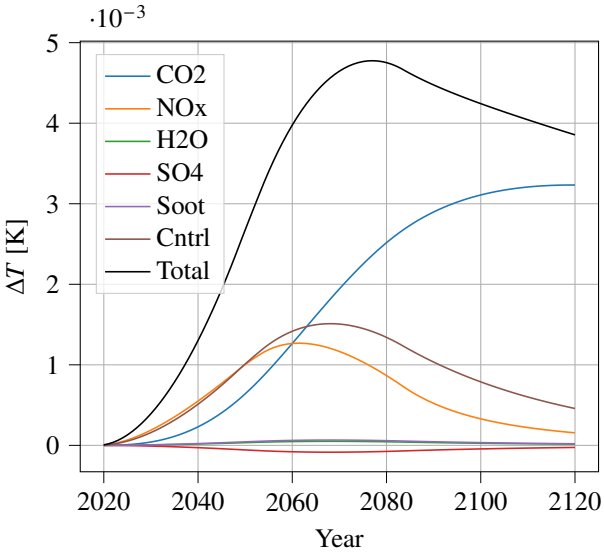

Fig. 6 Surface temperature change of every climate forcer for the cost-optimised design

longitudinal stability being the most limiting factor. This observation is evident in Table 8, where it is shown that the lengths of the more aft section L_3 and b_{outer} increased compared to the baseline configuration, the forward section L_1 decreased, resulting in a shift of neutral point towards the aft, resulting in an increased static margin.

The increase in the length of the fin was necessary due to constraints on the maximum deflection angle of the rudder during sideslip and when one engine is inoperative. The initial fin length of 7m by Horwitz was insufficient to provide control authority for all three designs [14]. Nevertheless, Nolet's research demonstrated that the incorporation of a split drag rudder could enhance yawing control by 55% and 150% during high angles of attack [43]. As the angle of attack increases, the winglet rudder control authority decreases significantly. However, this is not the case for a split drag rudder. However, subsequent analysis revealed that a longer fin length continued to be advantageous for enhancing aerodynamic performance.

The fin, which is 50% longer, led to a 170% increase in the weight of the fin. The weight increase mentioned does not take into account the impact of the increased structural load on the wing caused by carrying a heavier fin. This is because the weight of the wing is based on a simplified mass model. Nevertheless, the enlargement of the fin by 50% has led to a notable enhancement of 9% in the effective aspect ratio, consequently reducing the drag caused by lift.

The fleet size of the climate-optimised designs is 22% and 20% larger than that of the cost-optimised and fuel-optimised designs, respectively, as indicated in Table 9. This research does not consider the costs and climate impact of increasing production capacity by approximately 20%. Nevertheless, it can be argued that this heightened production results in a greater climate impact and overall life cycle expense of the fleet.

B. Multi Objective Optimisation Results

This section illustrates the results of the multi objective optimisation for ATR_{100} and COC. The relationship between ATR_{100} and COC is demonstrated in Figure 7 using a Pareto front analysis. Significantly, the Pareto front unveils three sections with two significant transitions.

The initial section from the left to the right indicated with the orange points in Figure 7 are for a flying-V which operate at an altitude of 6km and a Mach number from 0.60 to 0.62. The operational cost here is significantly higher, due to the fact that a second captain and copilot is required at block times longer than 10 hours, which is the case at these velocities. Nevertheless, as it is just above the 10 hours for this specific mission. These additional captain and copilot will not be on board lowering the costs with 14%. This was also the reason for the high operational costs of the single objective climate-optimised Flying-V, when for that design no additional pilots are applied the cost will reduce from 36% to 22%. However, it is important to consider that this is intended for an average mission, where in many instances the mission will cover a greater distance, thus necessitating the presence of extra pilots operating also at higher speeds.

The second part of Figure 7 after the first transition indicated with blue show a trend from an altitude of 6km and a

Mach of 0.62 to an altitude of 7.7km with a Mach of 0.80. The altitude and cruise velocity are the most influential design variables, as they have the most significant impact on the ATR and COC, where the other design variables are slightly changed to fly optimally at the altitude and velocity at hand.

The final section indicated in Figure 7 with green corresponds to a significant change in altitude. Contrail effects have a substantial impact on ATR_{100} from an altitude of around 8000 km and higher. However, the influence of this effect decreases from an altitude of 11km. In addition, as the altitude increases, there is a decrease in CO_2 emissions. Therefore, designs that are specifically designed for high altitudes show advantageous performance for both ATR and COC. This can be attributed to the capacity to operate efficiently at higher speeds as a result of the decreased air density at higher altitudes and the crew costs tends to decrease as velocities increase and block times are reduced, leading to fewer aircraft and reduced crew salaries.

It is noteworthy that the second section concludes at an altitude of 7.7km, rather than 8km, where the contrails will start to form. The reason for this is the continuous climb during the cruise phase, which causes the Flying-V to fly at an altitude where contrails are likely to form. This effect becomes more pronounced as the mission's distance increases, necessitating the aircraft to start cruising at an even lower altitude in order to maintain the same benefits of flying at a lower height. Alternatively, the aircraft could maintain a constant altitude, although this would necessitate flying with a less than optimal lift coefficient. To mitigate the impact of this sub-optimal lift coefficient, one could initiate the cruising phase before reaching the lowest point on the drag polar, allowing the aircraft to pass through its minimum drag point during the flight.

The Pareto front in Figure 7 illustrates that decreasing the ATR_{100} by 16% results in a minimal 1% change in COC. This occurs when the aircraft is operating at an altitude of 12km and Mach 0.86. Afterwards, the cost begins to escalate more rapidly, reaching 6% when the ATR reduction is 27%, until reaching the transition point where it has to fly at such a low altitude that prevents the formation of contrails. Thus, in order to reduce ATR while minimising cost increases, it is advantageous to maintain high altitude and velocity during operations, as illustrated in Figure 8. From an operational standpoint, this approach is advantageous because commercial aircraft typically operate at high altitudes and are less susceptible to weather conditions. From a commercial standpoint, people prefer flying because it is the most efficient mode of transportation, making it more economically advantageous to keep flying at a high velocity.

However, the lowest ATR occur when flying at a low altitude and velocity, specifically after the transition to an altitude of 7.3km and a Mach number of 0.80 until an altitude of 6km and Mach of 0.60. After the transition it is again possible to achieve a substantial 8% reduction in ATR with only a 1% increase in costs. However, after this point, the costs begin to increase rapidly while the decrease in ATR is limited.

Despite the fact that there is some fluctuation in some of the plots in Figure 8, some other trends beside the trends in operational variables could be observed. Initially it should be noted that at the two extremes, where ATR is lowest or where COC is lowest similar designs as for climate-optimised and cost-optimised single objective optimisation were expected. However, this was not the case for all design variables. The ATR and COC of these extreme designs were marginally lower with 1.9mK for the climate-optimal and $1.40 \cdot 10^{12}$USD for the cost-optimal. This shows that the multi objective optimisation had a better convergence, which could be expected as it had ten times more evaluations.

The BPR plot in Figure 8 indicate despite the fluctuation a high BPR of 11.2 at the lowest altitude and velocity than a decrease to 9.5, as the velocity starts to increase after which it maintains around the 10.8. This is similar to the values obtained for the single objective optimisation in Table 8, which indicated a BPR of 11.5 at the climate optimal design and 10.8 for the cost optimal design.

The fan's pressure ratio exhibited a comparable pattern to that observed in single objective optimisation, wherein the pressure ratio rises with higher altitudes. This is due to the necessity of compressing the thinner air more effectively in order to generate thrust with the bypass air. $\Pi_{\text{fan}_{\text{cr}}}$ decreased while the $\Pi_{\text{fan}_{\text{cr}}}$ increased in order to maintain a low OPR. This is advantageous from both environmental and economic perspectives. The TIT exhibits a clear upward trend since a lower TIT is advantageous for an aircraft optimised for climate conditions, resulting in reduced formation of NO_x. However, at higher altitudes, a higher TIT is necessary because the thinner air reduces the mass flow through the turbofan.

L_1 and L_3 show significantly different trends in Figure 8 than for the single objective optimisations in Table 1, as here the the length of the first section is around the 25.8m with only for the climate optimal design having a slightly shorter section 1 at 25.6m, while for the single objective optimisation both climate and cost were 19.2m and 20.4m respectively. The length of the third section is almost everywhere at its minimum bound of 8.8m with slightly higher value at the climate optimised side and an outlier, while this was at 15.4m and 14.2m for the climate and cost optimal designs respectively. This differences result from the fact that the multi objective optimisation moved to a design with a long and slender outer wing, as the taper ratio remains at a minimum of 0.07 and the outer span remains around the

18.2m which is approximately 2m longer than for the single objective optimisation. The slender outboard led together with the increase in sweep angle led to a reduction in fuel tank volume, which required a larger section 1 than 3, as more fuel is stored in the first section.

The length of the fin remains for most part at its upper bound of 10.5m. This bound was set, as there are several uncertainties in the weight estimation of the fin. The normalised chord of the third section also remains constant at its lower bound of 1.017 with the exception of one outlier and slight fluctuations. The normalised chord of the first section shows a decreasing trend until it is also at its minimum bound of 1.0, the higher chord near the lower ATR was also required to fit the increased fuel volume at a lower L_1.

However, it should be mentioned that taper ratio and fin length are at their maximum and the chord in section three is at its minimum so might be kept constant during a following optimisation.

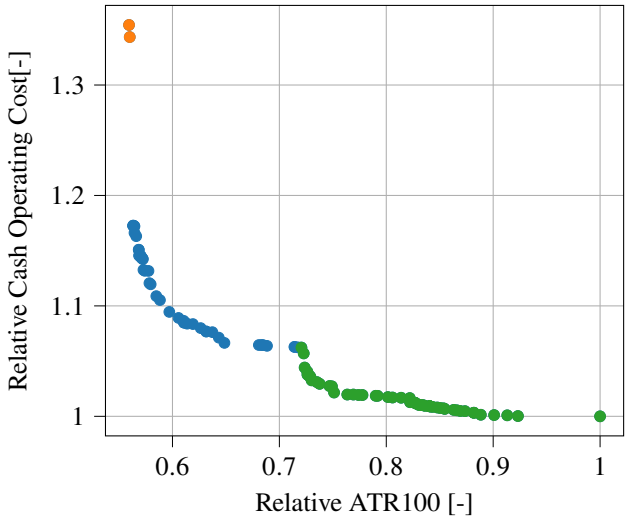

Fig. 7 Pareto front between cost and climate objectives (data are normalized with respect to the cost-optimal Flying-V)

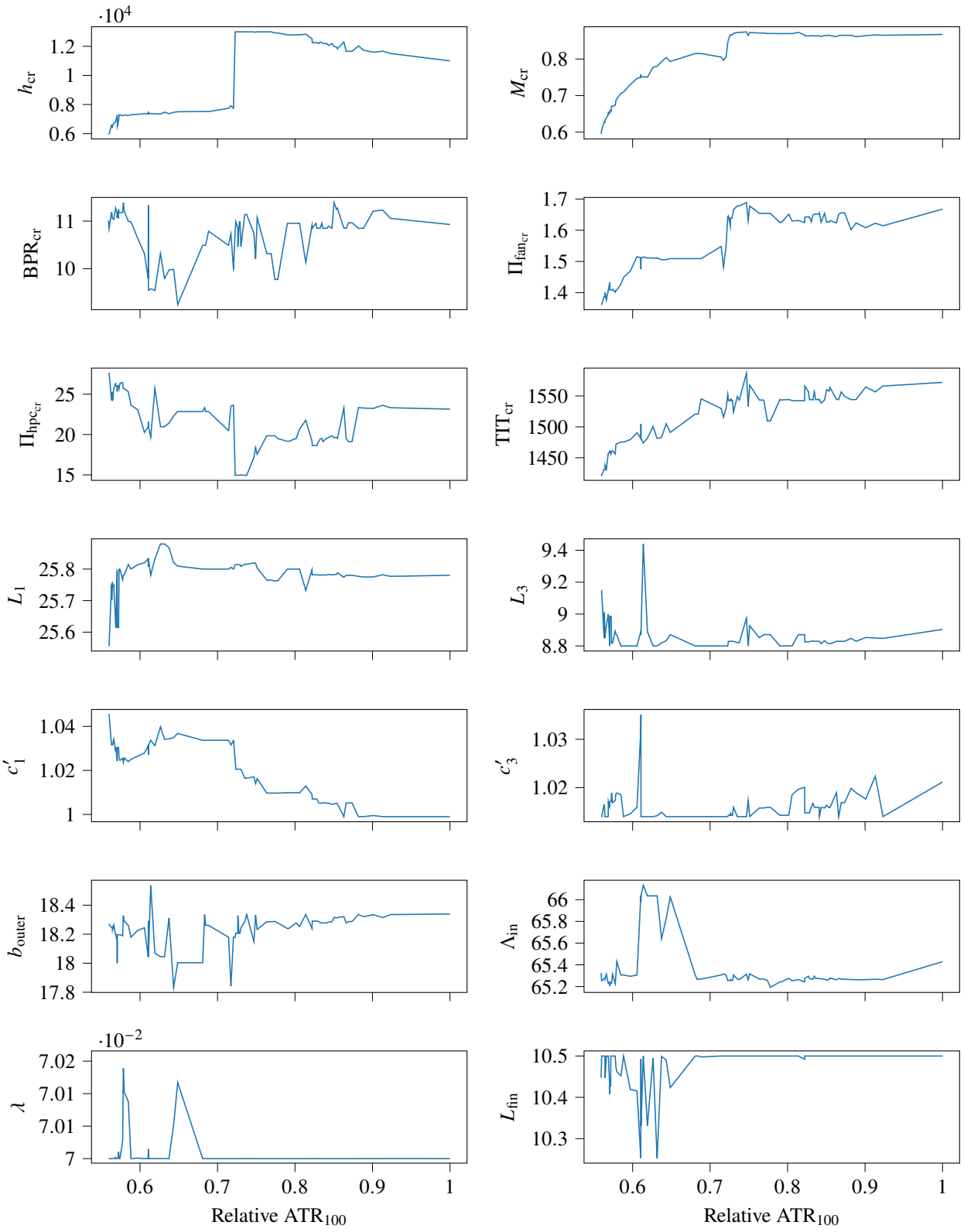

Fig. 8 The trend in design variables of the multi objective optimisation moving from the climate-optimised design to the cost-optimised design

V. Conclusion

The purpose of this study was to assess the potential of the Flying-V-900 aircraft in reducing climate impact and compare it to the operational cost optimal Flying-V and to a conventional long range aircraft. This analysis aimed to examine the trade-off between cost and climate considerations and to evaluate its potential for promoting sustainable aviation and its competitiveness in the aircraft market. Consequently, a multidisciplinary analysis and optimisation framework was developed to optimise the Flying-V aircraft for multiple objectives, including reducing global warming impact (measured in average temperature response), minimising cash operating cost (measured in USD), and optimising fuel efficiency (measured in kg). This also enabled the examination of the impact of geometry, turbofan, and mission design variables on these objectives. It established a framework for analysing the ATR_{100} and cash operating costs of current and future Flying-V configurations.

The results indicate that transitioning from a Flying-V design that prioritises fuel efficiency or cost to a climate-optimised Flying-V-900 could potentially decrease ATR_{100} by around 38%. However, this decrease is accompanied by a substantial increase in operational costs 36%, due to the need for an additional pilot and long flight time. Although the model contains inherent uncertainties, the comparative approach effectively reduces the influence of these assumptions.

The climate-optimised design exhibits distinct characteristics that prioritise operating at lower altitudes and velocities to minimise the formation of contrails and NO_x emissions. However, this transition requires an increase of 20% in fleet size to maintain the required level of productivity, which could potentially counterbalance the positive environmental effects resulting from increased manufacturing emissions.

The climate-optimised Flying-V-900, in comparison to a conventional long-range aircraft optimised for cost, is capable of reducing the ATR_{100} by 60%. Additionally, it can achieve a 28.6% greater reduction in ATR_{100} compared to the climate-optimised conventional aircraft. However, this comes at a 32% higher cost compared to the cost-optimised conventional aircraft and a 6% higher cost compared to the climate-optimised aircraft. This is such a significant factor that it could impede its potential for development. Nevertheless, the cost-optimised Flying-V-900 has the capability to decrease the ATR_{100} by 36% compared to the cost-optimised conventional aircraft, while reducing operational cost with with 3% and consuming 10% less fuel.

To conduct thorough fleet analyses, it would be beneficial to incorporate the effects of manufacturing, although there may be difficulties in implementing this, as it might be hard to quantify. In addition, future research should take into account more realistic routing networks in order to more accurately evaluate the impact of climate and optimise mission trajectories, in conjunction with aircraft design, to further reduce emissions.

In order to improve the study of the Flying-V's environmental influence more advanced structural analysis tools and further refining the aerodynamic model beyond a basic drag polar would be suggested. Additionally, it is advisable to utilise a more sophisticated climate model, as the existing model relies on various assumptions that overlook crucial factors such as the geographical location and time of day of emissions. Ultimately, conducting research on the climate-optimised Flying-V with advanced engine technologies, alternative configurations, or different fuels could provide valuable insights for future research directions.

Appendix

A. XDSM

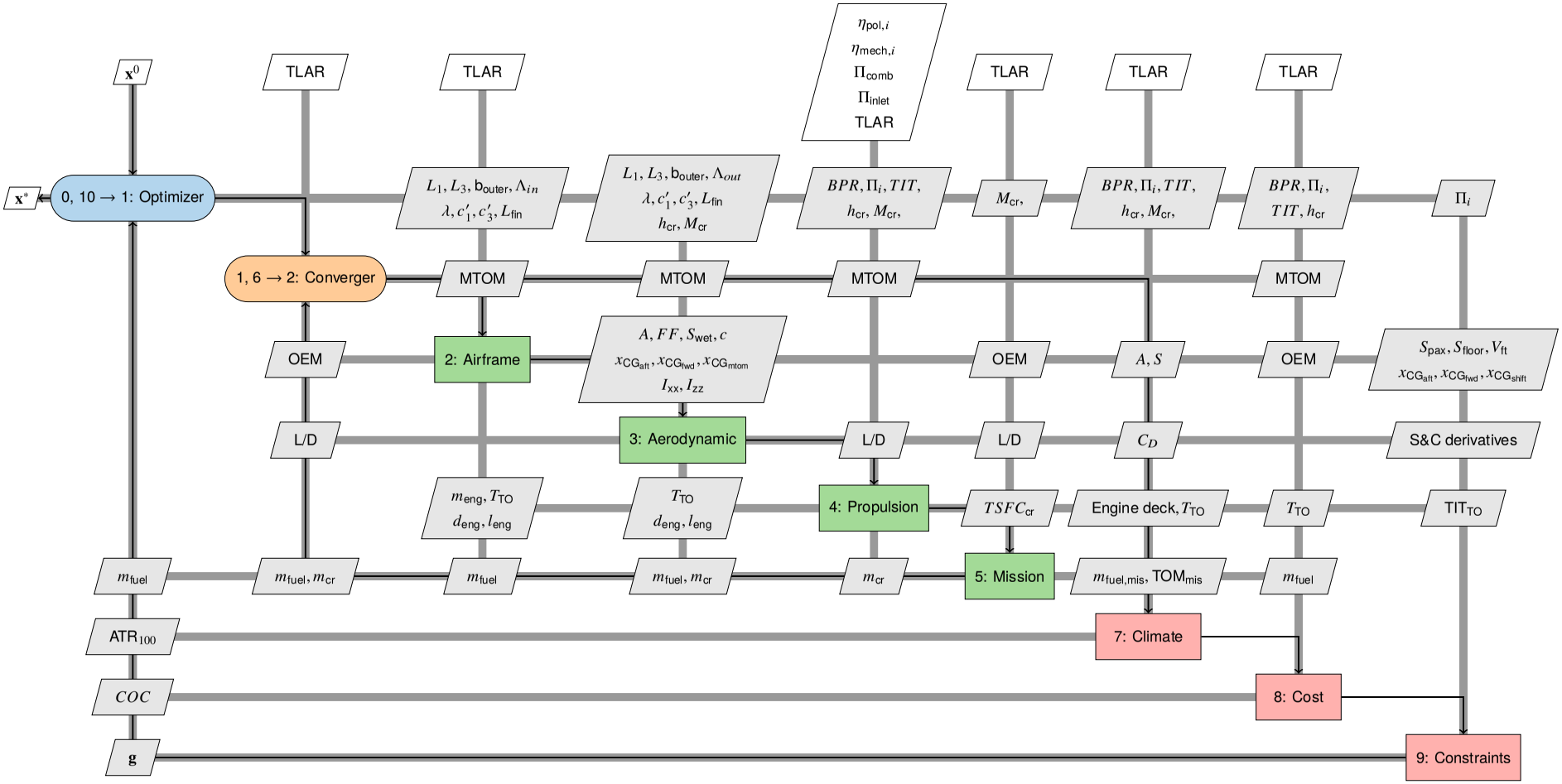

Fig. 9 Extended design structure matrix of multidisciplinary design optimisation setup [11]

References

[1] UNFCCC, "The Paris Agreement," *Paris Climate Change Conference - November 2015*, 2018.

[2] Lee, D., Fahey, D., Skowron, A., Allen, M., Burkhardt, U., Chen, Q., Doherty, S., Freeman, S., Forster, P., Fuglestvedt, J., Gettelman, A., León, R. D., Lim, L., Lund, M., Millar, R., Owen, B., Penner, J., Pitari, G., Prather, M., Sausen, R., and Wilcox, L., "The contribution of global aviation to anthropogenic climate forcing for 2000 to 2018," *Atmospheric Environment*, Vol. 244, 2021, p. 117834. https://doi.org/10.1016/j.atmosenv.2020.117834, URL https://doi.org/10.1016/j.atmosenv.2020.117834.

[3] Organization, I. C. A., "ICAO Long-Term Traffic Forecasts: Passenger and Cargo," Tech. rep., ICAO, 2016.

[4] Benad, J., "The Flying V A new Aircraft Configuration for Commercial Passenger Transport," 2015. https://doi.org/10.25967/370094, URL https://publikationen.dglr.de/?tx_dglrpublications_pi1[document_id]=370094.

[5] Matthes, S., Lim, L., Burkhardt, U., Dahlmann, K., Dietmüller, S., Grewe, V., Haslerud, A. S., Hendricks, J., Owen, B., Pitari, G., Righi, M., and Skowron, A., "Mitigation of Non-CO2 Aviation's Climate Impact by Changing Cruise Altitudes," *Aerospace*, Vol. 8, No. 2, 2021, p. 36. https://doi.org/10.3390/aerospace8020036, URL http://dx.doi.org/10.3390/aerospace8020036.

[6] Reekers, M., "Climate Effects of the Flying-V," Master's thesis, Technische universiteit Delft, 2021.

[7] Oosterom, W., "Flying-V Family Design," , 2021. URL http://resolver.tudelft.nl/uuid:9e8f9a41-8830-405d-8676-c46bf6b07891.

[8] van der Toorn, M., "Flying-V Family Design for Stability and Control," , 2022.

[9] Proesmans, P.-J., and Vos, R., "Airplane Design Optimization for Minimal Global Warming Impact," *Journal of Aircraft*, Vol. 59, No. 5, 2022, p. 1363–1381. https://doi.org/10.2514/1.c036529, URL http://dx.doi.org/10.2514/1.C036529.

[10] Hillen, M., "Parametrisation of the Flying-V Outer Mould Line," , 2020.

[11] Lambe, A. B., and Martins, J. R. R. A., "Extensions to the design structure matrix for the description of multidisciplinary design, analysis, and optimization processes," *Structural and Multidisciplinary Optimization*, Vol. 46, No. 2, 2012, p. 273–284. https://doi.org/10.1007/s00158-012-0763-y, URL http://dx.doi.org/10.1007/s00158-012-0763-y.

[12] Proesmans, P.-J., and Vos, R., "Comparison of Future Aviation Fuels to Minimize the Climate Impact of Commercial Aircraft," *AIAA AVIATION 2022 Forum*, American Institute of Aeronautics and Astronautics, 2022. https://doi.org/10.2514/6.2022-3288, URL http://dx.doi.org/10.2514/6.2022-3288.

[13] Kulfan, B. M., "Universal Parametric Geometry Representation Method," *Journal of Aircraft*, Vol. 45, No. 1, 2008, p. 142–158. https://doi.org/10.2514/1.29958.

[14] Horwitz, J., "Parametric Design of the Flying-V Winglets for Improved Lateral-Directional Stability and Control," , 2021.

[15] Torenbeek, E., *Advanced Aircraft Design*, Wiley, 2013. https://doi.org/10.1002/9781118568101, URL https://doi.org/10.1002/9781118568101.

[16] Schmidt, K., and Vos, R., "A Semi-Analytical Weight Estimation Method for Oval Fuselages in Conventional and Novel Aircraft," *52nd Aerospace Sciences Meeting*, American Institute of Aeronautics and Astronautics, 2014. https://doi.org/10.2514/6.2014-0026, URL https://doi.org/10.2514/6.2014-0026.

[17] Vos, R., and Hoogreef, M., "Semi-Analytical Weight Estimation Method for Fuselages with Oval Cross-Section," *54th AIAA/ASME/ASCE/AHS/ASC Structures, Structural Dynamics, and Materials Conference*, American Institute of Aeronautics and Astronautics, 2013. https://doi.org/10.2514/6.2013-1719, URL https://doi.org/10.2514/6.2013-1719.

[18] Claeys, M., "Flying V and Reference Aircraft Structural Analysis and Mass Comparison," , 2018. URL http://resolver.tudelft.nl/uuid:ee7f2ecb-cdb6-46de-8b57-d55b89f8c7e6.

[19] Souders, T. J., and Takahashi, T. T., "VORLAX 2020: Benchmarking Examples of a Modernized Potential Flow Solver," *AIAA AVIATION 2021 FORUM*, American Institute of Aeronautics and Astronautics, 2021. https://doi.org/10.2514/6.2021-2459, URL http://dx.doi.org/10.2514/6.2021-2459.

[20] Miranda, L., Elliott, R., and Baker, W., "A Generalized Vortex Lattice Method for Subsonic ans Supersonic Flow Applications," Tech. Rep. CR 2865, NASA, 1977.

[21] Faggiano, F., Vos, R., Baan, M., and Dijk, R. V., "Aerodynamic Design of a Flying V Aircraft," *17th AIAA Aviation Technology, Integration, and Operations Conference*, American Institute of Aeronautics and Astronautics, 2017. https://doi.org/10.2514/6.2017-3589, URL https://doi.org/10.2514/6.2017-3589.

[22] Raymer, D. P., *Aircraft design*, 1st ed., American Institute of Aeronautics & Astronautics, Reston, VA, 2004.

[23] Chiozotto, G. P., "Improving Aircraft Conceptual Design with Methods for Wing Loads, Aeroelasticity and Mass Estimation," Ph.D. thesis, ????

[24] van Laar, Y., "Aerodynamic Design of a Flying V Aircraft in Transonic Conditions," , 2023. URL http://resolver.tudelft.nl/uuid:591093b2-5cdc-41c5-b564-3786f43d51db.

[25] de Zoeten, G. J., Varriale, C., and Vos, R., "Flight Performance Evaluation of the Flying-V," *AIAA AVIATION 2023 Forum*, American Institute of Aeronautics and Astronautics, 2023. https://doi.org/10.2514/6.2023-3484, URL http://dx.doi.org/10.2514/6.2023-3484.

[26] Roskam, J., *Airplane Design: Part VII (Part 7) - Determination of Stability, Control and Performance Characteristics: FAR and Military Requirement*, DARcorporation, 1985.

[27] Kay, J., Mason, W. H., Durham, W., Lutze, F., and Benoliel, A., "Control Authority Issues in Aircraft Conceptual Design: Critical Conditions, Estimation Methodology, Spreadsheet Assessment, Trim and Bibliography," Tech. rep., VPI-Aero-200, 1996.

[28] Mattingly, J. D., Heiser, W. H., and Pratt, D. T., *Aircraft engine design, second edition*, American Institute of Aeronautics and Astronautics, Reston ,VA, 2002.

[29] Walsh, P. P., and Fletcher, P., *Gas Turbine Performance*, 2nd ed., Blackwell Science, Philadelphia, PA, 2004.

[30] Greitzer, E., and et al., P. B., "N+3 Aircraft Concept Designs and Trade Studies, Final Report Volume 2: Appendices—Design Methodologies for Aerodynamics, Structures, Weight, and Thermodynamic Cycles," CR 216794/VOL2, NASA, 2010.

[31] Bourget, G., "The effect of landinggear implementation on Flying V aerodynamics, stability and controllability," , 2020.

[32] Roskam, J., *Airplane design part I: Preliminary sizing of aiplanes*, DARcorporation, 1985.

[33] Sausen, R., and Schumann, U., ""Estimates of the Climate Response to Aircraft CO2 and NOx Emissions Scenarios"," *Climatic Change*, Vol. 44, No. 1/2, 2000, p. 27–58. https://doi.org/10.1023/a:1005579306109, URL http://dx.doi.org/10.1023/A:1005579306109.

[34] Dallara, E. S., Kroo, I. M., and Waitz, I. A., "Metric for Comparing Lifetime average Climate Impact of Aircraft," *AIAA Journal*, Vol. 49, No. 8, 2011, p. 1600–1613. https://doi.org/10.2514/1.j050763, URL http://dx.doi.org/10.2514/1.J050763.

[35] Dallara, E. S., "Aircraft design for reduced climate impact," Ph.D. thesis, Stanford University, 2011.

[36] Schumann, U., "Influence of propulsion efficiency on contrail formation," *Aerospace Science and Technology*, Vol. 4, No. 6, 2000, p. 391–401. https://doi.org/10.1016/s1270-9638(00)01062-2, URL http://dx.doi.org/10.1016/S1270-9638(00)01062-2.

[37] Zhang, Y., Macke, A., and Albers, F., "Effect of crystal size spectrum and crystal shape on stratiform cirrus radiative forcing," *Atmospheric Research*, Vol. 52, No. 1-2, 1999, pp. 59–75. https://doi.org/10.1016/s0169-8095(99)00026-5, URL https://doi.org/10.1016/s0169-8095(99)00026-5.

[38] Stuber, N., and Forster, P., "The impact of diurnal variations of air traffic on contrail radiative forcing," *Atmospheric Chemistry and Physics*, Vol. 7, No. 12, 2007, pp. 3153–3162. https://doi.org/10.5194/acp-7-3153-2007, URL https://acp.copernicus.org/articles/7/3153/2007/.

[39] Roskam, J., *Airplane Design: Part VIII (Part 8) - Airplane Cost Estimation: Design, Development, manufacturing, and Operating*, DARcorporation, 1985.

[40] Vos, R., and Farokhi, S., *Introduction to Transonic Aerodynamics*, Springer Netherlands, 2015. https://doi.org/10.1007/978-94-017-9747-4.

[41] Torenbeek, E., *Synthesis of subsonic airplane design*, Springer Netherlands, 1982. https://doi.org/10.1007/978-94-009-9580-2.

[42] Köhler, M. O., Rädel, G., Dessens, O., Shine, K. P., Rogers, H. L., Wild, O., and Pyle, J. A., "Impact of perturbations to nitrogen oxide emissions from global aviation," *Journal of Geophysical Research: Atmospheres*, Vol. 113, No. D11, 2008. https://doi.org/10.1029/2007jd009140, URL http://dx.doi.org/10.1029/2007JD009140.

[43] Nolet, S., "Improving the Flying V Directional Control Power by the Implementation of Split Flaps," , 2022. URL http://resolver.tudelft.nl/uuid:18847b0d-597d-4539-968f-ebc8a14c905e.

Part II

Literature Study
previously graded under AE4020

Abstract

The aviation industry's significant contribution to global warming has prompted a search for new aircraft designs to replace traditional tube-and-wing configurations. The Flying-V, with its higher aerodynamic efficiency and lighter weight compared to the Airbus A350-900, holds promise for lowering fuel consumption and associated emissions. However, the relationship between fuel performance and climate impact is complex, with NO_x and H_2O emissions and exhaust contrail formation having varying climate impacts depending on location and timing of emission. A postdesign climate assessment has shown that the A350-900 has a lower global warming impact than the Flying-V, due to the optimal operating conditions at a higher altitude. This literature study investigates the global warming analysis, operating cost analysis and preliminary design aspects of the Flying-V in order to develop a research plan for a subsequent thesis study.The following thesis will investigate the global warming impact and operational cost in the conceptual design stage, optimising the preliminary designs of the Flying-V to assess its potential for future development.

Furthermore, this study looks into the potential and challenges of unconventional aircraft configurations, emphasising their aerodynamic efficiency and weight savings while highlighting stability and control issues. It also delves into climate response modelling, mitigation techniques, and the trade-off between computational costs and accuracy in aerodynamic, propulsion, and mission models. Finally, the study delves into multi-disciplinary optimisation, discussing the utility of genetic algorithms as well as the significance of finalising design variables and constraints. The findings emphasise the importance of early-stage climate assessment and the trade-offs in modelling and optimisation processes between computational costs and accuracy.

Preface

This literature study on the climate impact and operational costs of the Flying-V aircraft is the first step towards completing a master thesis in aerospace engineering. The objective of this research is to investigate and analyse the potential effects of the Flying-V aircraft design on both climate impact and operational costs.

The purpose of this research is to shed light on the intricate relationship between aircraft design, environmental impact, and economic considerations. I hope to identify opportunities for optimising the design and operation of future aircraft by investigating the Flying-V's climate impact and evaluating its operational costs.

I'd like to thank Pieter-Jan Proesmans and Roelof Vos for giving me such an interesting topic to work on, as well as for their guidance, support, and expertise throughout this literature study.

I am excited to begin this academic journey, and I hope that this literature study will serve as the foundation for a thorough and insightful master thesis. My sincere hope is that this research will contribute to a broader understanding of sustainable aviation and inspire further research in this critical field.

Rowan de Voogt
Rotterdam, May 2023

Contents

List of Figures

Nomenclature

Abbreviations

AGTP	Absolute global temperature potential
AGWP	Absolute global warming potential
ATR	Average temperature response
AVL	Athena Vortex Lattice
BWB	Blended wing body aircraft
CH_4	Methane
CO_2	Carbon dioxide
Eff	Efficacy
FEM	Finite element method
G	Green's function (climate impulse response function)
GSP	Gas Turbine Simulation Program
GTP	Global temperature potential
GWP	Global warming potential
H_2O	Water
ICAO	International Civil Aviation Organization
IDF	Individual disciplines feasible
LTO	Landing and take-off phase
MDA	Multi-disciplinary design analysis
MDAO	Multi-disciplinary design analysis and optimisation
MDF	Multiple disciplines feasible
MDO	Multi-disciplinary design optimisation
MOOP	Multi-objective optimisation problem
MTOW	Maximum take-off weight
MZF	Maximum zero fuel weight
NO_x	Nitrogen Oxides
O_3	Ozone
OEM	Operational empty weight
OML	Outer mould line
Q3D	Quasi three-dimensional solver
RANS	Reynolds-averaged Navier Stokes equations
RPK	Revenue passenger kilometres
SO_4	Sulfate
USD	United States Dollars
VLM	Vortex lattice method
XDSM	extended design matrix

Greek Symbols

α	Angle of attack, deg or Coefficient
β	Sideslip angle, deg
χ	Concentration of species, ppmv
Δ	Difference
δ	Orientation angle, deg
η	Efficiency
Γ	Dihedral angle, deg
Λ	Sweep angle, deg
λ	taper ratio or climate sensitivity parameter
Π	Pressure ratio
ρ	Density, kg/m^3
τ	Perturbation time

Symbols

α	Coefficient
b	Wing span
BPR	Bypass Ratio
C	Cost, USD
c	chord or curve coefficient
C_D	Drag coefficient
C_L	Lift coefficient coefficient
C_l	Roll moment coefficient
C_m	Pitching moment coefficient
C_n	Yaw moment coefficient
C_y	Side force coefficient
E	Absolute emission, kg
EI	Emission index of species, kg/kg
EPNL	Effective percieved noise level
ERF	Effective radiative forcing, W/m^2
f	Objective function
H	Height, m
H	Time horizon or Humidity
h	Altitude, m
i	Incidence angle
L	Length, m

L/D	Lift-to-drag Ratio
LHV	Lower heating value, MJ/kg
M	Mach number
m	Mass, kg
N	Number
OPR	Overall engine pressure ratio
P	Pressure, Pa
R	Range
RF	Radiative forcing, W/m^2
RF*	Normalized radiative forcing
S	Wing area, m
s	forcing factor
SFC	Specific fuel consumption, kg/N
SM	Static margin
T	Thrust, kN; or Temperatur, K
TIT	Turbine inlet temperature
V	Velocity
W	Width, m or Weight, w
w	Weight function
X	Climate forcer
x	X-location

Subscripts

0	initial value
t	at wing tip location
bl	block
CO_2	carbon dioxide
cr	cruise
hpc	high pressure compressor
i	species
lpc	low pressure compressor
ops	direct operating
p	roll rate
pax	passengers
ref	reference
TO	take-off
w	wetted
yr	operational years

1 Introduction

As evidenced by the increasingly stringent regulations put forth in the Paris agreement during UN climate change conferences intended at keeping the global warming below the 2°C, the issue of climate change has gained significant prominence in the field of engineering[8] The aviation sector, which contributes significantly to global warming, has not been spared from this trend. Indeed, the aviation sector alone is estimated to account for 3.5% of net anthropogenic effective radiative forcing by 2018, and as the fastest-growing transport sector with an axpected annual growth until 2035 of 4.3%, neglecting the effects of the COVID pandemic, its influence on global warming is increasing [2, 9]. While carbon-neutral solutions, as electrical propulsion are becoming more common in sectors such as the land-based transportation, the adoption of electric flight for long-range commercial aircraft remains a distant possibility, because of the strict weight and power constraints. As a result, alternative solutions for reducing aircraft's climate effect must be investigated.

These solutions could take the form of novel aircraft configurations that combine multiple functionalities into a single component, reducing the number of components required. The goal is to improve the overall efficiency of the concept by reducing the weight and drag associated with additional components. The Flying-V is one of these concepts, which improves aerodynamic efficiency by removing the aircraft's fuselage and integrating it with the wings. Figure 1 depicts a model of the Flying-V[10]. This demonstrates the placement of two tubular pressurised cabins carrying passengers and cargo in a V-shape inside the wing with a high sweep angle. The high-sweep angle had several benefits. It ensured that the control surfaces had a long lever arm and also reduced the increased wave-drag associated with thick airfoils[11].

Changing the operating conditions could lead to further advancements. Nowadays, aircraft are optimised for minimal operating costs while flying high and fast. However, studies have shown that flying at a lower altitude and velocity can significantly reduce an aircraft's global warming impact [4]. Even the Flying-V faces this challenge, despite the fact that it is already designed for minimal fuel consumption and thus lower CO_2 emissions. The Flying-V flies at a higher altitude than conventional tube-and-wing aircraft, which has a greater impact on global warming due to non-CO_2 effects such as NO_x emissions and contrail formation, which tend to increase with altitude [12]. As a result, it is worthwhile to investigate the Flying-V's climate performance at lower altitudes. However, flying at this lower altitude increases the direct operating cost because of longer flights and this necessitate more flights.

The goal of this study is to analyse and optimise the Flying-V design for multiple objectives, including climate impact and direct operating costs, and then compare the findings to those of a conventional aircraft. This will be achieved through the creation and implementation of a model that considers various design factors such as Flying-V geometry, engine type, and mission, as well as the use of appropriate optimisation algorithms.

The ideal outcome of this study would be to identify a Pareto-optimal solution and to create a reusable model to assess the Flying-V's climate impact and operating costs. The model will include an MDAO workflow and design guidelines that will allow future Flying-V iterations to be optimised for climate effect and direct operating costs.

The following is the structure of the literature study. It will begin by reviewing the existing research on the Flying-V in section 2. Then it will examine existing methods for assessing the climate effects of the aviation industry and mitigation techniques in section 3. section 4 examines operating cost models briefly. Then the various additional models required to assess the performance of the flying-V are described in section 5, section 6 and section 7 that describe various aerodynamic models, propulsion models and mission models respectively. The various optimisation techniques and an investigation in a suitable design space and MDAO workflow are described in section 8. section 9 proposes the research plan that will be applied in the subsequent master thesis. Finally, section 10 draws a conclusion from the research and makes suggestions for further research.

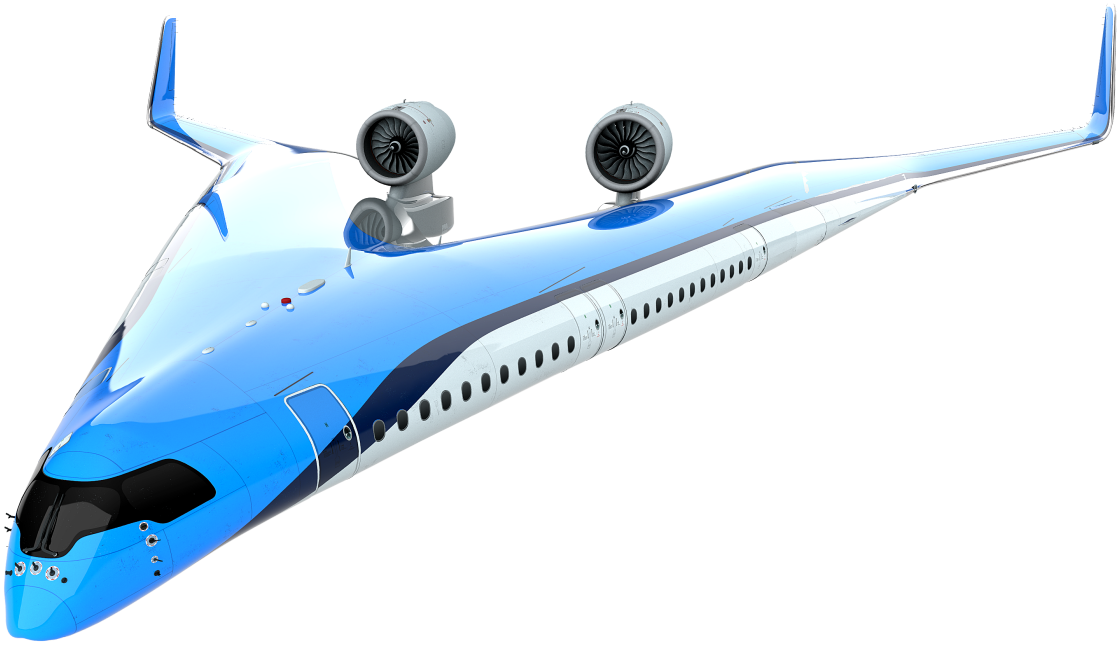

Figure 1: The Flying-V

2 Flying-V

The current state of development of the Flying-V, the subject of the research project, is examined in this section. Beginning with an explanation of the flying wing configuration and a discussion of the benefits and drawbacks of employing a flying wing configuration. The Flying-V is then thoroughly discussed, as are various studies conducted for this concept, with a focus on research related to this study.

2.1 Flying Wing and Blended Wing Body aircraft

Flying wings are a type of aircraft configuration that is tailless and lacks a well-defined body that houses the crew and payload, so everything is housed inside the main wing, which has been researched by aerospace engineers for over a century. Igo Etrich first proposed the concept of a flying wing as a glider in 1904. However, John Dunne was the first to develop a flying wing aircraft, the D-8, in 1911, which was a swept and twisted wing biplane [13]. Later, Alexander Lippisch and the Horton brothers conducted additional research into tailless aircraft configuration, with Lippisch producing the first delta wing glider and the Horton brothers developing the first jet powered flying wing known as the HO 229 during WWII [14, 13]. However, in the 1940s, Jack Northrop developed one of the first functioning large-scale flying wings, the XB-35, which later evolved into the YB-49. Because the goal of this prototype bomber was to carry out bombing missions over Germany from the United States, an unusually long range for the time was a driving requirement in the design [15]. Northrop's solution was to remove as many drag-creating parts of the aircraft as possible, improving the lift-to-drag ratio (L/D) and paving the way for an all-wing design, but it was never produced due to its poor handling qualities [13]. In the decades that followed, advancements in flying wing configurations slowed until the successful development of the Northrop-Grunman B2-Spirit, which breathed new life into flying wings and blended wing bodies.

Robert Liebeck of the then McDonnell Douglas Corporation (MDC) now Boeing Company conceptualised the blended wing body (BWB) aircraft, as it is known today in 1988, after realising that the conventional tube-and-wing configuration was the only shape applied to long-haul commercial aircraft for almost 40 years and improvements were getting to an asymptote [16]. Blended wing bodies (BWB) are a type of aircraft configuration that shares many of the advantages and disadvantages of flying wings, as the lifting surfaces and fuselage are integrated into a single aerodynamic shape. However, a BWB features smoothly blending of the wing into the body, where passengers are accommodated, while a pure flying wing has a straight leading and trailing edge and the payload has to be stored in the wing [17]. Since, then various studies have been performed and have identified significant obstacles as well as significant potential benefits of the setup.

The fundamental advantage of a BWB concept is that it combines the structural function of fitting the payload with the aerodynamic function of creating lift in a single structure [13]. When compared to the BWB concept, conventional tube-and-wing aircraft have a greater wetted area and more friction drag since a separate fuselage is needed to hold the payload [16]. A BWB also has reduced interference drag because of the seamless transition between its body and wing. Additionally, the BWB's shape is more area-ruled than a conventional aircraft, resulting in wave drag that is reduced at high velocities [18]. This all leads to an increase in lift-to-drag ratio (L/D), which can translate into improved fuel efficiency and range [16]. Because the chord of a flying wing is larger than that of a conventional aircraft, the L/D of a flying wing is improved even further. The drag is reduced even further, due to the absence of a horizontal tail. The lower static margin on a flying wing raises the L/D. All these beneficial aerodynamic properties of a BWB result in a higher aerodynamic efficiency. For the same load cases, this could result in a 20% increase in L/D compared to a conventional aircraft[19]. This increase in aerodynamic efficiency results in a reduced fuel burn and therefor also a reduced CO_2 emission compared to a conventional tube-and-wing with similar mission characteristics [10].

Furthermore, because of shielding, the engines of a BWB are frequently mounted on top of the wing, resulting in less noise perceived by the ground. Additionally, a BWB lacks a tailplane and high lift devices, which reduces noise. Finally, because the payload is located in the same parts as the lift, it relieves the bending moment caused by lift generation.[18].

However, designing flying wings and BWB presents a number of difficulties. First, there are issues with stability and control, as the lack of tail makes the aircraft unstable in most cases. Another, difficult part is integrating the fuselage with the wing. For starters, designing a wing planform that can accommodate passengers and cargo as well as onboard systems like engines and fuel tanks is difficult. The requirement of a 90-second evacuation time is either a challenge, particularly for BWB, because there are many passengers in the middle of the aircraft, far from the exits. Furthermore, the pressurised body's non-circular shape introduces additional

stresses, resulting in a structural weight penalty [18]. Commonality between different sizes, application and manufacturing techniques either faces difficulties in designing BWB. Commonality between different sizes is much more difficult than for a conventional aircraft, as it could not be easily stretched, due to the highly three dimensional geometry of the centerbody, resulting in limited possibilities for family design [20].

The flying wing configuration has a long history in aviation and provides several benefits in terms of aerodynamic efficiency and stealth capability. However, its inherent instability and structural design challenges must be carefully considered when developing modern aircraft concepts like the Flying-V. Therefore, the development of a blended wing body and flying wing feature to be inherently multidisciplinary and require the need for multidisciplinary design optimisation from the start [18].

2.2 Flying-V

The Flying-V concept is a pure flying wing passenger transport aircraft designed to reduce the traditional challenges associated with flying wings and BWBs as previously described in subsection 2.1. The Flying-V's early developments are described first. Following that, key aspects of the concept are described in greater detail.

2.2.1 Development of the Flying-V

The development of the Flying-V began in 2013 at Airbus Future Projects in Hamburg and was presented as the new aircraft configuration for commercial passenger transport. The goal of the design was to have a mass as low as possible and an L/D as high as possible for a given number of passengers. Furthermore, it was not allowed to violate the following constraints [10]:

- Pressurized passenger and cargo section available
- Level of comfort must be as high as in existing configurations
- Aircraft must be possible to trim, aircraft must be longitudinally stable
- Fast emergency evacuation must be possible
- Aircraft must be able to take-off and land at existing airports
- Aircraft must be compatible with the ground infrastructure of existing airports

To meet the objectives, the design had to include an almost circular cabin cross section and an elliptical spanwise mass distribution for a low mass, as well as a low wetted area, a high wing span, an elliptical lift distribution, engines close to the centre axis, low transonic drag, and a short cabin length in flight direction to achieve a high L/D. Other considerations included having enough wing area to avoid the need for high lift devices, shielding the engine from the ground, simple and straight lines, and few moving parts. As a result of these design considerations, a configuration with two cylindrical pressurised payload sections swept back in a V-shape and placed inside the front section of a wing with the same sweep angle was created, where a second pressurised cylinder was placed for the cargo due to available space in the wing. For structural efficiency, the engines of this design were placed over the landing gear. The following benefits were provided by the highly swept wing: [10]:

- When the cylindrical pressurised section is cut streamwise, it forms a flat ellipse and thus fits conventional airfoils well.
- It shifted the neutral point further back, so that it is now behind the centre of gravity, providing longitudinal stability.
- It generates a long lever arm of the control surfaces to the center of gravity of the aircraft.

The initial design's wing twist was optimized, resulting in a promising almost elliptical wing distribution without the use of reflexed camber lines. This resulted in a 10% greater L/D than the A350-900, which has a similar capacity, wingspan and cruise speed. However, because the aerodynamic model used did not account for wave drag, more research into this area was required, as described in subsubsection 2.2.2. The initial mass estimate

resulted in a 2% lighter weight than the A350-900. However, this was a greatly simplified mass, and more research in this area was required, as described in subsubsection 2.2.3. Finally, the Flying-V with a dihedral and a sufficiently large outerwing is directionally stable [10] and longitudinal and lateral control is provided by implenting elevons, but further research showed some unstable modes that are described in subsubsection 2.2.4.

2.2.2 Aerodynamic Design

Following the promising results of the initial design, the aerodynamic feasibility of the Flying-V was examined in greater depth. Because it did not estimate the wave drag, the 3D lattice vortex method used in the initial design was replaced by an Euler solver and empirical estimations for the profile drag. The Euler solver was used because it could compute the three-dimensional pressure distribution in transsonic conditions, predict shockwave formation and estimate the inviscid drag components (vortex induced drag and wave drag), at a lower computational cost than Reynolds-averaged Navier Stokes (RANS) equations, making it more suitable for optimisation. However, unlike RANS equations, it does not allow for the calculation of viscous or heat effects. As a result, a separate empirical viscous model based on Daniel Raymer's methods was developed to estimate profile drag, which was valid until drag divergence[21]. The profile drag consists of three components: skin friction, pressure, and lift-related profile drag, where the lift-related profile drag could be neglected for cruise condition [22]. With this aerodynamic model, the flying-V design was optimised for high L/D in cruise conditions, resulting in a 25% increase in L/D compared to the NASA common research model [23].

The Flying-V was also optimised for a family design, but as this required a lot of iterations, a less computationally expensive aerodynamic model was required. The AVL (Athena Vortex Lattice) model was used for this optimisation because it costs only a few seconds to run and was already available in the ParaPy framework in which the optimisation was performed[5]. AVL employs the vortex lattice method and can be used to compute the stability derivatives from the mass distribution, as well as to find the lift and moment distribution over lifting surfaces, trim the aircraft by defining the control surfaces and trim conditions[24, 5]. However, AVL is inviscid and cannot evaluate at high mach numbers, as in the transonic regime. Because it was only a comparative study with the Airbus A350, the fact that it does not allow for high Mach numbers was deemed less important than computational cost. Since AVL is inviscid, the stability derivatives that are less influenced by viscous effects, such as C_{l_p} and C_{n_p}, are determined more precisely, and an additional viscous model was required to calculate drag and L/D[24, 5]. The additional viscous model applied was the same as used by Faggiano et al[23].

In order to verify the aerodynamic calculations made by the various models wind tunnel and flight tests were performed on the Flying-V. The wind tunnel experiment made use of a 4.6%-scale half span model to determine the aerodynamic coefficients by changing the angle of attack, wind speed and elevon deflections. Only the lateral force coefficient C_y, was not determined due to high uncertainties and to the exclusion of fins [25]. This research showed a lift curve slope shifted to the right compared to results obtained from a VLM called odilla [26]. The wind tunnel test discovered a maximum lift coefficient of 1.08 at a 42-degree angle of attack. When compared to conventional aircraft, the maximum lift coefficient is lower and the stall angle of attack is greater. Due to vortex effects, the lift slope at low angles of attack was around 1.9 per radian and increased to a maximum of 2.4 per radian at around 13 degrees angle of attack [27].

A single flight test on a 4.6% scale flying-V model was performed, but as only one flight test was performed there were still several uncertainties. However, it did show a similar lift curve slope as the wind tunnel testing only with a shift with respect to the angle of attack. Furthermore, did it show a significantly larger drag, due to the drag from the landing gear, pylon, nacelles etc . At last, it experienced an unstable dutch roll mode [28].

Research into the flight control system of the Flying-V applied an aerodynamic model that combined VLM and the aerodynamic model identified by the wind tunnel test. The VLM model was applied as this is able to calculate all the aerodynamic derivatives, but at a high uncertainty and was not able to identify pitch break. The aerodynamic model identified from the wind tunnel test had a much lower uncertainty, but had limited lateral-directional aerodynamic coefficients such that the unstable dutch roll mode could not be evaluated [25]. By combining the two it resulted in a more accurate model that could compute both the dutch roll and pitch break. The flight test was not considered, as there was still a high uncertainty and a lot of coefficients were not determined [28].

2.2.3 Structural Design and Weight Estimation

As already indicated Flying wings and BWBs have structural advantages such as decreased wing loading because the lift is distributed over a greater surface area and a considerable inertia relief since the payload is situated over the lift generating surfaces, bringing the planform weight distribution close to the aerodynamic load distribution. All of this improves the structural efficiency of BWBs [16]. However, due to the non-circular form of the cabin cross-section, the main structural challenge for a flying wing or BWB is efficiently carrying pressurisation loads during high-altitude cruise flight. The initial Flying-V design mitigated this problem by using a single-shell structure that could support pressurisation stresses as well as aerodynamic and inertial loads, with a double pressurised cylinder in each wing, where a cargo cylinder was located behind the cylindrical passenger cabin that is mounted in the leading edge of the wing layout, which was ideal for structural considerations. This layout did not afford adequate design flexibility, thus it was replaced by an oval pressurised cross section, which made a further aerodynamic optimisation and more efficient use of space possible [23]. The oval pressurised cross section was presented as a solution for a BWB's centerbody. Prior to the oval-cross section, there were two conceptions in the literature: integrated and segregated. However, both have shortcomings. The segregated requires a complex structure to connect the pressurised vessel with the aerodynamic shell, while the integrated has decreased passenger comfort due to structural member interruptions and a decreased structural efficiency due to bending moments[29]. The Oval concept had its own shortcomings, as it required two horizontal structural components loaded in compression and two vertical structural members loaded in tension. Because the force on these structural components increases with radius of curvature, it is best suited for relatively short widths less than 15m, as the force on the horizontal structural member would result in a significant weight penalty. [29].

The Flying V's initial weight was calculated by adding the scaled weights of existing aircraft parts. More study was required because this was not accurate enough and still included two cylindrical pressurised cabins in each wing. The preliminary structural design and weight estimation with an oval cabin demonstrated that the oval Flying-V pressurised cabin design was feasible and increased volume efficiency and planform design flexibility, but it did not result in a correct mass estimation, necessitating the development of a new model generation procedure [30]. Therefore, more research was done using a finite element method (FEM) analysis, that included more three-dimensional structural aspects into consideration, such as dividing the the cross section in several sections with transitions and the placement of structural components. Furthermore, did it contain a taper in the aft section of the pressurised cabin to ensure a better fit with the aerodynamic design. This research did result in a correct mass estimation, finding a reduction of 17% FEM weight with a reference aircraft [31]. However, both these methods were computationally costly and the FEM weight is not equal to the total structure weight.

In order to perform a multi-disciplinary optimisation (MDO) a less computationally costly weight estimation method was required, which was also able to estimate the weight of the individual components to generate the centre of gravity that is needed for stability analyses. Hence, at least a Class-II weight estimation method was required as this estimates the mass per component. The most well known and applied empirical class-II methods are by Raymer, Torenbeek, General Dynamics and Roskam. The method by Torenbeek is considered as providing the most consistent results with a mean error of 1% [32].

The mass estimation method for the MDO of the flying-V family design consisted of a semi-analytical approach that is a hybrid approach of structural analysis and empirical relationships [5]. In which the mass of parts that were similar to a conventional aircraft, such as the systems, payload items, landing gear, engine, operational items and cabin provisions were estimated using Torenbeek. The mass of the outer wing of the Flying-V, which is also similar to a normal aircraft wing was estimated using EMWET, as empirical relations was deemed not accurate enough for such a crucial part of the aircraft. EMWET is a quasi-analytical method developed at Delft University of Technology and is able to calculate the wing weight based on the aerodynamic loads, engine loads and fuel loads within seconds [33]. At last, the mass of the inner wings oval fuselage was calculated using an semi-analytical method made by Schmidt and Vos in 2014. This method provides more detail than the initial oval weight estimation method, as it allows sizing of all primary structural members and offers great flexibility in changing loads on all members. Furthermore, this method is extensively verified and validated [34, 35]. The mass estimations following from this model were validated by comparing it to earlier studies and to the results obtained by the FEM analysis of Claeys. This all showed small deviations, hence the model provide sufficient results for optimisation and a comparative study [5].

This method was elaborated upon by incorporating the results from the FEM analysis into the semi-analytical method [36]. This method scales the primary structure weight as obtained from the Torenbeek class-II method with the results obtained from the FEM analysis applying conversion factors. After which it accounts for differences in weight and geometry between the FEM analysis and analysis at hand by scaling it with the maximum zero fuel weight (MZF), that is obtained from the method developed for the flying-V family design

by Oosterom [36].

2.2.4 Stability and Control

For the flying-V to ever be produced it has to comply with stability and handing requirements imposed by the various flight authorities, such as the ICAO, EASA and FAR.Several studies were conducted to model and assess the Flying-V's stability and handling qualities. The majority of these studies evaluate the stability and handling qualities of full-size aircraft in relation to the military standards imposed by the EASA, which are the most stringent and thoroughly documented. Initially, a six-degrees-of-freedom flight dynamic toolbox was used, with inertia estimation using a lumped mass method and aerodynamic coefficients from VLM [26]. However, the aerodynamic data was linearised, which does not perform well at critical conditions on the flight envelope's corners and causes errors when deviated too far from the linearisation points.

These studies concluded that the Dutch roll is unstable, which was confirmed by a test flight of a small scale model of the flying-V and is a well-known feature of flying wings [26]. Dutch roll is a type of lateral instability and oscillatory motion that can occur. It is distinguished by a yawing and rolling motion combination. The aircraft alternates between sideslip and roll during a Dutch roll, producing a side-to-side motion similar to that of a pendulum. It is primarily caused by the aerodynamic interaction of the yawing and rolling moments of the aircraft. The main component in dutch roll is $\frac{\partial M_z}{\partial p}$, that means the change of moment around the z-axis with change in roll rate, that is mostly influenced by the C_{n_p} and C_{y_p}, these coefficients represent the yawing moment generated due to a change in roll rate and a side force generated due to a change in roll rate respectively. Dutch roll is unstable when C_{n_p} is negative and C_{y_p} is positive. Further study into the flying-V showed that C_{n_p} gets more negative with increasing angle of attack and forward shifting of the centre of gravity and that C_{y_p} becomes positive at larger angles of attack and forward shifting of the centre of gravity. This results into an unstable dutch roll mode at high angles of attack and at a the forward centre of gravity location [28]. This was opposite to results obtained from earlier research, as this showed that the only stable duth roll mode was at the most forward centre of gravity position [26]. The wing dutch roll performance could be increased by redesigning the wing and placing the fins more upward and forward.

Half-span sub-scale wind tunnel tests were conducted prior to the small scale test flights. These tests were carried out to evaluate the flying-V's longitudinal stability. When encountering disturbances, an aircraft must create a pitching down moment in order to maintain longitudinal stability, which happens when Equation 1 is fulfilled. This occurs when the neutral point, the point at which the centre of gravity produces zero longitudinal static stability, is located behind the centre of gravity. Because flying wings lack an empennage, the neutral point coincides with the wing's aerodynamic centre, the point at which the pitching moment is independent of the angle of attack [37].

$$C_{M_\alpha} < 0 \tag{1}$$

The half-span sub-scale wind tunnel experiments yielded the optimal centre of gravity and the range within which the aircraft could be trimmed to achieve statically stable performance. Furthermore, if the angle of attack exceeded $19 degree$, it displayed statically unstable behaviour due to the formation of strong vortices over the wing surface [38, 27]. This unstable pitch break could be delayed by using fences, which also reduces the absolute pitching moment coefficient [39].

These experiments did not evaluate the dynamic longitudinal stability qualities, due to limitations imposed by the test setup inside the windtunnel. The short period and phugoid modes are of interest for an aircraft's dynamic longitudinal stability. Short period oscillations are characterised by rapid changes in pitch attitude, with the nose moving up and down in a relatively short period of time, and are typically caused by disturbances that cause a momentary change in angle of attack, such as a gust of wind or pilot control inputs. The short period has requirements in the form of a minimum damping ratio or as a control anticipation parameter, which is a measure of the pilot's ability to predict the aircraft's ultimate response [40, 28]. The phugoid mode represents slower and more pronounced climb and descent cycles involving pitch attitude and airspeed changes. Because the dynamic stability properties of conventional aircraft and BWB are similar, both of these modes can be assessed using eigen values [37]. According to research, the flying-V has a positively damped short period, with the worst performance during cruise at the most forward centre of gravity location, and a positively damped stable phugoid during cruise and approach [26].

Additional wind tunnel experiments were performed on a 4.6% scale half model to quantify the engine integration

effects. These experiments showed an increase in nose down pitching moment of angles of attack between the 5° and 12.5°, but this is followed by an increase in nose up pitching moment between 12.5° and 22.5° [41]. This further showed that the aircraft is trimmable with control surface deflections $\delta \in (-10°, 10°)$, but this comes with an increase in power requirement at low speeds, while it reduces power requirements at higher velocities [41].

Directional static stability means that when a sideslip angle occurs due to a disturbance a positive yawing moment would be created to push the aircraft back into its original state without sideslip. This is expressed as a formula by $C_{n_\beta} \geq 0$. This positive moment will be created when the two vertical fins are placed behind the centre of gravity, resulting in a stabilising effect. It is normal to set the yawing moment limit to 0.0005 to ensure a safety margin [42]. However, for this configuration, this derivative could not be accurately calculated using empirical methods, necessitating the use of RANS or SU2, which is beyond the scope of this research [23].

When an aircraft exhibits lateral static stability, it returns to an equilibrium position with its wings level after experiencing a roll disturbance. This happens when the sideslip-induced rolling moment is negative ($C_{l_\beta} < 0$).

An aircraft must comply with a single engine inoperative condition at take-off, according to safety regulations. In this case, the control forces generated by the fins should be able to balance the yawing moment caused by one engine being inoperative, so that the aircraft maintains a zero degree slip angle at take-off speed at the most aft centre of gravity position, as this is considered the worst case scenario [21]. The maximum rudder deflection is not permitted because the aircraft must still be able to manoeuvre in this position. As a result, the maximum rudder deflection should be set at a 20° angle. In this condition, the yawing moment coefficient with respect to rudder deflection is used to calculate the rudder deflection required. This can be calculated using an empirical relationship, similar to Sadraey's method [43]. Research showed limited controllability of the flying-V during this condition [26].

Maximum crosswind landing conditions correspond to a wind speed equal to 20% of takeoff speed. The sideslip angle must not be greater than 11.5° in this case. The aircraft must still be manoeuvrable in this condition, so a maximum rudder deflection angle is not permitted [5]. There are three modes of dynamic lateral-directional stability. The periodic dutch roll, as previously described. The ability of an aircraft to generate a roll rate quickly after a roll control input is applied and return to zero when the input is removed is referred to as aperiodic roll. When $C_{l_p} < 0$, this motion is damped, resulting in a negative rolling moment when a rolling disturbance occurs. When the real eigenvalues are negative, this is stable. A roll time constant, which indicates how long it takes to achieve a specific roll rate, specifies the requirements for this mode [28]. Finally, spiral motion is a flight path that is uncoordinated and distinguished by a descending spiral turn. When the aircraft is unbalanced and the horizontal component of lift is insufficient to keep the plane level, this occurs. Instead of a slowly increasing roll angle, this motion is stable when the aircraft returns to wing level after a roll disturbance. Both of these modes were determined using the Flying-V's eigenvalues, resulting in a stable spiral mode and aperiodic roll during cruise and approach [26, 28]. All of these dynamic stability requirements, however, are dependent on the aircraft's design and necessitate stability derivatives that provide significant uncertainty when computed using simple aerodynamic models, such as a VLM [23]. Hence, a decision has to be made to implement them into the model generated in the subsequent thesis.

Another research investigated the effect of stability and control constraints of the Flying-V family performance in detail. With the exception of the rudder power for steady sideslip and one engine inoperative trim, this research demonstrated that the initial design optimised for fuel burn almost met all of the stability constraints. These constraints could be met by increasing the fin length, resulting in a less than 1% fuel burn penalty. As a result, the control constraints are not a driving requirement as long as the fins are large enough to accommodate rudders. However, it should be noted that large uncertainties existed in the aerodynamic model applied [44].

Control is provided by two types of control surfaces elevons mounted to the trailing edge of the outer wing and rudders added to the fins. Various studies applies different elevons, where research by Toorn applies one per side, research by Cappuyns two and the wind tunnel test Overeem apply three [26, 28, 44]. The three elevon design strategy was that the most inboard elevon was used as elevator, the centre elevon for both lateral and longitudinal control and the outboard elevon provided mostly lateral control [38].

2.2.5 Parametrisation of the Flying-V

The aerodynamic design of the Flying-V consists of three groups the wing, the two vertical fins and the two engines. The Flying-V is a unconventional aircraft, hence traditional empirical approaches do not apply, due to

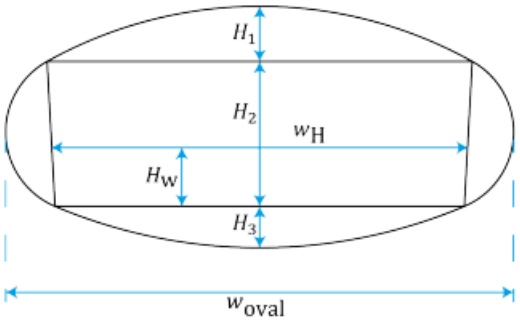

Figure 2: Oval cross section with design variables [1]

the lack of available data. Therefore, the wing has to be parameterised and a shape optimisation is required. First, Faggiano proposed a geometric model that could be used to evaluate the aerodynamic design of the flying-V. This geometric model took into consideration an oval pressurised fuselage with the four structural support panels. However, further study showed that this parametrisation suffered from the following problems [1]:

- The cabin area was too small to position all the payload.
- It had excess space between the fuselage and the outer mould line (OML) in the tapered aft part of the fuselage.
- The fuselage did not fit the OML near the root.
- It did not reflect the proposed primary structure design.
- All the wing trunks are tapered, resulting in a harder to manufacture design.
- It did not provide the structural requirements near the root

This resulted in the generation of a new wing parametrisation. The new wing parametrisation changed the orientation of the surface smoothness discontinuities resulting in more manufacturable and robust design. In this method is the wing build around the fuselage, since the transportation of payload is the main reason an aircraft is built.

Firstly, the oval cabin of the flying-V is described in subsubsection 2.2.3. To incorporate this oval cross section into the design, four additional panels must be added so that when pressurised, the horizontal panels bear compression loads and the vertical panels bear tension loads. Furthermore, by connecting all of these panels, it functions as a wing box carrying the torsion load. As a result, a structurally efficient and flexible cabin design for integrated blended wing bodies and flying wings is created. The parametrisation of this wing box is shown in Figure 2 and results in the five additional parameters listed below [1]:

- H_1: Crown height, height from top to upper horizontal panel
- H_2: cabin height, height between both horizontal panels
- H_3: Keel height, height form lower horizontal panel to the bottom of oval
- H_{arm}: Arm rest height
- W_{cabin}: Cabin width at arm-rest height

This parametrisation applies one additional parameter compared to the parametrisation by Faggiano, the arm rest height. This parameter is added because the side panels could be at an angle hence it might be of interest to analyse the width at the arm rest height instead of the floor. The floor, ceiling and oval width could all be determined from these five parameters [1].

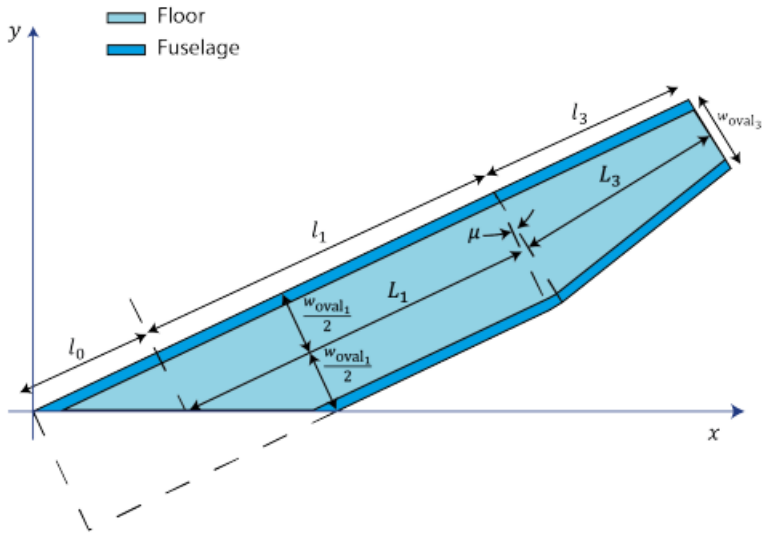

Figure 3: The planform of the fuselage [1]

The planform of the fuselage consists of four parts. A nose part, a constant cross section part, a transition part and a tapered end part. The constant cross sectional part was required for the easy stretching and shortening such that a flying-V family design was possible. The tapered end part made it able to have a constant leading edge sweep on the inboard section of the wing. This resulted in the parametrisation given in Figure 3, that made it able to calculate the fuselage planform from the following four parameters:

- L_1: untapered fuselage length
- L_3: Tapered fuselage length
- W_{H_1}: Width at input height section 1
- W_{H_3}: Width at input height section 3

The airfoil shape of the inboard wing section is generated around the fuselage in a method similar to Faggiano. However, that method thought the airfoil parallel to the flow direction (symmetry plane), while the new parametrisation constructs the airfoils orthogonal to the centreline of the fuselage. This method consists of constructing 3 curves; one for the nose and two for the rear part, with four conditions imposed to them tangency at start, curvature continuity at start and pass through start and end points. These curves could be constructed from the following 6 parameters [1]:

- $\bar{c}'$: Planform chord, normalised
- z_{TE}: Vertical position of trailing edge
- c_{up}: Upper curve coefficient
- c_{low} : Lower curve coefficient
- $\bar{x}_{S_{\mathrm{up}}}$:Upper curve starting location
- $\bar{x}_{S_{\mathrm{low}}}$:Lower curve starting location

The airfoil shape of the outboard wing was parameterised with the Class function/Shape function Transformation (CST) method for curve parametrisation of Kulfan, as this section of the wing is not restricted to the oval shape [45].

The wingplanform parametrisation is shown in Figure 4. This results in addition with dihedral and twist in the final wing parameters given below:

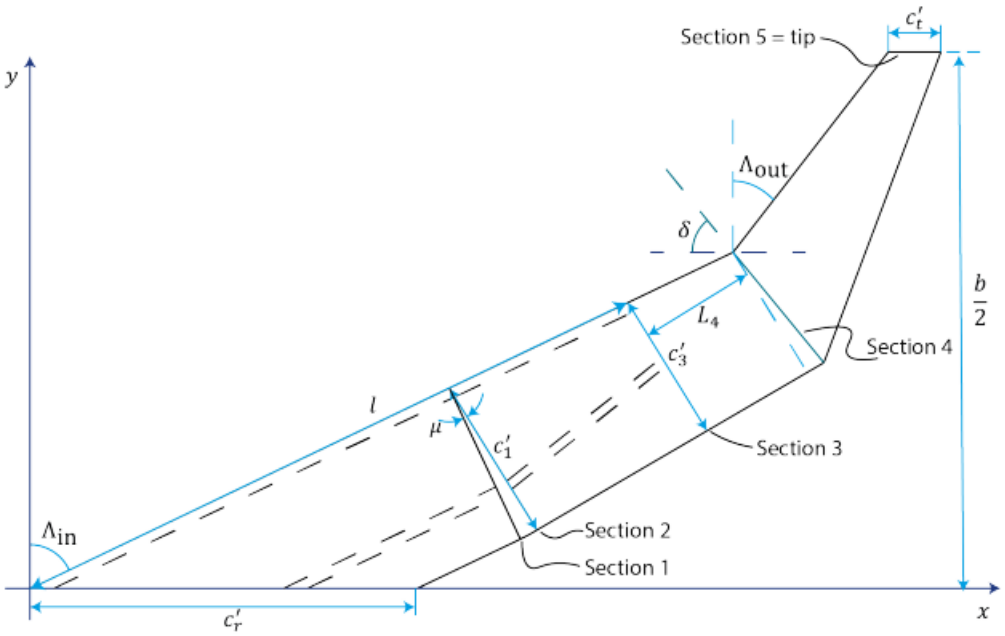

Figure 4: Wingplanform of the flying-V [1]

- b: Span
- $\bar{c_1'}$: Planform chord of section 1
- Λ_{in}: Leading edge sweep of inboard wing
- Λ_{out}: Leading edge sweep of outboard wing
- λ: Taper ratio
- $\bar{L_4}$: Virtual fuselage extension length to leading edge kink
- $\bar{c_3'}$: Planform chord of section 3
- δ: Orientation angle of section 4
- Γ_4: Dihedral of trunk 4
- Γ_5: Dihedral of trunk 5
- i_4: Incidence angle of section 4
- i_5: Incidence angle of section 5

The twin fins on the flying-V are added to ensure the aircraft's stability and control. Because without the fins, the aircraft would be unable to provide directional static stability, perform take-off with one engine inoperative, and land in maximum crosswind conditions. In order to satisfy these condition as described in the section above, the fins have to be sized. A minimum fin area is desired, because this would result in minimal zero lift drag and weight. Hence the fin area is of importance. A good way to parameterise the fin area with minimal design variables is describing the fin area with the fin sweep (Λ_{fin}), fin aspect ratio (A_{fin}) and fin taper ratio (λ_{fin}). Horowitz, on the other hand, provided a better parameterisation by using winglet length, cant angle, leading edge sweep angle, taper ratio, and overall taper ratio. As a result, the number of design variables has increased, but the foundation for ensuring directional stability has improved. It did, however, show that the effect of wing and winglet taper ratio had such a limited effect on the stability characteristics that they could be considered constant [46].

3 Climate Analysis

This section discusses the various climate models used in aviation and how they can be used to predict aviation's climate impact. It examines the impact of all climate forcers in aviation as well as the models available to investigate their response. Furthermore, mitigation techniques for reducing aircraft's climate impact are described. Finally, climate modelling uncertainties are addressed.

3.1 Introduction to Climate Analysis

The assessment of the environmental impact is normally at a postdesign analysis phase in which an aircraft is analysed to see if it fulfills the requirements imposed by authorities such as the ICAO. In most cases small adjustments are required to comply to the regulations resulting in a sub optimal overall design, but since these effects are still small is this approach feasible. Nevertheless, due to the relatively insignificant impact of these adjustments, this approach remains viable. However, with the increasing stringency of environmental regulations, the cost and complexity associated with achieving compliance during the post-design phase have considerably escalated. Therefore, it is imperative to consider the environmental impact at an early stage of aircraft design [47].

The impact of aviation on climate change is widely documented, and is mostly attributable to carbon dioxide (CO_2) emissions and non-CO_2 aviation effects. Although early climate impact studies focused primarily on CO_2 emissions due to their direct association with fuel use and being the principal driver of global warming across all sectors, it is now recognised that aviation's contribution to global warming is not restricted to CO_2 emissions alone. Non-CO_2 effects, which include NO_x, water vapour, aerosols, soot, and contrail formation, accounted for 66% of aviation's net effective radiative forcing (ERF) in 2018, with contrail formation accounting for the most, followed by CO_2 and NO_x. An overview of the ERF of all climate forcers in aviation are given in Figure 5 [2]. As a result, detailed models evaluating the non-CO_2 effects are required. Modelling non-CO_2 effects, on the other hand, are a difficult endeavour that involves a variety of atmospheric physical processes such as plume dynamics, chemical transformations, microphysics, radiation, and transport [2].

Numerous research have been conducted to evaluate the various components that contribute to ERF. However, few have examined the whole impact of aviation on climate[2]. Furthermore, quantifying the societal cost and harms caused by emissions would ideally be undertaken, however this is not achievable due to significant uncertainties[7]. As a result, different climate measures are utilised in different studies, making it difficult to incorporate results into a comprehensive model for measuring the climate impact of an aircraft or fleet. It is challenging to select the appropriate climate metric. The many climate metrics used in research are listed below, with ATR regarded as the best for long-term evaluations because it takes into account the location of the emission, is climate-relevant by giving a temperature change, and is independent of time horizon, but every metric has its own specific application [48].

- Emission amount: the amount of a species emitted.
- Radiative Forcing (RF): RF is defined as the change in net irradiance at the boundary between the troposphere and stratosphere caused by a concentration change an relative to pre-industrial times.
- Effective Radiative Forcing ERF: ERF represents the change in net top of atmosphere downward radiative flux after allowing for atmospheric temperatures, water vapour and clouds to adjust, but with global mean surface temperature or a portion of surface conditions unchanged
- Absolute Global Warming Potential (AGWP): AGWP is defined as temporal integral over RF from time of emission until a given time horizon.
- Global Warming Potential (GWP): GWP is the AGWP in relation to the absolute climate indicator of a reference species (CO_2 in most cases) with the same mass.
- Absolute Global Temperature Potential (AGTP): AGTP is equal to the near-surface temperature change at a given time horizon.
- Global Temperature Response (GTP): GTP is the AGWP in relation to the absolute climate indicator of a reference species (CO_2 in most cases) with the same mass.

- Average Temperature Response (ATR): Mean surface temperature change over a certain time span. In a lot of cases a time span of 100 years is taken such that the metric is called ATR_{100}.
- Average Temperature Response Potential (ATR-P): ATR-P is the ATR in relation to the absolute climate indicator of a reference species (CO_2 in most cases) with the same mass

The formulas of some of the climate metrics are given below, where H is the timespan, X the climate forcer and RF the radiative forcing.

$$GWP^X(H) = \frac{\int_{t_0}^{t_0+H} RF^X(t)dt}{\int_{t_0}^{t_0+H} RF^{CO_2}(t)dt} \tag{2a}$$

$$\text{GTP}^X(H) = \frac{\Delta T^X(H)}{\Delta T^{CO_2(H)}} \tag{2b}$$

$$ATR_H = \frac{1}{H}\int_{t_0}^{t_0+H} \Delta T(t)dt \tag{2c}$$

Because each climate metric has its own specialised use, ambiguity in the application of climate metrics must be avoided. The ambiguity could be greatly eliminated by clearly framing the question so that only a small number of climatic metrics are appropriate. The following five-step approach could be used to accurately formulate the question [49]:

- Pose the respective question precisely.
- Deduce an adequate reference from the question.
- Deduce an adequate emission scenario from the question.
- Deduce an adequate climate change metric from the question.
- Deduce an adequate time horizon from the question.

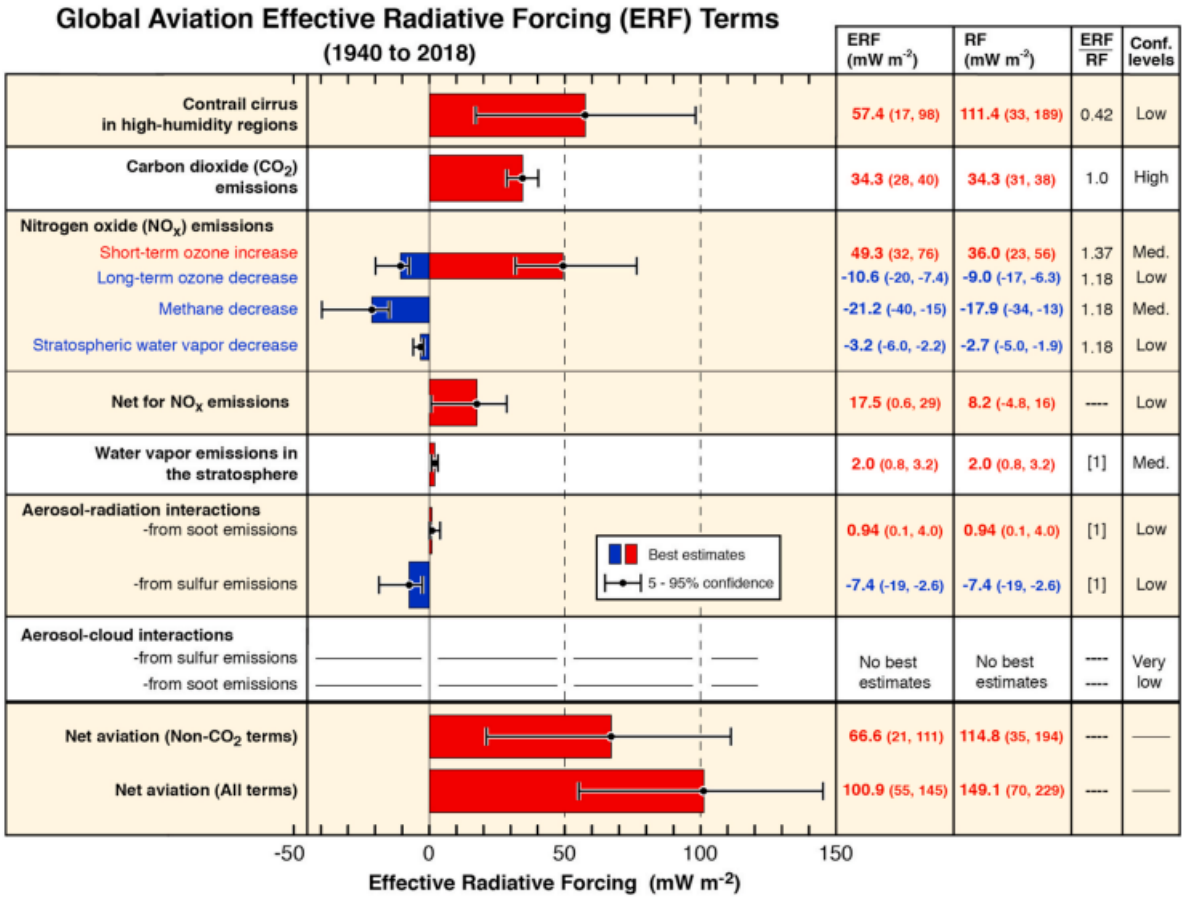

Figure 5: Best-estimates for climate forcing terms from global aviation from 1940 to 2018 [2]

3.2 Climate model types

A climate response model is applied to determine the impact of emissions on concentrations, radiative forcing and the climate. The traditional approach of a response model consists of the following steps:

- Step 1 determine the emissions
- Step 2 determine the atmospheric changes with the use of an Atmosphere-Chemistry model
- Step 3 determine the radiative forcing with an global climate model
- Step 4 determine the temperature change with a linear temperature response model

However, there are now a variety of models that use look-up tables and relationships between emissions and radiative forcing to reduce the need for an Atmosphere-Chemistry model and an Atmosphere-Ocean model. As a result, the model's complexity decreases while the computational time increases.

An Atmosphere-Chemistry model computes the composition and chemical processes occurring in the atmosphere, such that the change in concentrations of various species, due to emissions and later on depletion could be determined. The global climate model simulates the dynamic behavior of the atmosphere, ocean, land and sea ice components of the Earth's climate system and captures their complex interactions, feedback mechanisms, and energy exchanges. Thereby determining the transport and exchange of heat, momentum and gases between atmosphere, ocean and land such that the effect of a species concentration on the global temperature could be determined. However, these models are computationally expensive.

A linear temperature response model represents the climate system based on results from a global climate model. These models estimate averaged conditions instead of time-varying results, thereby reducing the complexity and decreasing the computational costs, while increasing the uncertainty.

Grewe's AirClim model is an example of a linearised temperature response climate-chemistry model that evaluates the impact of local emissions for 7 latitudes with each 12 altitude zones using precalculated look-up tables that contain non-linear relationships between localised emissions and radiative forcing. Using these look-up tables, it is possible to obtain similar results to the E39CA model in seconds on a desktop computer rather than the 3 weeks required for E39CA on a supercomputer. As a result, the primary goal of this model is to rapidly evaluate changes and compare mitigation options [50]. However, this model has already an increased complexity due to dependence on geographical location of emission.

A simple linearised temperature response model could easily independent on geographical location be constructed, by applying relations between the radiative forcing and emission of a species obtained from global climate models. The radiative forcing of well mixed green house gasses could be used to calculate the global mean temperature (Δ_{surf}) by multiplying with a climate sensitivity parameter (λ), as given in Equation 3a. However, this is not as effective for gasses where the location matters. In most cases the climate sensitvity parameter is taken constant and equal to the parameter for a doubling of CO_2, such that the sensitivity is then independent form an individual model. The effects of the other climate forcers are then calculated with Equation 3b, where the efficacy (Eff) is the ratio between the sensitivity of the species an CO_2.

$$\Delta T_{\text{surf}} = \lambda \cdot RF \qquad \text{(3a)} \qquad\qquad \Delta T_{\text{surf}} = \lambda \cdot Eff_x \cdot RF \qquad \text{(3b)}$$

The method above is independent of time. Hence, a more accurate way to calculate the temperature change is by implementing a climate impulse response function to find a time time-varying global mean temperature, as given in Equation 4 [50]. RF_i^* is the normalised radiative forcing of the various species involved. This is one for a doubling in CO_2 compared to preindustrial times, and can be calculated for all the species with Equation 5. Furthermore, G_T is a climate impulse response function and result from global climate models, Dallara describes and compares various of these climate impulse response functions and applies the method by Boucher and Reddy [3, 51], while Airclim and research by Proesmans applies the results from Sausen and Schumann [52, 50, 7].

$$\Delta T(t) = \int_{t_0}^{t} G_T(t-\tau) \left(\sum_i RF_i^*(\tau) \right) d\tau \qquad (4)$$

$$\mathrm{RF}_i^*(t)\mathrm{Eff}_i \cdot \frac{\mathrm{RF}_i(t)}{\mathrm{RF}_{2\times \mathrm{CO}_2}} \tag{5}$$

The radiative forcing is calculated from the emissions with two methods one for species that have a are long-lived applying a convolution integral with a response function or a simpler method for short-lived species. Equation 6 and Equation 7 gives the equation for the long-lived and short-lived species respectively, where s(h) is a forcing factor to include altitude dependency that not is not included to all the species, E is the emission of the species in kilograms and A_i, τ_i and $\mathrm{RF}_{ref}/\mathrm{E}_{ref}$ are a coefficient, the perturbation lifetime and the radiative forcing per unit of emission respectively and are originally computed with a global climate model, but are taken from literature.

$$\mathrm{RF}_i(t,h) = s_i(h) \int_{t_0}^{t} G_i\left(t-t'\right) \cdot E_i\left(t'\right) \mathrm{d}t' \mathrm{with} G_i(t) = A_i \cdot e^{-t/\tau_i} \tag{6}$$

$$\mathrm{RF}_i(t) = s(h) \cdot \left(\frac{\mathrm{RF}_{\mathrm{ref}}}{E_{\mathrm{ref}}}\right)_i \cdot E_i(t) \tag{7}$$

3.3 Climate Forcers of Aviation

The numerous species that have an impact on the climate as a result of aviation, including CO_2, NO_x, water vapour, aerosols and contrails. Their sources, atmospheric lifetimes, and radiative forcing values will be discussed.

3.3.1 Carbon Dioxide

CO_2 is a greenhouse gas, as it absorbs outgoing infrared radiation from the earth, hence an increase in the concentration of a greenhouse gas will warm the earth and increase the surface temperature. The emission of CO_2 is directly related to the burning of fossil fuels that contain carbohydrates, by the reaction given in Figure 6. The amount of a species emitted with the burning of a specific fuel is given by the emission index (EI), which has for the combustion of kerosene for CO_2 a value of 3.16kg/kg. The change in the concentration of CO_2 in the atmosphere, due to the emission of CO_2 has a very long lifetime in the order of centuries. Because CO_2 has such a long lifetime the place of emission is not relevant for the impact on the climate, which is the case for some of the more short lived climate forcers. Furthermore, a convolution integral with a response function is required, due to the long lifetime of CO_2.

A method to determine the normalized radiative forcing of CO_2, due to the change in CO_2 concentration in the atmosphere is given in Equation 8, where the concentration change is calculate with the convolution integral and impulse response function given in Equation 9. The E_{CO_2} is the absolute CO_2 emissions in year t, α_i are coefficients corresponding to the perturbation lifetimes τ_i, and χ represents the concentration with $\chi_{CO_2,0}$ the background concentration of CO_2 having a value of 380ppmv (parts per million volume)[52]. The IPCC proposes another method similar to how the RF is calculated is calculated for long-lived species only the decay of radiative forcing G is computed with 7 parameters instead of 2 [3, 53]. This method does however, still require to be adjusted to normalised radiative forcing, but does decrease the amount of parameters from 10 to 9 including the conversion and has an uncertainty of 15%.

$$\mathrm{RF}^*(t) = \frac{1}{\ln 2} \cdot \ln\left(\frac{\chi_{\mathrm{CO}_2,0} + \Delta\chi_{\mathrm{CO}_2}(t)}{\chi_{\mathrm{CO}_2,0}}\right) \tag{8}$$

$$\Delta\chi_{\mathrm{CO}_2}(t) = \int_{t_0}^{t} G_{\chi_{\mathrm{CO}_2}}\left(t-t'\right) \cdot E_{\mathrm{CO}_2}\left(t'\right) \mathrm{d}t' \text{ with } \quad G_{\chi\mathrm{CO}_2}(t) = \sum_{i=1}^{5} \alpha_i \cdot e^{-t/\tau_i} \tag{9}$$

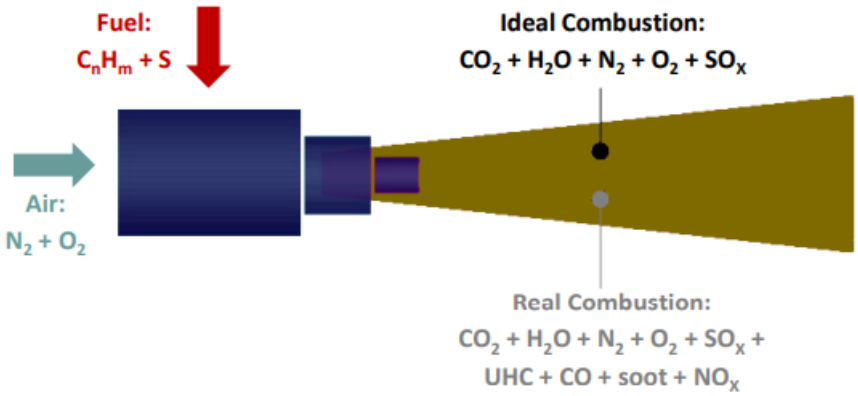

Figure 6: Products of aircraft carbohydrate fuel combustion [3]

3.3.2 Nitrogen Oxides

In a turbofan engine, nitrogen oxides (NO_x), which consist of NO and NO_2, are primarily formed in three ways: thermal NO_x, prompt NO_x, and the N2O mechanism. Thermal NO_x is produced when nitrogen and oxygen in combustion air combine at high temperatures in a flame. As a result, thermal NO_x is highly dependent on flame temperature, but also on the equivalence ratio, because nitrogen and fuel compete for available oxygen, resulting in a peak NO_x formation near equivalence ratios of 0.9. Prompt NO_x forms from the rapid reaction of atmospheric nitrogen with hydrocarbon radicals. The N2O mechanism occurs in the presence of an oxygen atom and a third molecule, where nitrous oxide is formed at a low activation energy instead of nitric oxide and this nitrous oxide is then further oxidized into 2 nitric oxides. Prompt NO_x is only a small portion of the total NO_x production. Furthermore, the ratio between NO_x formed due to the thermal way and N2O mechanism is heavily related to the turbine inlet temperature and operating pressure[54].

The fact that NO_x emissions consist of multiple species and that those are formed under different circumstances keep the emission index from being constant, but dependent on engine and combustor conditions. Hence, the emission index has to be determined for the various operating conditions and engines, by the means of fuel flow methods or analytical expressions. An easy to use method is given in Equation 10, which has only a small amount of parameters, namely P_{T3}, T_{T3} and H_0, which are the pressure and temperature at the inlet of the combustor and the specific humidity respectively [3]. Although, at the NASA Glenn Research Center they apply Equation 11 that makes use of the the combustor exit temperature (T_4) rather than the specific humidity. Both these equations show that the formation of NO_x is not only dependent on the temperature, but also on the pressure [47]. However, both these methods require engine operating conditions or detailed engine models. Fuel flow correlation methods exist that compute the NO_x emissions based on ambient conditions, fuel flow rate and ICAO landing and take-off certification data. The Boeing Method 2 is an example of a fuel flow correlation model [55].

$$\mathrm{EI}_{\mathrm{NO}_x} = 0.0986 \cdot \left(\frac{p_{T3}}{101325}\right)^{0.4} - e^{T_{T3}/194.4 - H_0/53.2} \tag{10}$$

$$\mathrm{EI}_{\mathrm{NO}_x} = 0.004194 T_4 \left(P_3/439\right)^{0.37} e^{(T_3 - 1471)/345} \tag{11}$$

Nitrogen oxides are not greenhouse gasses itself as they self do not trap heat in the atmosphere. However, they indirectly have a net warming effect as they react with greenhouse gasses as methane (CH_4) and ozone (O_3). In the short term, NO_x raises the O_3 concentration in the atmosphere, which causes it to warm. This is calculated with Equation 7, as it is a short effect. However, NO_x reduces the lifetime and abundance of CH_4 in the long term, which has a cooling effect. The decrease in CH_4 causes a decrease in O_3 and stratospheric water vapour, both of which have a cooling effect. Both these long term effects are calculated with Equation 6. So NO_x causes an increase in O_3 in the short term but a decrease in the long term. However, the short-term warming effects of NO_x outweigh the long-term cooling effects, resulting in a positive net ERF when all of these effects are added together [2]. Because NO_x works with multiple species and on different timescales makes the net RF dependent on the background concentrations and chemical rate coefficients such that it is dependent on the location and time of emission [56].

3.3.3 Water Vapour

Water vapour (H_2O) is similar to CO_2 also a potent green house gas and is directly related to the burning of fossil fuels, hence the absolute emission of water from burning kerosene could be computed with the emission index, which is $EI_{H_2O} = 1.26$ kg/kg. However, water vapour is governed by the hydrological cycle rather than the carbon cycle, which has a significantly shorter perturbation lifetime ranging from a week to a month depending on altitude[3, 50]. As a result, it has only a minor climate influence, although this increases with flying at higher altitudes this effect could be neglected [4]. Water vapour's short residence period and negligible altitude dependence, result in a further simplified method shown in Equation 12 [7]. Finally, water vapour does play a role in the formation of aerosol particles and clouds [57].

$$\mathrm{RF}_i(t) = \left(\frac{\mathrm{RF}_{\mathrm{ref}}}{E_{\mathrm{ref}}}\right)_i \cdot E_i(t) \tag{12}$$

3.3.4 Sulphate

Jet A fuel contains around 400 ppm sulphur, which is oxidised inside the combustor to produce sulphur dioxide, sulphur trioxide, and sulphuric acid (H_2SO_4). H_2SO_4 coagulates with H_2O, increasing in size and hence increasing sulphate aerosols. These sulphate particles reflect incoming solar radiation, resulting in net cooling. These particles have a four-day residence duration, which is rather brief. As a result, the impact might be computed using the same formula as for water vapour, as stated in Equation 12. Sulphate aerosol emissions have a minor direct impact, due to the short residence time and few emitted particles with an EI of $4.0{\cdot}10^{-5}$kg/kg, but sulphate particles can play a role in the development of contrail and cirrus clouds [3].

3.3.5 Soot

In the combustion chambers of aircraft engines, carbon soot particles made of graphite carbon and organic compounds are produced. These soot particles are formed in fuel-rich region, such a close to the fuel spray. The formation of soot is a complex physical process governed by atomisation and fuel-air mixing, instead of kinetic and thermodynamic processes making it hard to predict soot formation. However, it is known that soot formation increases when engine throttle increases, due to more fuel being injected in the combustor, but also due to a higher pressure. Soot formation is heavily dependant on the combustor, its fuel atomizer and its operating conditions, but also the fuel type, as this could induce local fuel rich regions and have a resistance to carbon formation [54].

Because of how much soot absorbs solar energy, there is a little warming impact. Soot particles have very brief atmosphere lifetimes, on the scale of a week or less, hence the radiative forcing is determined similar to water vapour and sulphate with Equation 12. Soot particles typically have few direct effects, but they serve as nucleus for heterogeneous ice nucleation, which is crucial for the development of contrails [57]. Studies have shown that a reduction in soot emission would reduce the amount of initial ice crystals, which result in a decrease in contrail radiative forcing [58, 59, 60].

3.3.6 Contrails

Condensation trails (contrails) are ice clouds formed by jet aircraft. Contrails can be short- or long-lived, depending on the surrounding atmospheric conditions, if they last at least 10 minutes. This induced cloudiness may scatter incoming solar radiation during the day, resulting in a cooling effect. It does, however, trap outgoing radiation during the day and night, resulting in a warming effect. Contrails are the single most significant contributor to aviation-induced radiative forcing, according to research, hence precisely modelling contrail generation is critical [2].

According to Schmidt's thermodynamic model, contrails form when hot and moist jet engine exhaust expands and mixes with dry and cold ambient air, lowering the temperature and humidity of the exhaust. During this mixing, the air becomes saturated with liquid water and droplets form. When temperatures fall below 235 K, these supercooled droplets freeze and contrails form. When the ice is supersaturated, the contrails persist for longer, but dissolve when it is subsaturated.

To assess the creation of contrails, the ambient temperature must be less than 235K. Second, the Schmidt-Appleman criterion, which states that the hot exhaust air must become saturated with liquid water during the mixing process with the surrounding air, must be met. A mixing line is used to represent the mixing process in the graph of water vapour partial pressure against ambient temperature. This mixing line can be approximated by a linear relationship that is dependent on the overall efficiency of the engine, the ambient conditions (pressure, temperature, and relative humidity), and the fuel (Emission index of water, specific heat content)[61]. Finally, the mixed exhaust has to reach the ambient temperature below the saturation line for liquid water and above the saturation line for ice in order for the contrails to persist. Sonntag's Formula, which gives the saturation pressure of water as a function of temperature, determines the saturation lines for ice and water [62].

The radiative forcing for linear contrails could be calculated using a modified version of the short term equation that includes the altitude forcing (s(h)) and the length in kilometres, as shown in Equation 13 [3]. The length in this equation is determined by evaluating for all flight phases if all three criteria for persistent contrails are met, and when that is the case for a flight phase, the distance travelled during that phase is applied.

$$\mathrm{RF}_{\mathrm{contrails}}(t,h) = s_{\mathrm{contrails}}\,(h) \cdot \left(\frac{\mathrm{RF}_{\mathrm{ref}}}{L_{\mathrm{ref}}}\right)_{\mathrm{contrails}} \cdot L(t) \tag{13}$$

This model, however, excludes the nucleation mechanisms that generate ice crytsals. Microphysically seen, aerosol particles (mostly soot, volatile particles, and sulphate) in exhaust and ambient air combine with water vapour to generate water droplets from supersaturated vapour [63]. Soot Particles are the most prominent in droplet formation caused by kerosene emissions and have an impact on the number of droplets that condense into ice particles. Contrails have a longer lifetime and increased radiative forcing when there are many tiny particles in them [60].

Furthermore, linear contrails could spread resulting in contrail-cirrus. This is estimated to increase the contrail coverage by 1.8, but the effect of contrail cirrus on radiative forcing is highly uncertain and is therefore omitted in most models [3].

3.3.7 Noise

Another thing to consider is that noise contributes significantly to the climate impact of aviation. This may be the most directly harmful of all, as it causes poor sleep for people who live near airports. Despite noise reductions, there is still an increase in complaints near airports. This has resulted in significant noise constraints.

However, noise is only important during the landing and take-off phase (LTO), because it is perceived the best there. As a result, noise certifications, which are measured in total time integrated noise, also known as effective perceived noise (EPNL), are measured in the LTO at three points: the approach, sideline, and flyover, where the sideline and flyover are perceived the loudest due to jet noise. [47].

There are some noise-computing models available. The Aircraft Noise Prediction Programme (ANOPP) is used by NASA Langley Research Centre. It is a semiempirical code that computes the time averaged EPNL by incorporating noise prediction schemes and models for fan noise, jet noise, and airframe noise.

3.4 Mitigation Techniques for Climate Impact in Aviation

The engines are the biggest contributing factors to the climate impact, as it is the system that emits the exhaust gasses. therefore, significant reductions to the climate impact can be made by optimising the engine. There are multiple ways an engine could reduce its emission. Firstly, it can lower the emission index by improving the combustor or fuel type, as this would reduce the amount of pollutant emitted per kilogram of fuel burned. Secondly, the amount of fuel consumed could be reduced, by changing the engine cycle, such as increasing the overall pressure ratio resulting in more complete combustion. However, this would result in an increase in combustion temperature and an increase in NO_x, due to thermal NO_x formation and an increase in soot formation. Hence, the engine operating conditions for NO_x and CO_2 reductions have conflicting requirements, such that a trade-off between the two is required [54]. Increasing the bypass ratio also decreases the fuel consumption until a certain point, but as a bypass ratio exceeds the 10 the fan and nacelles will get so big that there is a large increase in parasite drag leading to a increase in fuel consumption. Furthermore, the NO_x and

soot production increases with a higher bypass ratio as a bigger fan needs more power to be extracted from the low pressure turbine leading to an increase in pressure and combustion temperatures [47].

By incorporating new combustor designs, such as a lean premixed combustor, an RQL combustor, or Catalytic combustors, NO_x production can be reduced without increasing CO_2 production. However, all of these designs have flaws, and more research is needed before they can be used confidently in an aircraft engine[54].

As previously stated, fuel combustion in aircraft engines is a major contributor to climate change. This fuel, however, is consumed solely for the purpose of transporting the payload. To accommodate the payload, a dedicated fuselage is currently used, which adds significant weight and aerodynamic drag to the aircraft. As a result, a significant amount of fuel is required to propel the aircraft. As demonstrated in section 2, the use of a blended wing body (BWB) or Flying-V aircraft design, in which the wings and fuselage are integrated into a single component, could significantly reduce fuel consumption. This improved aerodynamic design change could result in a 20% reduction in fuel mass, resulting in a corresponding reduction in CO_2 emissions and a significant reduction in non-CO_2 emissions.

The climate impact of aviation could be reduced even further by changing the operating conditions. Reduced flight altitude would have a significant impact on the climate. To begin, contrails will not form when flying below 9 kilometres because the ambient pressure is greater than 235K. Furthermore, the total impact of other emissions will be reduced because they will be emitted in the troposphere rather than the sensitive tropopause. The effect of always flying 2000 feet lower or higher has been evaluated and is depicted in Figure 7[4]. The AirClim model is used to calculate the changes in radiative forcing. These figures clearly show that flying lower reduces all non-CO_2 effects while increasing only CO_2 effects and vice versa for flying higher. Furthermore, it demonstrates the importance of non-CO_2 effects in assessing the climate impact. As a result, flying lower could significantly reduce the climate impact of aviation, but more research into this area is needed, as there is a large uncertainty in the cloud related aviation effects [4]. Furthermore, this model assumed that flying at this suboptimal lower altitude required 1% more fuel. However, an aircraft has to be specifically optimised to fly at this lower altitude in order to minimise the reduction in performance and increase in fuel consumption.

A lower cruise Mach number is known to be required for efficiently flying at a lower altitude, as the density of the air increases when flying lower, increasing friction drag. To achieve a similar aerodynamic performance, the aircraft must fly slower to compensate for the increase in drag. This increases the flight duration and thus the operational costs, from a cost standpoint, this is not advantageous. Finally, flying at a lower altitude may increase the impact of weather on operating conditions.

Various studies confirm that flying lower and slower reduces an aircraft's environmental impact, but at the expense of increased operational costs [47]. Furthermore, the impact varies depending on the climate force for which it is designed. So, designing for a minimal fuel would result in a 10% fuel savings with a 2% increase in operating costs. However, designing for minimal NO_x emissions would already increase operating costs by 10% while reducing NO_x formation by nearly 55%. This also confirmed that there is a large conflict between designing for fuel and NO_x, as the design for NO_x had a 22% higher fuel consumption than the optimal design for fuel. Finally, designing for low noise would result in a 26% increase in operating costs with cumulative noise reductions up to 25dB[47]. therefore, it is of the utmost importance to keep in mind what the goal of the design is.

Other studies that implemented a blended wing body to decrease the environmental impact with respect to conventional tube-and-wing aircraft with same mission characteristics did result in overall worse climate performance. For example, the Flying-V was initially optimised to have a minimum fuel burn, such that most CO_2 emissions and other directly to fuel burn related emissions decrease. However, this resulted in the aircraft to fly higher than the conventional reference aircraft resulting in an increase in contrail and NO_x formation, such that when a more inclusive climate metric was applied (ATR_{100}) the flying-V performed worse than the A350-900 reference aircraft. Although, it did found that when both aircraft flown at the same altitude the Flying-V performed better even though this conditions was sub-optimal [12].

The AHEAD multi-fuel BWB faced similar problems. The AHEAD multi-fuel BWB is an aircraft that incorporates a novel combustor that burns liquid hydrogen or methane in the first combustion chamber and a part of this exhaust is inserted into a combustion chamber with bio kerosene[64]. The initial burning of liquid hydrogen or methane reduces the CO_2 emissions, while the second combustor burns kerosene in a lean low oxygen environment resulting in low NO_x emissions. The blended wing body was added have an efficient structure to fit the large cryogenic tanks. This should result in lower emissions, hence a lower climate impact. However, initial investigation that was focused on low CO_2 and NO_x emissions showed worse climate performance (ATR_{100}) than conventional aircraft adjusted for the future, due to the aircraft flying higher and thereby increasing the contrail

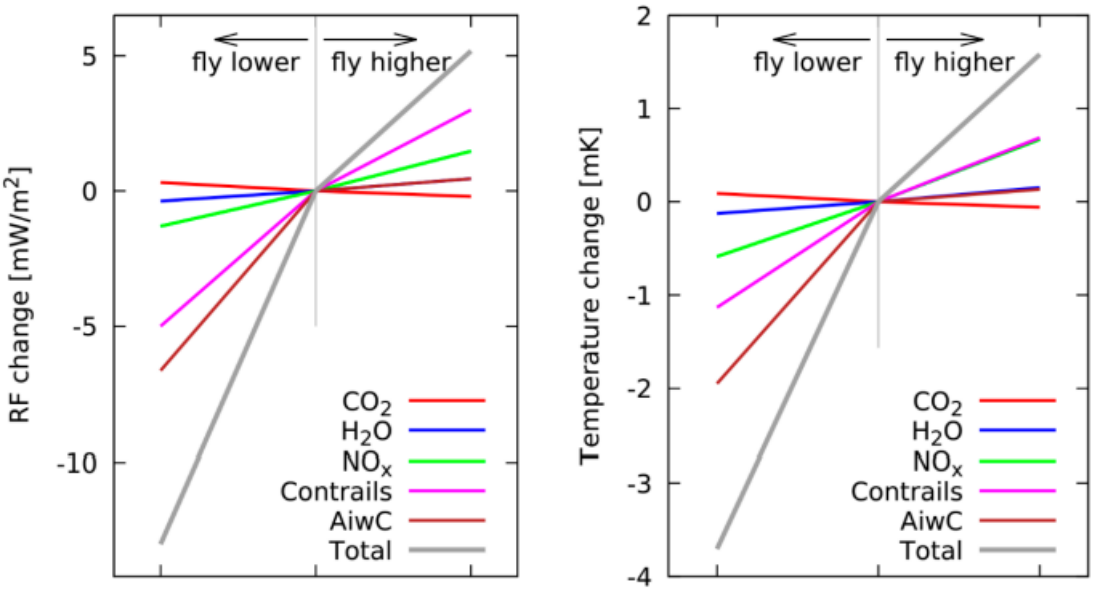

Figure 7: The effect of changing the altitude on the radiaitve forcing and temperature of the climate forcers: CO_2, water capour,net nitrogen oxides induced impact, contrail cirrus, aerosol indirect effect on warm clouds(AiwC)[4]

formation, which has the largest contribution to the climate impact of aircraft[2]. Only when the aircraft was designed for ATR_{100} did it perform better than a conventional aircraft with a conventional combustion chamber [64].

Another operational measure that could be implemented to reduce the climate impact of aviation is formation flying, which is similar to bird flight. This would result in a 14% reduction in fuel consumption and a 24% reduction in NO_x emissions for the following aircraft, with only a 3% increase in both measures for the leader, resulting in a group of two with a 6% reduction in fuel consumption and an 11% reduction in NO_x emissions. For this total, it is determined that both aircraft fly together for 83% of the flight and 3% of the distance to the rendezvous [65].The advantage of this mitigation option is that it does not require a lengthy development period; however, it is only applicable to a small portion of flights and advances in air traffic control are required.

Finally, intermediate stop operations in which intermediate stops are made for refueling could decrease the fuel consumption and thereby also the operational cost. This strategic operational measure could reduce the fuel consumption and CO_2, H_2O and SO_2 emissions by 4.8 % and decrease the NO_x emissions by 4.6%. However, this increases the CO and HC emissions by 33% and 43% respectively, as these are released during landing, descent and approach. Furthermore, it is shown that this results in an increase in warming effect (ATR_{100}), due to the aircraft flying higher when applying this procedure [66].

Noise reduction could be obtained by increasing the bypass ratio of the engine. As more airflow is passed around the combustion chamber with respect to passing through it allows the exhaust velocities to be reduced more due to mixing. This reduced exhaust velocity could result in a 8dB lower noise when going from a bypass ratio of 6 to 14[47]. However, increasing the bypass ratio above 10 would decrease the fuel performance due to significant parasite drag of the large fans and a decrease in sealevel thrust [47]. Furthermore, the nozzle design could incorporate a serrated design known as chevron, which improves the mixing of the exhaust flow with the atmosphere and results in less noise [67]. Finally, most blended wing body designs position the engines on top of the body, shielding the ground from noise, resulting in less noise perceived on the ground.

3.5 Uncertainties in Climate Modeling

Climate response modeling consist of integrate non-linear relations between the emissions and the earth's climate system. However, it is important to acknowledge that there are several gaps in the understanding of climate modeling and that most models are constructed with significant assumptions. This ensures that significant uncertainties arise in these climate response models. Several sources of uncertainty in the climate response

modeling in aviation are:

- Radiative forcing of contrails: There is a significant uncertainty in quantifying the radiative forcing of contrails as they are dependent on the contrail coverage and optical depth [68].
- Aerosol-contrail interactions: Aerosols have an impact on the formation on contrails, but due to the complexities of this process uncertainties exist, that could result in an increased warming effect or even cooling effects.
- Climate sensitivity: There exist uncertainties in the exact value of climate sensitivity, such that the magnitude of the climate response could be modeled inaccurate.
- Regional variation: As described by Grewe regional variations in atmospheric conditions, including temperature, humidity, and wind patterns should be taken into account [50]. Uncertainties exist in accurately representing these regional variations and their influence on the climate response, if they are even accounted for.
- Emission scenarios: The emissions directly proportional to fuel burn could be determined accurate, but for example NO_x and soot emissions are heavily dependent on the operational engine conditions, such that uncertainties arise. Furthermore, alternative fuel sources would also increase the uncertainties of emission scenarios.

Dallara performed uncertainty quanitifcation studies with a Monte Carlo analysis that demonstrated that a 66% likelihood ranges exist for reductions in ATR relative to the reference aircraft. This implies that for comparative studies reductions in ATR could be considered with some certainty, due to the fact that the same model is applied with the same uncertainties. Furthermore, did it show that it was more probable to have greater reductions than smaller reductions in ATR than computed [3].

4 Operational Cost

This section provides an overview of operational cost and their significance. Following that, a model for calculating direct operating costs is described.

4.1 Introduction to Operating Cost

Operational cost is an important design goal in aircraft design because it directly impacts an aircraft's economic viability and success. Lowering operational costs boosts airline and operator profitability and competitiveness. Operating costs such as fuel consumption and maintenance can be reduced by designing for efficiency, which includes aerodynamic optimisation, lightweight materials, and advanced propulsion systems. This not only improves financial sustainability but also makes air travel more affordable for passengers. Aircraft designers can meet market demands, deliver financially viable solutions, and contribute to aviation industry sustainability by prioritising operational costs. This have led to the fact that the primary focus of commercial aircraft design is on producing aircraft that meets the requirement at minimum operating conditions [47].

Additionally, reducing operational costs could align with environmental goals, as it often leads to lower fuel burn and lower emissions. For example research on a BWB showed a 20-25% reduction in fuel burn, which translated in a 10-12% reduction in direct operating cost [13, 16]. However, later studies have shown that designing for operational cost does not align with designing for minimising the global warming impact not even when a design for minimal fuel consumption is considered. Because the mach number is higher of an aircraft design for minimum operational cost, as the costs are heavily depend on the flight time does it fly at a sub-optimal velocity [47, 7, 66].

4.2 Direct Operating Cost Estimation Method

A method presented by Roskam could be used to estimate an aircraft's operational costs [69]. This method calculates the cash operating cost of an aircraft design in US dollars per seat per kilometre or for an entire fleet by taking two major contributions into account: flight-related costs and maintenance costs.

Fuel and oil costs, crew salaries, and insurance are all part of the flight costs. The costs of fuel and oil per seat per kilometre are calculated using Equation 14 and Equation 15, respectively [69]. These equations show that the cost of fuel and oil is affected not only by the properties of the fuel and oil, but also by the range, mass, time, and passengers.

$$C_{\text{fuel}} = \frac{m_{fuel,\text{bl}}}{r_{\text{bl}} \cdot N_{\text{pax}}} \cdot \frac{C_{f,\text{gal}}}{\rho_{\text{fuel}}} \tag{14}$$

$$C_{\text{oil}} = \frac{m_{\text{oil}}}{r_{\text{bl}} \cdot N_{\text{pax}}} \cdot \frac{C_{\text{oil, gal}}}{\rho_{\text{oil}}} = \frac{0.7 \cdot N_{\text{eng}} \cdot t_{\text{bl}}}{r_{\text{bl}} \cdot N_{\text{pax}}} \cdot \frac{C_{\text{oil,gal}}}{\rho_{\text{oil}}} \tag{15}$$

The costs of a single flight crew are estimated in USDs per seat per kilometre with Equation 16, which shows that this is dependent on the flight time amount of passengers and salaries. Finally, an annual hull insurance rate in USDs per USDs per airplane per year is required.

$$C_{\text{crew member}} = \frac{1}{N_{\text{pax}} \cdot V_{\text{bl}}} \cdot \left[(1 + k_j) \cdot \frac{\text{sal}_{\text{crew member}}}{\text{ah}_{\text{crew member}}} + t_{\text{ef}} \right] \tag{16}$$

These equations from flight-related costs show that flying at a high velocity may be advantageous because it reduces oil costs and crew costs by having a shorter block time. However, this may increase the amount of fuel used.

The labour rates of the airframe and engine engineers, as well as the costs for spare parts, are included in an aircraft's maintenance costs. The prices for the airframe and engine spares are computed with Equation 17 and Equation 18 respectively. These equations are dependent on the operational empty weight in kilograms and the static take-off thrust in kilonewtons respectively.

$$P_{\mathrm{AC},2020}[2020 \text{ USD }] = 0.0052 \cdot \mathrm{OEM}^{0.927} \cdot 10^6 \tag{17}$$

$$P_{\mathrm{eng},2020}[2020 \text{ USD }] = 0.1604 \cdot T_{\mathrm{TO,\,eng}}^{0.878} \cdot 10^6 \tag{18}$$

Depreciation and other fees associated with financing and operations could also be taken into account, but will be assumed outside the scope of the research, as these categories are thought to be more uncertain and influenced by company choices. The cost of financing, for instance, may change depending on whether the aircraft is purchased or leased. Indirect operating costs like those associated with passenger services, station operations, promotion, and administration are also not taken into consideration in the analysis.

Finally, the operational costs are all calculated per kilometre per passenger per aircraft. However, for the analysis in this research the entire fleet is of importance, because the climate impact is either determined over the entire fleet. As a result, the fleet's direct operational cost should be calculated, which could be done with Equation 19, where $\mathrm{RPK}_{AC,ann}$ is the annual amount of revenue passenger kilometres by one aicraft, N_{yr} is the operational life of an aircraft and N_{AC} is the total fleet size. The N_{yr} and N_{AC} are variable due to differences in block time and thus productivity.

$$\begin{aligned} &C_{\mathrm{ops,fleet}} = C_{\mathrm{ops,\,AC}} \cdot \mathrm{RPK}_{\mathrm{AC,ann}} \cdot N_{\mathrm{yr}} \cdot N_{\mathrm{AC}} \\ &= (C_{\mathrm{fuel}} + C_{\mathrm{oil}} + C_{\mathrm{crew}} + C_{\mathrm{insurance}} + C_{\mathrm{maintenance}}) \\ &\cdot \mathrm{RPK}_{\mathrm{AC,ann}} \cdot N_{\mathrm{yr}} \cdot N_{\mathrm{AC}} \end{aligned} \tag{19}$$

5 Aerodynamics

This chapter describes provides an overview of the procedure for aerodynamic analysis. The cruise performance, wing geometry, and maximum lift coefficient are the most important parameters that must be determined by the aerodynamic analysis. The Flying-V has only one maximum lift coefficient, because it lacks high lift devices. The cruise performance is critical for determining the amount of fuel burned and the emissions produced. Wing geometry is important for wing loading and weight, and the maximum lift coefficient is required to evaluate stall speed, approach speed, take-off performance, and climb performance.

5.1 Initial Sizing of the Wing

In order to evaluate the drag polar of a wing an initial sizing procedure is required. The initial sizing of an aircraft is in most cases performed by a class-I sizing method. These method describe the overall design variables from simple analytical relations. The wing area (S) and take-off thrust (T_{TO}) are initially sized with this method. These are determined by computing the maximum required sea-level thrust-to-weight ratio for three critical performance conditions as described by the ICAO: take-off distance, the cruise mach number at the beginning of cruise and the second-segment climb gradient with one-engine inoperative condition. Roskam provides such a method [70].

After the initial sizing is computed the drag polar has to be computed as a function of its geometry. The geometry is influenced by selected design variables and is parameterised for the Flying-V in subsubsection 2.2.5.

5.2 Drag Polar

This drag polar must be iterated multiple times because it is required back into the class-I sizing, propulsion, and mission sizing. As a result, it should be evaluated using simple methods that rely on Kutta-conditions, such as the Euler method or potential flow panel methods with integral boundary layer equations, rather than methods that require expensive computational work, such as RANS or even real-life experiments, such as wind tunnel testing. However, the RANS equation can measure turbulence, viscosity, and heat transfer, whereas the Euler model cannot. As a result, viscosity-related drag is not taken into account, but it accurately predicts shock waves and their effects, providing a good estimate for wave drag in the transonic regime [71]. Finally, because potential flow assumes irrotational flow, it does not account for these shockwaves, resulting in no wave drag approximation and overestimation in the transonic regime.

The drag polar could be determined by the method described by obert which assumes a quadratic drag polar that consists of a part of drag dependent to lift that depends on the aspect ratio an Oswald factor (e) and a part of drag independent to lift, which consists of friction, profile and excrescence drag. According to this method the pressure drag of all the components need to be determined with a flow solver method as lifting line method, which will be described below. Furthermore the aircraft size-dependent and independent excrescence could be determined with analytical relations. Finally, summing all these drag components would lead to the final drag polar [72, 7].

A simpler method is to determine the zero-lift drag coefficient from earlier obtained zero lift drag coefficients. In this method the drag coefficient is assumed only dependent on the difference in wetted wing area, as given in Equation 20, where the hat indicated the earlier reference value [36]. The advantage of this method is that if research is available on the zero lift drag of the aircraft under investigation no further aerodynamic model is required to compute all the separate drag components. However, it does rely on several assumptions that make it only applicable if only small changes are made in the wing geometry such that the wing loading remains similar. This will not be the case for an optimisation of the climate effects as earlier research show large variations in planform design [7, 47].

$$C_{D_0} = \hat{C}_{D_0} \frac{s_{\mathrm{w}}/s_{\mathrm{ref}}}{\hat{s}_{\mathrm{w}}/\hat{s}_{\mathrm{ref}}} \tag{20}$$

5.3 Aerodynamic Flow Solvers

There are several aerodynamic flow solver methods available to compute the lift and drag of an aircraft. The decision on the aerodynamic model is a trade-off between computational cost and accuracy of the result. Ranging from results that rely on a lot of simplifying assumptions as the lifting line method that gives result in a matter of seconds or computational fluid dynamical models that could take days to converge to a solution. Several of these models are described below.

The lifting line method is a technique for aerodynamic analysis that approximates a wing as a row of lifting elements known as horseshoe vortices. It computes the lift distribution along the wing span, moment distirbution and induced drag using vortex theory and mathematical equations such as the Kutta-Joukowski theorem and the Biot-Savart law. The lifting element is associated with a circulation, which determines the strength of the vortices generated. The lift distribution along the span can be calculated by satisfying the boundary conditions at the wingtips [73]. This model has to lowest computational cost, but also the lowest accuracy, as it relies on irrotational, inviscid, two-dimensional flow. XFLR5 is an example of a program that applies the lifting line method.

An extension of the lifting line method is the Vortex lattice method (VLM) ass a sequence of lifting lines are used. VLMs leverage the idea that the normal component of the induced velocity on any point of this surface should be zero since no flow crosses the lifting surface and describe a lifting surface as a sheet of horseshoe vortices[73]. Vortex lattice methods analyse the aircraft lift, moment and induced drag in a computationally efficient manner, making them appropriate for conceptual design studies, performance prediction, and optimisation. These methods, however, rely on simplifying assumptions, such as inviscid, incompressibility, thin surfaces and small angles of attack, which restrict their accuracy. Athena Vortex Lattice (AVL) is a program that applies this method. The advantage of AVL over a simple lifting line method is that it allows the computation of stability derivative from provided mass distributions and trimming of the aircraft from defined control surfaces. AVL computes the stability derivatives with the direct approach such that the force and moment equations are implicitly differentiated with respect to the various parameters using the chain rule [5]. Since AVL is inviscid, the stability derivatives that are less influenced by viscous effects, such as C_{l_p} and C_{n_p}, are determined more precisely [24]. These values are important parameters for the lateral-directional stability of the aircraft, hence accurate estimation of these parameters is beneficial. Several studies On the flying-V also applied this method. Faggiano applied AVL to check the feasibility of design vectors before optimising it with more extensive models and Oosterom applied it in combination with a viscous model to evaluate the aerodynamic performance of the flying-V family design [23, 5]. Odilla is another vortex lattice method that computes the lift, moment and induced drag of an aircraft. It relies on the same assumptions, hence it ommits thickness and viscosity, but does account for nacelles, high lift devices, control surfaces, taper, twist and camber.

Quasi three-dimensional solver (Q3D) is an aerodynamic model made by Mariens, Elham and Van Tooren at Delft University of Technology. This model overcomes the limitation of AVL, that gives fast three-dimensional inviscid results by combining it with a viscous drag approximation model for a 2D airfoil (XFoil, VGK & MSES). This makes it possible to quickly calculate the lift, moment and also drag of an aircraft such that it could be applied in multi-diciplinary optimisation [74]. The 2D airfoil models implemented differ in the fact that XFoil is limited to Mach numbers below 0.7 and the other two are applicable in the transonic regime, but both increase the computational time required.

XFLR5 is a similar method that combines a lifting line method, vortex lattice method or 3D panel method with the 2D airfoil model XFoil, but as already stated above this is limited to mach numbers below 0.7, hence it is not applicable to the transonic flying-V [5].

6 Propulsion

This section discusses various methods for modelling the propulsion unit. The first method outlines how to employ a real reference engine. Following that, two models based on thermodynamic cycle calculations are described briefly. Finally, some potential improvements to turbofan engines are discussed.

6.1 Application of a Reference Engine

Estimating fuel burn and emissions accurately is critical for assessing an aircraft's environmental impact. To accomplish this, a suitable model for evaluating the propulsion unit must be chosen. The use of a comparable engine is one method of analysing the Flying-V aircraft's propulsion system. To achieve accurate results, it is necessary to account for the differences in take-off weight between the two aircraft. The A350-900, which has performance characteristics similar to the Flying-V, is an appropriate reference aircraft for engine analysis. Given this similarity, using the Trent-XWB-84 engine, which meets the power requirements of the A350-900, is a viable option. As a result, it is reasonable to consider using this engine in the analysis of the Flying-V aircraft.

However, the Flying-V's lower take-off weight must be considered. To ensure accurate results, the engine should be scaled down proportionally to the A350-900's take-off weight. This scaling methodology assumes that both aircraft have a consistent thrust-to-weight ratio, implying that the Flying-V's thrust-to-weight ratio scales similarly with wing loading. It is important to note that additional research is needed to validate this assumption, specifically for the Flying-V aircraft [5].

Given the Flying-V's unique wing configuration and loading characteristics, additional research is required to confirm the thrust-to-weight ratio assumption. These analyses should take into account the Flying-V's unique design features, such as the blended wing-body, which may influence the scaling relationship between thrust, weight, and wing loading.

Another problem with this model is the fact that it only gives an insight in the on design performance of the propulsion unit. However, for the evaluation of the environmental impact the off-design performance are also off importance, as for example a large portion of the NO_x formation happens at take-off and landing.

A method to calculate the NO_x emissions at off-design phases is the fuel flow correlation method. The Fuel flow correlation methods computes the NO_x emissions based on ambient conditions, fuel flow rate and ICAO landing and take-off certification data. The Boeing Method 2 is an example of a fuel flow correlation model [55].

6.2 Thermodynamic Cycle Calculations

The accurate modeling of an engines design and off-design performance could be done with external programs, such as Gas Turbine Simulation Program (GSP). This program makes it possible to model the steady state and transient performance of a turbine engine by drag and dropping the required components to make the desired engine configuration. This allows for the creation of existing turbofan engines with the real performance maps. By applying thermodynamic cycles and a full thermo-chemical gas properties model it is possible to evaluate the gas conditions, species and fuel flow at the given design points[75]. Hence this could be applied to model the design and off-design performance of a comparative engine, but it is a lot more computationally expensive.

Another option is to design a less accurate engine model based on the assumption of constant component efficiencies, reducing the need for component maps while still evaluating off-design performance using thermodynamic cycle calculations. Such a model would be able to calculate the pressure and temperature at each stage, fuel flow, and overall efficiency of the turbofan engine from standard engine variables such as the different pressure ratios (fan pressure ratio Π_{fan}, low pressure compressor ratio Π_{lpc} and high pressure compressor ratio Π_{hpc}) turbine inlet temperature, bypass ratio, component efficiencies (mechanical efficiency, polytropic efficiency, and pressure losses), and ambient conditions. This method has the advantage of being computationally efficient for a simple twin spool turbofan engine with no additional features. This method has the advantage of being computationally efficient for a simple twin spool turbofan engine with no additional features such as a reheater, intercooler, or recuperator. However, it does allow for the inclusion of design variables that are important for an aircraft's climate assessment and could take into account the variation of specific heat with temperature

[76, 77, 7].

Both the thermodynamic cycle calculations only provide the thermodynamic properties and efficiencies. While for the analysis of the entire aircraft the weight and size of the engine is also of importance, as these are required for the aerodynamic and structural calculations. The fan diameter could be calculated from thermodynamic properties, axial mach number, bypass ratio, core mass flow and hub-to-tip ratio[76]. The mass of the engine could be calculated with software as WATE++, but a relation depending on the core mass flow, core pressure ratio and bypass ratio will either suffice [7].

6.3 Turbofan Engine Design Trends and Improvements

Several engine design features can improve the performance of a turbofan engine. A reheater, also known as an inter turbine burner, is an additional burner placed between high and low pressure turbine that increases specific power output while increasing heat rejection, resulting in a lower thermal efficiency. An intercooler is installed between the two compressors to cool the air in front of the high pressure compressor. This reduces the amount of work required by the high pressure compressor while increasing the amount of heat required to reach the turbine inlet temperature. As a result, it increases fuel flow while decreasing efficiency. A recuperative system transfers heat from the turbine to the flow in front of the combustor, lowering heat rejection and increasing thermal efficiency. This, however, results in less thrust power. Finally, an additional spool or gear could be installed to allow the fan to spin independently of the low pressure compressor. This improves the fan's efficiency because it can run at its optimum velocity, but both options result in increased weight and mechanical complexity. All of these effects could be combined into a single engine, resulting in a more efficient and higher thrust outputting engine, but this would increase the design and model's complexity. Furthermore, would this result in the addition of design variables that are unrelated to the research at hand. As a result, these features are disregarded because engine-specific research is more appropriate to study this.

Increased thermal efficiency and propulsive efficiency of an engine could improve overall engine efficiency. However, the manner in which both increase is in conflict. When the component efficiencies improve, so does the thermal efficiency. Furthermore, it rises with turbine inlet temperature and overall pressure ratio as more energy is extracted from the flow in the turbine. Although this reduces SFC and CO_2 production, it increases NO_x formation.

The bypass ratio could be increased to improve propulsive efficiency, but because this results in a larger fan diameter with a higher mechanical power requirement, the fan pressure ratio must be reduced. The fan pressure ratio must also be reduced so that the tips do not rotate excessively fast. Furthermore, increasing the temperature of the turbine inlet increases heat losses inside the core nozzle, resulting in a decrease in propulsive efficiency.

7 Mission Analysis

A relevant mission must be designed in order to evaluate the total performance of an aircraft fleet over its lifetime. This standard mission profile is depicted in Figure 8. The mission profile includes all of the phases that an aircraft must be able to complete. Most of these phases are not carried out during a normal flight, but the reserve fuel for the diversion to another airport and loitering must be carried on board and adds to the maximum take-off weight (MTOW), such that the aircrfat structure is designed for it, hence it could not been omitted from the analysis. The initial cruise altitude is kept as a variable in this mission profile because it has a significant impact on the climate, as described in section 3. However, it is constant during an analysis meaning it does not apply a step-climb procedure, which is in reality often the case. Finally, the cruise range is kept constant to the design range.

An aircraft is designed such that it can transport payload over a certain range. However, the range an aircraft could fly is dependent of the payload mass as with less mass the aircraft requires less thrust. A payload-range diagram, as depicted in Figure 9, gives the payload over range of aircraft, for various design conditions. In this research the cruise range is the design cruise range, which is given by the point D in the figure. At this point an aircraft is able to have an increased range with less weight or carry additional payload for a shorter range.

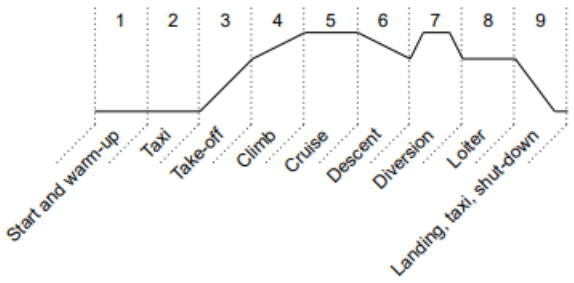

Figure 8: The standard mission design [5]

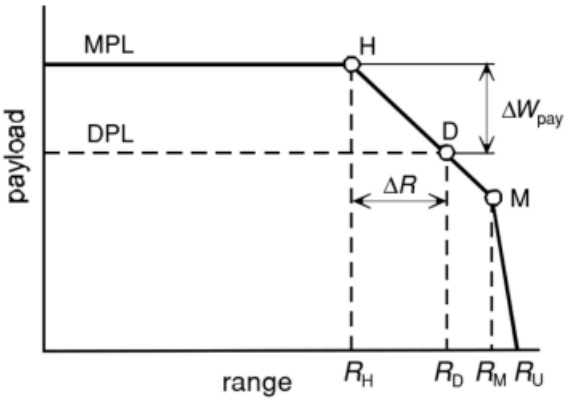

Figure 9: Generic payload-range diagram from Torenbeek[6]

In the mission analysis it is of interest to see how much fuel is required to complete this mission. There are multiple approaches that could be applied to calculate the amount of fuel required. The lost-range method is on of them. This method computes the fuel mass to takeoff mass ratio for the standard mission from the cruise range, altitude, lift-to-drag ratio and engine overall efficiency according to Equation 21, where the first term accounts for the cruise phase, second for the take-off and climb phase and the last term for maneuvering. Two additional formulas are needed to account for loitering and diversion, such that the total ratio could be calculated with Equation 22.

$$\begin{aligned} \frac{m_{\text{fuel,mission}}}{m_{\text{TO}}} &= \frac{r_{\text{cr}}/R_H}{p + (1/2) \cdot r_{\text{cr}}/R_H} + \frac{h_{\text{cr,eq}}}{0.7 \cdot \eta_{\text{ov,cr}} \cdot R_H} + \frac{0.0025}{\eta_{\text{ov,cr}}} \\ \text{where } R_H &= \frac{\text{LHV}}{g}, \quad p = \eta_{\text{ov,cr}} \cdot \left(\frac{L}{D}\right)_{\text{cr}}, \quad h_{\text{cr,eq}} = h_{\text{cr}} + \frac{V_{\text{cr}}^2}{2 \cdot g} \end{aligned} \tag{21}$$

$$\begin{aligned} \left(\frac{m_{\text{fuel}}}{m_{\text{TO}}}\right)_{\text{total}} &= \frac{m_{\text{fuel,mission}}}{m_{\text{TO}}} \cdot \left[1 + \left(\frac{\Delta m_{\text{fuel}}}{m_{\text{fuel,mission}}}\right)_{\text{div}} + \left(\frac{\Delta m_{\text{fuel}}}{m_{\text{fuel,mission}}}\right)_{\text{hold}}\right] \\ \text{with } \left(\frac{\Delta m_{\text{fuel}}}{m_{\text{fuel,mission}}}\right)_{\text{div}} &= 1.20 \cdot \frac{r_{\text{div}}}{r_{\text{harm}}} \\ \text{and } \left(\frac{\Delta m_{\text{fuel}}}{m_{\text{fuel, mission}}}\right)_{\text{hold}} &= 0.20 \cdot t_{\text{hold}} \cdot \frac{R_H}{r_{\text{harm}}} \cdot \left(1 - \frac{m_{\text{fuel,mission}}}{m_{\text{TO}}}\right) \end{aligned} \tag{22}$$

Another approach in estimating the fuel weight is the so called fuel fraction method. The fuel fraction method describe the ratio between start and end weight of an aircraft per mission segment. For almost all the phases

are estimates for transport jets given by Roskam, except for the cruise, diversion and loiter phase. The fuel faction of the cruise phase could be determined with the Breguet range equation, which is given in Equation 23. This equation calculates the fuel fraction from the specific fuel consumption(SFC), cruise velocity, L/D and design range. The diversion and loiter phase is taken into account by adding 5% reserve fuel [70], but could also be calculated with the Breguet range and endurance equations. Finally, this method does not take into account the distance flown in the climb and descend phase, since this could be in different directions than the destination is [6].

$$R = \frac{V}{SFC}\frac{L}{D}\ln\left(\frac{W_{cr_{\text{start}}}}{W_{cr_{\text{final}}}}\right) \tag{23}$$

Both methods depend on engine performance and aerodynamic performance to evaluate the mission fuel burn, but the lost range method applies a more elaborate way of determining the diversion and loitering phase. Furthermore, it has a higher dependence on the altitude, as it is already in the equation instead of incorporated in the velocity. Finally, the Breguet range equation already uses the specific fuel consumption, where the lost range method uses the overall engine efficiency and a separate lower heating value (LHV), hence it is more dependent on the fuel quality.

The advantages of these methods are that they are fully analytical and can be quickly executed, which is ideal for the convergence to the MTOW. However, this method misses a lot of components that are required for the evaluation of the climate impact. Because the emission of NO_x is heavily dependent on off-design performance of the engine and the ambient conditions do play a significant role in the formation of NO_x and contrails, as described in section 3. Therefore, a more detailed mission analysis is needed for the evaluation of the climate impact.

8 Optimisation and Design Space

The multidisciplinary analysis and optimisation (MDAO) workflow and design space exploration are described in this section, as the goal of this research is to assess and minimise the flying-V's climate impact and direct operating cost. A vast design space must be explored using a multidisciplinary approach in order to achieve optimal aircraft design. The various disciplines involved in optimisation have already been discussed in the preceding sections. However, all of these disciplines must be coupled and arranged, and all relevant design variables must be determined. This section will begin with the optimisation problem, followed by an overview of the relevant design variables. Finally, the workflow for optimisation is described.

8.1 Optimisation Problem

An optimisation problem always consist of five components: the objective function, the design vector, inequality constraints, equality constraints and boundaries. The main purpose of this research is to perform a multi-objective optimisation creating a Pareto-front from which a trade-off between a design for climate impact and direct operating cost could be made. However, first due to the complexity of a multi-objective optimisation, two separate single objective optimisation of the climate impact and the direct operating cost of the flying-V has to be performed.

8.1.1 Single Objective Optimisation

The single objective optimisation problem for the optimisation of the climate impact and the direct operating cost of a fleet of flying-V is defined as follows:

$$\min_{x} \text{imise} F(\mathbf{x}) = \text{ATR}_{100}(\mathbf{x}) \text{ or } C_{\text{ops,fleet}}(\mathbf{x}) \tag{24}$$

The design vector $\mathbf{x}$ still has to be determined. However, an analysis of the parameters that are considered are described in further detail in subsection 8.2. The constraints either need to be determined in a further research, but the sources and possible constraints are described in subsubsection 8.1.2.

The goal of an optimisation problem is in most cases to find a minimum or maximum. The optimum point of the problem could be found in various ways, but is always an iterative process that starts from an initial guess and iterate until no better design is found.

The simplest way to do this is calculating almost every point, but this in most cases to exhaustive, so that it could take decades. Methods according to this way are called zeroth order, as they do not rely on gradients. Other methods of this order are Nelder-Mead, Genetic algorithms and Particle Swarm and have the advantages that they as robust and suitable for global search without deep knowledge of the models. Genetic algorithm are also known as evolution algorithms and are described in subsubsection 8.1.3.

Higher order functions as first order methods, that rely on first derivatives (Steepest descent, conjugate and Quasi newton) and second order methods that rely on first and second derivatives (Newton) are computationally more efficient and allow for mathematical verification. However, they do not ensure that the minima found is global or local and are not capable for discontinuous or discrete design variables and functions.

8.1.2 Constraints

In optimisation problems, constraints are critical for ensuring feasibility, safety, regulatory compliance, operational efficiency, and system integration. They help define the parameters within which an optimal solution must be found while taking real-world constraints and requirements into account. Different authorities establish safety regulations in the aviation industry, but the ICAO establishes international standards. As a result, there are numerous constraints.

The most important constraints for preliminary aircraft sizing imposed by the ICAO are airport requirements. The Flying-V will be classified in the same category as the A350-900, and thus will be subject to the same

ICAO regulations, which are code E and aircraft approach category C [78].

In category C, the minimum approach speed of 135 to 140 knots limits wing loading at maximum lift coefficient. The ICAO code E specifies the minimum field length, which is 1800 metres. Furthermore, it establishes hangar size requirements, as the aircraft must be stored in a hangar. The regulations state that the wingspan must be between 52m and 65m, and the tail height must be less than 20.1m and its outer main landing gear span within 14m.

Another constraint could be imposed on the TIT during take-off because the material must be able to withstand high thermal loads, which could result in material failure and a decrease in thermal efficiency; this limit could be set at 2000K [77].

The lift coefficient could be constrained in a variety of ways. For starters, as the lift coefficient decreases with wing sweep, so does the maximum attainable lift coefficient; thus, a maximum lift coefficient limit may be required. Finally, in transonic flight during cruise, buffeting may occur, which should be avoided by setting a limit on the lift coefficient at which buffeting occurs.

The CS25 ans FAR25 impose a lot of requirements on the stability and control of transport aircraft to ensure a safe handling of the aircraft. The CS25 part 171, 173, 175 and 177 are on stability and control in general, longitudinal, directional and lateral respectively and should be abide to by the Flying-V.

Static longitudinal stability has to be ensured. A constraint for this parameter is often given in the form of a static margin, which is the allowed location of the centre of gravity in front of the neutral point, as given in Equation 25a . A minimum of 5% static margin should provide sufficient stability, but makes it also possible to trim the aircraft at high angles of attack [27]. Furthermore, no pitch break at high angles of attack should occur.

Directional stability is ensured when the yawing moment derivative is positive or even above 0.0005, as given in Equation 25b and lateral stability is ensured when Equation 25c [23]. Dynamic stability should either be ensured such that the dutch roll mode, short period, phugoid, aperiodic roll and spiral are stable.

The ICAO proposes additional safety regulations considering special manoeuvres. First, the aircraft should be able to take-off in one engine inoperative condition. Secondly, the aircraft should be able to land in maximum cross wind condition.

$$\mathrm{SM} = \frac{(x_{\mathrm{np}} - x_{\mathrm{cg}})}{\bar{c}} > 0.05 \quad (25a)$$

$$C_{n_\beta} \geq 0.0005 \quad (25b) \qquad C_{l_\beta} \leq 0 \quad (25c)$$

The ICAO also establishes regulations for overall CO_2 emissions and NO_x emissions during the landing and take-off cycle, but because the focus of this research is on minimising aircraft's climate impact, these are ignored. However, it may be worthwhile to assess how well it performs in relation to these values. The noise regulations are either ignored or ignored because noise estimation is considered outside the scope of this research.

RAMS (reliability, availability, maintainability, and safety) constraints are not considered; however, availability and maintainability are considered in the form of an aircraft's lifetime, number of flights per year, and maintenance cost.

8.1.3 Multi-objective Optimisation

As already described in section 3 climate climate impact and direct operating cost are conflicting objectives, hence no single solution exists that is a minimum for both objectives. However, it is of interest to find a set of trade-off optimal solutions known as Pareto optimal solutions or non-dominated solutions. These are the solutions, that arise from a multi-objective optimisation problem (MOOP), for which there are no other solution better than the current one in some objective function without worsening other objective functions, hence a non-dominated set is better compared to the rest of the solutions.

There are three major distinctions between single objective and multi-objective optimisation. For first of all, there are multiple optimal solutions rather than just one. This could also exist in a multi modal single objective

optimisation, but in MOOPs, the Pareto-optimal solutions have decision values that have similarities, which is not the case in multi modal problems [79]. Second, MOOPs have two goals: convergence to Pareto-optimal solutions and retaining the greatest possible spread among the set of solutions. Finally, there are multiple search spaces that allow for flexibility in search algorithms [80].

Finally, because every engineering problem should result in a single design, the MOOP must also result in a single solution. This could be accomplished using two approaches: a priori approach and a posteriori approach. The posteriori approach first finds a set of optimal solutions, after which a final design is chosen from higher level requirements. In the a priori approach, this is done the other way around, by first defining the higher level information, and then converting the MOOP into a SOOP using weight factors from a preference vector. However, without knowledge of the consequences, it is difficult to construct a good preference vector in this manner [80].

There are several methods available to perform a MOOP in the posteriori approach. These methods could be divided into three classes: Mathematical programming-based methods, Evolutionary algorithms and deep learning methods.

Mathematical programming-based methods run the same algorithm multiple times, where every run a single new Pareto-optimal solution is found. These methods solve the MOOP by constructing several scalarisations. Scalarisation is the classical method of solving a MOOP by constructing a SOOP from the set of objectives, with the application of scalarising parametres.

The simplest approach belonging to this category is the weighted-sum approach. In which each objective is multiplied with a weight forming the single objective optimisation, as described in Equation 26. The problem with this method that defining the weights is difficult, but could be avoided by first normalising the objective functions, before adding them to the composite objective function. Then the sum of the weights has to be one. However, applying this method to find a set of Pareto-optimal solutions result in two difficulties: firstly, a uniform choice of weight vectors does not always find a uniform set of Pareto-optimal solutions and this procedure can only find solutions on a convex portion of the Pareto-optimal front [80, 81].

$$\min_{x} \text{imise} F(\mathbf{x}) = \sum_{m=1}^{M} w_m f_m(\mathbf{x}) \tag{26}$$

The problem with non-convex objective spaces is solved by the ϵ-constraint method. In which the optimisation problem retains one objective and treats the other objectives as a constraint ϵ. The problem with this method is that the solution depends on the ϵ vector and no or wrong results can be obtained by having too large or too small values [80].

The subproblems must be executed many times in order to find a complete set of non-dominated solutions using these methods. However, evolutionary algorithms can simultaneously find a set of non-dominated solutions. Evolutionary algorithms emulate nature's evolutionary principles by searching for optimal solutions from a large population of solutions via a generational process of selection and elimination. Most evolutionary multi-objective optimisation algorithms consist of three operations: the non-dominated solutions are searched to find the Pareto-front, a niching operation is performed to maintain diversity among the solutions and an elite-persevering operation is applied to speed up convergence. Well known evolutionary multi-objective optimisation algorithms are the non-dominated sorting genetic algorithm (NSGA-II) and Strength Pareto Evolutionary Algorithm 2 (SPEA-2). Both these methods follow a population based evolutionary algorithm. A generic example of these strategies is described below [80]:

- Step 1 A population P and an empty archive A are initialized. The non-dominated solutions of P are copied in A
- Step 2 A set of λ new offspring solutions are created using P and A.
- Step 3 Every new offspring solution is checked for its inclusion in A by using a archive-acceptance criterion CA and for its inclusion in P by using a population-acceptance criterion CP. If an offspring is not to be included to either P or A, it is deleted.
- Step 4 Iterate step 2 and 3 until the termination criterion is satisfied
- Step 5 Before termination, the non-dominated set of the archive A is declared as the efficient set.

However, these methods do not guarantee convergence, hence a post-optimality study is needed after the computation. In order to check if the Pareto front found is the global Pareto-font and not a local one. EMO algorithms does have difficulties in handling a lot of objectives, but that is not of importance for this research, as only a bi-objective optimisation problem is of interest[80]. Finally, the process could be speed up and convergence could be improved by adding the extreme values obtained in the single objective optimisations to the initial population.

At last, there are new approaches that implement deep learning methods to generate Pareto optimal solutions. In these methods the deep learning algorithm finds the entire Pareto front from generalising some values on that front, this is called Pareto front learning, which makes use of HyperNetworks [82].

8.2 Design Variables

There are a lot of suitable design variables for the optimisation of the climate impact and operating cost of an aircraft, as there are various disciplines involved that are described in subsection 8.3. Although, all design variables fall under the categories: aircraft configuration, propulsion and mission profile.

Evaluating all the emitted species described in section 3, shows that the following variables have the most impact on the climate and the emitted species:

- Fuel mass (m_{fuel}), as a lot of emitted species are directly related to the burning of fuel, thus having a low fuel mass is definitely beneficial.
- Turbine inlet temperature (TIT), the production of NO_x is heavily dependent on the turbine inlet pressure, as thermal NO_x produces above 1850K.
- Engine pressure ratio (OPR), as a higher pressure ratio ensure more complete combustion, hence a reduction in fuel flow, CO_2 and UHC, but an increase in the production of NO_x and soot.
- Bypass ratio (BPR), a higher bypass ratio decreases the noise due to a decreased exhaust velocity and decreases the fuel consumption until a bypass ratio of 10, but increases NO_x and soot production as it is mostly paired with a higher OPR and TIT.
- Equivalence ratio, as a lot of the emitted species as UHC, NO_x and CO_2 will have a peak in emissions between the 0.9 and 1.05, but some as soot will only increase with equivalence ratio.
- Ambient pressure, as this is an important parameter for the formation of contrails en engine performance.
- Ambient temperature, as this is an important variable for the formation of contrails and engine performance.
- Ambient density, as this is important for the determination of the amount of fuel.
- Sea-level static thrust, as this is important for the sizing of the engine and its performance
- Engine efficiency, as this is important for the amount of fuel that is burned and the formation of contrails.

The ambient conditions could all be determined from the altitude, hence the altitude is a better option instead of three variables. Furthermore, the equivalence ratio will not be applied as it is heavily dependent on the combustor applied and the comparative study will use the same engine, as it is interested in the differences in aircraft configuration and engine operating conditions between the Flying-V designed for climate and cost and a conventional aircraft. At last, the fuel mass could be determined from the engine efficiency, which could be determined from the BPR, TIT and OPR.

The direct operating cost is the other objective that has to be optimised. The variables involved in the determination of this are the following:

- Fuel mass (m_{fuel})
- Oil mass (m_{oil})
- Operational empty weight (OEM)
- Take-off thrust(T_{TO})

- Amount of revenue passenger kilometers flown by one aircraft in one year ($\mathrm{RPK}_{AC,ann}$)
- Operational life of an aircraft (N_{yr})
- Total amount of aircraft in the fleet (N_{AC})
- Block time (t_{bl})
- Block range (r_{bl})
- Cruise Mach number (M_{cr})

The costs of everything, such as the fuel, oil and salary costs are not considered as a design variable as they will be considered constant. The oil mass will be determined with an analytical expression depending on the block time, as described in section 4. Furthermore, a standard amount of passenger over a standard mission profile will be analysed, hence the r_{bl} is constant and the $\mathrm{RPK}_{AC,ann}$, N_{yr}, N_{AC} and t_{bl} could be determined from the M_{cr}.

For the analysis of the fuel mass not only the engine efficiency and range is required, but also the mass and aerodynamic efficiency of the aircraft. In order to asses the mass and aerodynamic efficiency more design variables are required, that fall under the category aircraft configuration. The Maximum take-off weight (MTOW), wing area (S), airfoil parameters and wing sweep (Λ) could be considered. however, they are most likely to result from the parameterisation described in subsubsection 2.2.5. However, careful consideration has to be taken into what is required, such that the amount of design variables is taken to a minimum.

8.3 Multidisciplinary Analysis and Optimisation Workflow

The Flying-V is a complex system with various subsystems. In order to analyse and optimise the entire system has to be subdived into smaller managebale subsystems. The most convenient way to do this is to divide it by disciplines, because the interest of this research is in the entire system and not every small subsystem. The disciplines involved in the optimisation of the climate impact and direct operational cost of the Flying-V are the following:

- Airframe: This produces the design of the airframe by analysing the aerodynamics and the structure as described in section 2.
- Propulsion: This produces the design of the engine from performance analyses as described in section 6
- Mission: This calculates the fuel mass and block time and speed as described in section 7.
- Climate: This evaluates the climate impact of the design, as described in section 3.
- Cost: This evaluates the direct operating cost as described in section 4.

A design architecture must be implemented because the multiple disciplines involved in the analysis must be coupled. There are various multidisciplinary design optimisation (MDO) architectures for discipline coupling, with the two most common design architectures being solving the problem with an individual discipline feasible architecture (IDF) or a multiple disciplines feasible architecture (MDF).

All disciplines in an individual discipline feasible architecture are fully uncoupled and can be computed separately by adding target values for the coupled variables. Additional consistency constraints are used to ensure the consistency of these target values with the real values; thus, the optimiser is responsible for the consistency between the disciplines.

In an MDF architecture, the optimiser only has control over the design variables, whereas an multi-disciplinary analysis (MDA) process has control over the fully coupled MDA. As a result, the optimiser is unaware of the system's coupling relations, which are managed by a separate converger. The Gauss-Seidel numerical approach and the Jacobi approach are two common MDA procedures that can be used.

The Gauss-Seidel MDA procedure decouples the disciplines and feeds forward directly, but when an input that is the output of a subsequent analysis is required, the MDA coordinator will provide a target value. The MDA coordinator then iterates through these coupled variables until they converge with the target variables.

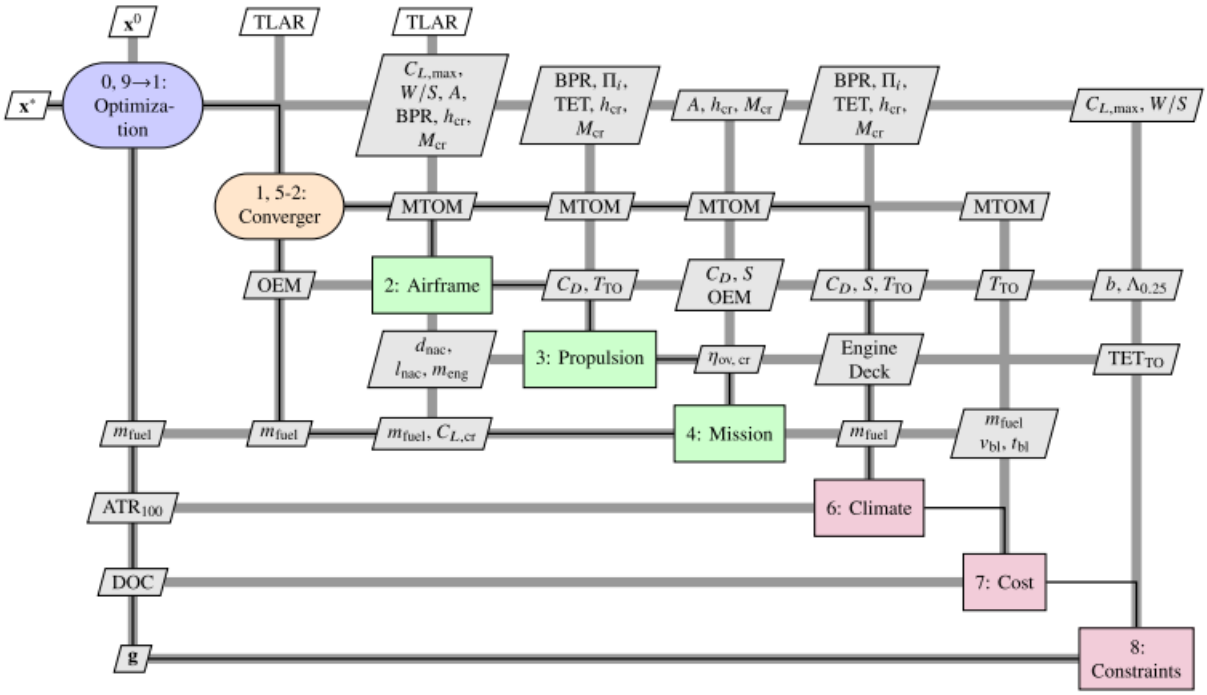

Figure 10: Extended design matrix for the multidisciplinary design workflow applied by research by Proesmans [7]

.

The Jacobi procedure completely decouples all disciplines, allowing them to run in parallel. As a result, the outputs are not feedforward, necessitating the addition of more target variables. These target variables are still provided by the MDA coordinator, who iterates until they converge.

The Gauss-Seidel method converges faster because it requires fewer target variables as the outputs are fed forward. However, if the number of target variables is not too different, parallel execution in the Jacobi procedure could result in a faster convergence.

An effective tool to represent the MDAO workflow is the extended design structure matrix (XDSM), as first introduced by Lambe and Martins [83]. In an XDSM all the coupling, information exchanges among the disciplines and architecture are presented. Figure 10 shows the XDSM applied in the research by Proesmans. This XDSM shows that it applies an MDF architecture with Gauss-Seidel procedure [7]. An almost similar workflow will be implemented in the subsequent thesis only the design variables and the models applied in the airframe discipline will change. Because the airframe discipline implemented by Proesmans was simplified and applied empirical relations that are only applicable to conventional transport aircraft,hence different models and design variable will be applied that are able to calculate the geometry, weight and aerodynamic performance of the Flying-V.

9 Research Plan

As a result of the extensive literature review on the climate impact of the Flying-V, this section establishes a clear research objective that will pave the way for an ensuing master thesis.

9.1 Research Question

This literature study provides a thorough review of the literature on the potential of Blended Wing Body (BWB) and flying wing configurations for future aerospace applications. According to the findings, these unconventional aircraft designs have the potential to improve aerodynamic efficiency, provide greater design flexibility, and yield significant benefits in terms of weight, fuel consumption, greenhouse gas emissions, and noise levels. However, several challenges must be addressed, including stability and control issues caused by the lack of a conventional tail, the complexities of designing a wing body that accommodates payload and integrates all onboard systems while meeting diverse requirements, and the requirement for a structurally and aerodynamically efficient design. Because of the inherent multidisciplinary nature of flying wing design, where multiple functions are integrated into a single component, multidisciplinary design optimisation must be applied from the initial stages of development. Furthermore, because there are no empirical relationships specific to these unconventional configurations, models encompassing all disciplines must be developed to effectively facilitate their design process.

The Flying-V is such an unconventional aircraft configuration having a V-shaped flying wing configuration that has the potential to increase an aircraft's aerodynamic efficiency by combining the fuselage and wings into a single structure. The Flying-V can reduce aerodynamic drag, which reduces fuel consumption and greenhouse gas emissions. This concept represents a significant advancement in aircraft design, promising increased sustainability and performance for the aviation industry.

The Flying-V promises to be a solution to the most imminent problem in the aviation industry, the climate impact. As the aviation industry is a significant contributor to the warming of the planet, by emitting CO_2, NO_x, H_2O, sulphate and soot. Moreover, aircraft produces contrails that leads to a further warming of the earth. The environmental impact of aviation does not only extend to the warming of the earth, but also the noise it produces that can have adverse effects on human health. Considering the rapid growth of the aviation industry and the increase in climate targets set by governments makes it crucial for the aviation industry to apply revolutionary ideas to reduce its emissions and transition toward a more sustainable industry.

The literature review investigated various strategies for reducing the aviation industry's climate impact, revealing that engine parameters, such as engine cycle parameters, alternative fuels, and novel combustor designs, can play a significant role. Furthermore, investigating changes in operational conditions revealed the possibility of significant climate impact reductions through lower and slower flight. Finally, the innovative Flying-V aircraft configuration demonstrated a significant increase in aerodynamic efficiency of more than 20%, resulting in significant fuel savings [23, 36].

Further investigation into the Flying-V design, however, revealed that configurations optimised for minimum fuel burn could have a worse climate impact than a conventional reference aircraft, which was the A350-900 for the Flying-V studies, due to increased contrail formation at higher altitudes [12]. This showed the need for climate impact analysis to move the postdesign phase to an earlier design stage. While most research on unconventional aircraft configurations has focused on addressing challenges and evaluating aerodynamic or structural performance, there has been little attention paid to their climate impact. Although, one study has examined the climate impact of a blended wing body from an inclusive aircraft metric such as the ATR_{100}, which is the AHEAD multi-fuel BWB research. This study yielded promising results, but the emphasis was on the application of the multi-fuel combustor [64]. As a result, additional research into the integration of a flying wing with a conventional engine to the ATR_{100} is required. A detailed study assessing the potential of a flying wing aircraft optimised for minimum ATR_{100} could provide researchers with the information they need to decide whether to pursue further development on this configuration, as the ultimate goal is to increase efficiency and reduce climate impact. It will be interesting to see how the design and operating conditions of the for ATR_{100} optimised Flying-V differ from the original design, as well as how they compare to an ATR_{100} optimised conventional reference aircraft.

Minimising operational costs is a critical goal for airlines. Research on BWB showed that the operating cost could reduce, due to increased efficiency and decrease in fuel consumption. nevertheless research has shown that

optimising an aircraft for ATR_{100} can result in higher costs due to aircraft flying lower and slower, resulting in longer flights and a greater number of flights. This cost consideration is critical because airlines will not invest in an aircraft that will be prohibitively expensive to operate. As a result, the Flying-V's direct operating cost must be evaluated, allowing for a trade-off between direct operating cost and ATR_{100} optimisation while comparing design and operating condition differences.

With the aim of addressing the aforementioned research gaps and exploring the trade-offs between global warming impact reduction and direct operating costs, the research objective of this study is to conduct a multi-objective optimisation analysis on the Flying-V aircraft. The primary goal of this investigation is to reduce the climate impact, as measured in ATR_100 units, while taking into account the relevant aspect of direct operating costs. The outcomes of this research project will significantly contribute to the ongoing assessment of the feasibility and potential benefits of adopting the Flying-V concept, as well as other flying wing configurations, for the future commercial aviation landscape. Furthermore, will it provide valuable insights and inform decision-making processes regarding the viability of the Flying-V by comparing the obtained results with those of a conventional aircraft. Finally, will it provide an conceptual design analysis model for the Flying-V, that is able to generate optimised preliminary aircraft designs for ATR_{100} and direct operating cost.

In order to obtain this goal the following research question needs to be answered:

How can the Flying-V aircraft's climate impact measured in ATR_{100} and direct operating costs measured in U.S. Dollars be minimised using a multi-objective optimisation approach?

For answering this question the following sub-questions are formulated to steer the reseach in the right direction and divide the work into manageble workpackages.

1. What is the global warming impact of the Flying-V measured in ATR_{100}?
    - How can the ATR_{100} of the Flying-V be determined?
    - What is the ATR_{100} of the baseline Flying-V?
    - What is the ATR_{100} of the optimised Flying-V?
    - How does the ATR_{100} of the optimised Flying-V differ from the baseline and from a conventional reference aircraft?
2. What is the direct operating cost of the Flying-V measured in USD?
    - How can the direct operating cost of the Flying-V be determined?
    - What is the direct operating cost of the baseline Flying-V?
    - What is the direct operating cost of the optimised Flying-V? How does the direct operating cost of the optimised differ from the baseline and from a conventional reference aircraft?
3. How can the multi-disciplinary design and optimisation be performed?
    - What design variables are applied?
    - What are the constraints?
    - What optimisation algorithm and architecture is applied?

9.2 The Scope

In order to analyse the research question a comprehensive model has to be developed and implemented that takes into account a variety of design parameters such as Flying-V geometry, engine type, and mission requirements and a variety of disciplines such as airframe (aerodynamics and structures), propulsion, performance, cost analysis and climate analysis. In addition, appropriate optimisation algorithms has to be used to efficiently explore the design space and find optimal solutions. In order to perform the multi-objective multi disciplinary optimisation in a limited timespan is it of importance to well define the scope. All the disciplines and an example workflow are given in subsection 8.3. The extended design matrix shown is the workflow used in the research by Proesmans [7]. The workflow applied in the subsequent thesis will be almost similar to this. However, the airframe module will be the most affected by the current research. Furthermore, because a simplified airframe

model based on empirical relations was used, the design variables will differ from those used by Proesmans. These empirical relationships could not be applied to the novel Flying-V configuration, necessitating the use of other geometry parameterisation and aerodynamic models, resulting in more and different design variables.

The airframe module has to be determined in detail and should especially result in an optimal geometry and accurate determination of the wing loading and maximum lift coefficient. The geometry investigated will be the parameterisation applied by Hillen, such that the results are still similar to the Flying-V with an oval fuselage. The propulsion unit will consist of a conventional twin spool turbofan engine working on kerosene and without additional features as an inter turbine burner, such that the research primary focus is on the flying wing configuration and operational conditions.

The mission analysis will consist of a standardised mission profile. The mission profile researched will be similar to previous research on the flying-V and will have a design range equal range of the reference aircraft A350-900. The difference with previous research is that the cruise altitude and mach number will be considered as design variables, as the climate impact is heavily dependent on these operational parameters. Other payload-range than the design payload and range will not be considered. Furthermore, other operational techniques as intermediate stop operations will not be considered.

The climate analysis will assess the ATR_{100} for the entire fleet, where the influences from CO_2, NO_x, water, soot and sulphate emissions and linear contrail formation are taken into account. In these analysis the international standard atmosphere and no specific geographic location will be considered. Furthermore, only the direct effect of soot and sulphate will be considered and not their effect on contrail formation, as there are significant uncertainties in research on these effects and would increase the complexity of the model.

Noise will be neglected from this research, despite the fact that noise is an important environmental factor, the focus of this research will be on the global warming impact measured in ATR_{100}. The inclusion of noise would further increase the complexity. Furthermore, noise is measured in another metric such that this would add an additional objective to the optimisation problem.

The cost analysis will assess the direct operating cost in U.S. dollars for the entire fleet. Depreciation, financing fees, operation fees and indirect operating costs will be neglected, as they are more uncertain.

Stability performance will be imposed with constraints. However, it still has to be decided if only the static stability has to be ensured or also the dynamic and the special cases described by the ICAO such as one engine inoperative, as these are harder to determine, posses more uncertainty and might require to computationally expensive models.

9.3 Models Applied

This section will briefly describe the models that will probably be applied and the reasoning for this decision for the investigation of the research question. However, these might change when further analysis is performed.

The airframe module will consist of of a class-I initial sizing, followed by an aerodynamical analysis to obtain the geometry after which the weight and centre of gravity is estimated. In order to obtain the geometry the parametrisation by Hillen will be applied, as this is the most robust parametrisation and is applied by various other researches on the Flying-V. This does require significantly more design variables than the research by Proesmans as there simple empirical relations were applied that are not applicable to the unconventional configuration of the Flying-V.

Furthermore, an aerodynamic model applying AVL with an empirical viscous model will probably by applied similar to the research by Oosterom, as this was computationally efficient, gives stability derivatives and gave reasonable results for the aerodynamic coefficients. The model by Overbeek looked promising, as it incorporated the wind tunnel data, however the design will probably change too much from the original design such that it loses its validity. The weight estimation will be performed by a method similar to the method applied by Oosterom or Nieuwenhuizen [5, 36].

The propulsion module will apply thermodynamic cycle calculations with constant component efficiencies, as applied in the research by Proesmans [7]. This model will be applied as it is computationally efficient, already available and verified. Earlier optimisations on the flying-V applied empirical relations. However, this optimisation requires off-design calculations, hence a more elaborate model is required.

The mission, climate and cost analysis will apply models similar to the research by Proesmans, as these are already available. The lost-range method in the mission analysis is applied, because this actually calculates the fuel used in all the flight phases instead of the fuel fraction method that assumes most stages. The climate model will calculate the emissions from the emission indexes, those emissions will be translated into normalised radiative forcing with relations from literature, after which the temperature change is approximated. This method is computationally efficient, however it contains more uncertainties than with more elaborate models, as the AirClim model.

The optimisation architecture will probably be a multiple discipline feasible with the Gauss-Seidel procedure, as this provides the ability to separate the convergence of the MTOW, with the convergence of the optimisation allowing a shorter computational time. Furthermore, the Gauss-Seidel procedure allows for feed forward further increasing the compuational speed.

The optimisation algorithm still has to be determined, although for the multi-objective optimisation a genetic algorithm as the NSGA-II will probably be applied. Because this has the ability to find the Pareto-front at reasonable computational speed, that could be increased by inserting the results of the single objective optimisation into the initial population.

9.4 Planning

The following planning is proposed:

- Mid-term meeting 12-10-2023
- Draft thesis 26-11-2023
- Green light review 7-12-2023
- Thesis hand-in 22-12-2023
- Defense after holiday (10-1-2024)

I will start working on my thesis on the 26th of june. Then the normal duration is 14 weeks to the mid-term review, but as this period will normally be the regular summer break did I add two weeks to this such that I have 16 weeks. Then the nominal procedure is applied of 6 weeks to the Thesis draft hand-in and 2 weeks later the green light review. Two weeks after that the Thesis hand-in, such that this is just before the christmas break. Finally, the defence will occur somewhere after the holidays, but will be planned by then. The resulting planning is showed as a Gantt-chart in Appendix A.

10 Conclusions

The literature study reviewed the literature on flying wing and blended wing body configurations and the research on the Flying-V. This showed that there is a lack of knowledge in the literature about the global warming impact of these unconventional configurations. Only a few studies performed a climate assessment of BWB or flying wing, which showed that only a postdesign climate analysis does not provide the desired results of reduction in global warming impact. Normally, postdesign climate analysis is performed, during which only minor adjustments are made to just satisfy the requirements imposed by authorities. However, in order to meet the future environmental regulations, it is of importance to consider the environmental impact already from the preliminary design phase.

The literature study showed that the Flying-V or other unconventional configurations have the ability to reduce operational costs, as it proposes an significant decrease in fuel consumption. However, studies did show that designing for reduced global warming impact does result in higher costs, due to longer flights. The conflict between the operational cost and global warming impact is not yet investigated for BWB or flying wing configurations. Therefor, is it interested to see how the design of a the Flying-V changes from the original design when optimised for either of these values and how they compare to a reference aircraft. Hence, a research plan is constructed to further investigate the potential of the Flying-V to reduce the global warming impact measured in ATR_{100} and direct operating cost in U.S. Dollars, by implementing a conceptual design model to generate optimised preliminary Flying-V designs.

The ideal outcome of this research would be the identification of a Pareto-optimal solution and the development of a reusable model to assess the Flying-V's global warming impact and direct operating costs. A MDAO workflow and design guidelines will be included in the model, allowing future Flying-V iterations to be optimised for global warming impact and direct operating costs. This will inform decision-making processes and significantly contribute to the ongoing evaluation of the feasibility and potential benefits of implementing the Flying-V concept.

References

[1] Marleen Hillen. Parametrisation of the flying-v outer mould line. 2020.

[2] D.S. Lee, D.W. Fahey, A. Skowron, M.R. Allen, U. Burkhardt, Q. Chen, S.J. Doherty, S. Freeman, P.M. Forster, J. Fuglestvedt, A. Gettelman, R.R. De León, L.L. Lim, M.T. Lund, R.J. Millar, B. Owen, J.E. Penner, G. Pitari, M.J. Prather, R. Sausen, and L.J. Wilcox. The contribution of global aviation to anthropogenic climate forcing for 2000 to 2018. *Atmospheric Environment*, 244:117834, January 2021.

[3] Emily Schwartz Dallara. *Aircraft design for reduced climate impact*. PhD thesis, Stanford University, 2011.

[4] Sigrun Matthes, Ling Lim, Ulrike Burkhardt, Katrin Dahlmann, Simone Dietmüller, Volker Grewe, Amund S. Haslerud, Johannes Hendricks, Bethan Owen, Giovanni Pitari, Mattia Righi, and Agnieszka Skowron. Mitigation of non-CO2 aviation's climate impact by changing cruise altitudes. *Aerospace*, 8(2):36, January 2021.

[5] Wilco Oosterom. Flying-v family design. 2021.

[6] Egbert Torenbeek. *Advanced Aircraft Design*. Wiley, May 2013.

[7] Pieter-Jan Proesmans and Roelof Vos. Airplane design optimization for minimal global warming impact. *Journal of Aircraft*, 59(5):1363–1381, September 2022.

[8] UNFCCC. The paris agreement. In *Paris Climate Change Conference - November 2015*, 2018.

[9] International Civil Aviation Organization. Icao long-term traffic forecasts: Passenger and cargo. Technical report, ICAO, 2016.

[10] J. Benad. The flying v a new aircraft configuration for commercial passenger transport. 2015.

[11] J. Benad and R. Vos. Design of a flying v subsonic transport. In *ICAS 2022*, 2022.

[12] Matthijs Reekers. Climate effects of the flying-v. Master's thesis, Technische universiteit Delft, 2021.

[13] Paul Okonkwo and Howard Smith. Review of evolving trends in blended wing body aircraft design. *Progress in Aerospace Sciences*, 82:1–23, April 2016.

[14] Rudolf Storck. *Flying Wings*. Bernard & Graefe, Bad Neuenahr-Ahrweiler, Germany, 2002.

[15] Tony Chong. *Flying wings & radical things: Northrop's secret aerospace projects & concepts 1939-1994*. Specialty Press, North Branch, MN, June 2016.

[16] R. H. Liebeck. Design of the blended wing body subsonic transport. *Journal of Aircraft*, 41(1):10–25, January 2004.

[17] Rodrigo Martinez-Val, Emilio Perez, Javier Perez, Francisco J Palacin, and EUIT Aeronautica. Optimising transport flying wings. In *25th International Congress of the Aeronautical Sciences (ICAS)*, 2006.

[18] Zhenli CHEN, Minghui ZHANG, Yingchun CHEN, Weimin SANG, Zhaoguang TAN, Dong LI, and Binqian ZHANG. Assessment on critical technologies for conceptual design of blended-wing-body civil aircraft. *Chinese Journal of Aeronautics*, 32(8):1797–1827, August 2019.

[19] A.L Bolsunovsky, N.P Buzoverya, B.I Gurevich, V.E Denisov, A.I Dunaevsky, L.M Shkadov, O.V Sonin, A.J Udzhuhu, and J.P Zhurihin. Flying wing—problems and decisions. *Aircraft Design*, 4(4):193–219, December 2001.

[20] Robert Liebeck. Blended wing body design challenges. In *AIAA International Air and Space Symposium and Exposition: The Next 100 Years*. American Institute of Aeronautics and Astronautics, March 2003.

[21] Daniel P Raymer. *Aircraft design*. American Institute of Aeronautics & Astronautics, Reston, VA, 1 edition, 2004.

[22] Ohad Gur, William H. Mason, and Joseph A. Schetz. Full-configuration drag estimation. *Journal of Aircraft*, 47(4):1356–1367, July 2010.

[23] Francesco Faggiano, Roelof Vos, Max Baan, and Reinier Van Dijk. Aerodynamic design of a flying v aircraft. In *17th AIAA Aviation Technology, Integration, and Operations Conference*. American Institute of Aeronautics and Astronautics, June 2017.

[24] Bruno Mialon, Alex Khrabrov, Saloua Ben Khelil, Andreas Huebner, Andrea Da Ronch, Ken Badcock, Luca Cavagna, Peter Eliasson, Mengmeng Zhang, Sergio Ricci, Jean-Christophe Jouhaud, Gilbert Rogé, Stephan Hitzel, and Martin Lahuta. Validation of numerical prediction of dynamic derivatives: The DLR-f12 and the transcruiser test cases. *Progress in Aerospace Sciences*, 47(8):674–694, November 2011.

[25] Alberto Ruiz Garcia. Aerodynamic model identification of the flying v using wind tunnel data. 2019.

[26] Thibaut Cappuyns. Handling qualities of a flying v configuration. 2019.

[27] Rob Viet. Analysis of the flight characteristics of a highly swept cranked flying wing by means of an experimental test. 2019.

[28] Simon van Overeem. Modelling, control, and handling quality analysis of the flying-v. 2022.

[29] R. Vos, F.J.J.M.M. Geuskens, and M.F.M. Hoogreef. A new structural design concept for blended wing body cabins. In *53rd AIAA/ASME/ASCE/AHS/ASC Structures, Structural Dynamics and Materials Conference¡BR¿20th AI*. American Institute of Aeronautics and Astronautics, April 2012.

[30] Luuk van der Schaft. Development, model generation and analysis of a flying v structure concept. 2017.

[31] Mathias Claeys. Flying v and reference aircraft structural analysis and mass comparison. 2018.

[32] D Decloedt. Investigation into the effect of relaxed static stability on a business jet's preliminary design. 2016.

[33] A. Elham, G. La Rocca, and M.J.L. van Tooren. Development and implementation of an advanced, design-sensitive method for wing weight estimation. *Aerospace Science and Technology*, 29(1):100–113, August 2013.

[34] Roelof Vos and Maurice Hoogreef. Semi-analytical weight estimation method for fuselages with oval cross-section. In *54th AIAA/ASME/ASCE/AHS/ASC Structures, Structural Dynamics, and Materials Conference*. American Institute of Aeronautics and Astronautics, April 2013.

[35] Kristian Schmidt and Roelof Vos. A semi-analytical weight estimation method for oval fuselages in conventional and novel aircraft. In *52nd Aerospace Sciences Meeting*. American Institute of Aeronautics and Astronautics, January 2014.

[36] Ties Nieuwenhuizen. Conceptual design optimisation of a flying v aircraft. 2021.

[37] Helena V de Castro. *Flying and handling qualities of a fly-by-wire blended-wing-body civil transport aircraft*. PhD thesis, Cranfield University, 2003.

[38] Marco Palermo and Roelof Vos. Experimental aerodynamic analysis of a 4.6%-scale flying-v subsonic transport. In *AIAA Scitech 2020 Forum*. American Institute of Aeronautics and Astronautics, January 2020.

[39] Jeroen van Uitert. Experimental investigation into the effect of aerodynamic add-ons on the aerodynamic characteristics of the flying v. 2021.

[40] Michael V Cook. The solution of the equations of motion. In *Flight Dynamics Principles*. Elsevier, 2013.

[41] Sjoerd van Empelen. Engine integration of the flying v: Quantification of engine integration effects using wind tunnel experiments. 2020.

[42] Courtland D Perkins and Robert E Hage. *Airplane performance, stability and control*. John Wiley & Sons Incorporated, 1949.

[43] Mohammad H Sadraey. *Aircraft design: A systems engineering approach*. John Wiley & Sons, 2012.

[44] Menno van der Toorn. Flying-v family design for stability and control. 2022.

[45] Brenda M. Kulfan. Universal parametric geometry representation method. *Journal of Aircraft*, 45(1):142–158, January 2008.

[46] Jackson Horwitz. Parametric design of the flying-v winglets for improved lateral-directional stability and control. 2021.

[47] Nicolas E. Antoine and Ilan M. Kroo. Framework for aircraft conceptual design and environmental performance studies. *AIAA Journal*, 43(10):2100–2109, October 2005.

[48] Volker Grewe. Aircraft emissions and climate effects part 5 climate responses and climate metrics. Lecture Slides, 2021.

[49] Volker Grewe and Katrin Dahlmann. How ambiguous are climate metrics? and are we prepared to assess and compare the climate impact of new air traffic technologies? *Atmospheric Environment*, 106:373–374, April 2015.

[50] V. Grewe and A. Stenke. Airclim: an efficient tool for climate evaluation of aircraft technology. *Atmospheric Chemistry and Physics*, 8(16):4621–4639, 2008.

[51] O. Boucher and M.S. Reddy. Climate trade-off between black carbon and carbon dioxide emissions. *Energy Policy*, 36(1):193–200, January 2008.

[52] Robert Sausen and Ulrich Schumann. Estimates of the climate response to aircraft co2 and nox emissions scenarios. *Climatic Change*, 44(1/2):27–58, 2000.

[53] Intergovernmental Panel on Climate Change. *Climate change 2007 - the physical science basis, Contribution of Working Group I to the Fourth Assessment Report of the Intergovernmental Panel on Climate Change*. Cambridge University Press, Cambridge, England, September 2007.

[54] Arthur H Lefebvre and Dilip R Ballal. *Gas turbine combustion*. CRC Press, Boca Raton, FL, 3 edition, July 2009.

[55] Doug DuBois and Gerald C. Paynter. "fuel flow method2" for estimating aircraft emissions. In *SAE Technical Paper Series*. SAE International, August 2006.

[56] Volker Grewe, Thierry Champougny, Sigrun Matthes, Christine Frömming, Sabine Brinkop, Ole Amund Søvde, Emma A. Irvine, and Lucia Halscheidt. Reduction of the air traffic's contribution to climate change: A REACT4c case study. *Atmospheric Environment*, 94:616–625, September 2014.

[57] D.S. Lee, G. Pitari, V. Grewe, K. Gierens, J.E. Penner, A. Petzold, M.J. Prather, U. Schumann, A. Bais, and T. Berntsen. Transport impacts on atmosphere and climate: Aviation. *Atmospheric Environment*, 44(37):4678–4734, December 2010.

[58] B. Kärcher and F. Yu. Role of aircraft soot emissions in contrail formation. *Geophysical Research Letters*, 36(1), January 2009.

[59] B. Kärcher, U. Burkhardt, A. Bier, L. Bock, and I. J. Ford. The microphysical pathway to contrail formation. *Journal of Geophysical Research: Atmospheres*, 120(15):7893–7927, August 2015.

[60] Ying Zhang, Andreas Macke, and Frank Albers. Effect of crystal size spectrum and crystal shape on stratiform cirrus radiative forcing. *Atmospheric Research*, 52(1-2):59–75, August 1999.

[61] Ulrich Schumann. Influence of propulsion efficiency on contrail formation. *Aerospace Science and Technology*, 4(6):391–401, September 2000.

[62] D. Sonntag. Fortschritte in der hygrometrie. *Meteorologische Zeitschrift*, 3(2):51–66, May 1994.

[63] Bernd Kärcher. Formation and radiative forcing of contrail cirrus. *Nature Communications*, 9(1), May 2018.

[64] Volker Grewe, Lisa Bock, Ulrike Burkhardt, Katrin Dahlmann, Klaus Gierens, Ludwig Hüttenhofer, Simon Unterstrasser, Arvind Gangoli Rao, Abhishek Bhat, Feijia Yin, Thoralf G. Reichel, Oliver Paschereit, and Yeshayahou Levy. Assessing the climate impact of the AHEAD multi-fuel blended wing body. *Meteorologische Zeitschrift*, 26(6):711–725, December 2017.

[65] Katrin Dahlmann, Sigrun Matthes, Hiroshi Yamashita, Simon Unterstrasser, Volker Grewe, and Tobias Marks. Assessing the climate impact of formation flights. *Aerospace*, 7(12):172, December 2020.

[66] Volker Grewe, Katrin Dahlmann, Jan Flink, Christine Frömming, Robin Ghosh, Klaus Gierens, Romy Heller, Johannes Hendricks, Patrick Jöckel, Stefan Kaufmann, Katrin Kölker, Florian Linke, Tanja Luchkova, Benjamin Lührs, Jesper Van Manen, Sigrun Matthes, Andreas Minikin, Malte Niklaß, Martin Plohr, Mattia Righi, Simon Rosanka, Angela Schmitt, Ulrich Schumann, Ivan Terekhov, Simon Unterstrasser, Margarita Vázquez-Navarro, Christiane Voigt, Kai Wicke, Hiroshi Yamashita, Andreas Zahn, and Helmut Ziereis. Mitigating the climate impact from aviation: Achievements and results of the DLR WeCare project. *Aerospace*, 4(3):34, June 2017.

[67] B. Callender, E. Gutmark, and S. Martens. Far-field acoustic investigation into chevron nozzle mechanisms and trends. *AIAA Journal*, 43(1):87–95, January 2005.

[68] David S. Lee, David W. Fahey, Piers M. Forster, Peter J. Newton, Ron C.N. Wit, Ling L. Lim, Bethan Owen, and Robert Sausen. Aviation and global climate change in the 21st century. *Atmospheric Environment*, 43(22-23):3520–3537, July 2009.

[69] Jan Roskam. *Airplane Design: Part VIII (Part 8) - Airplane Cost Estimation: Design, Development, manufacturing, and Operating*. DARcorporation, 1985.

[70] Jan Roskam. *Airplane design part I: Preliminary sizing of aiplanes*. Darcorporation, 1985.

[71] Roelof Vos and Saeed Farokhi. *Introduction to Transonic Aerodynamics*. Fluid mechanics and its applications. Springer, Dordrecht, Netherlands, 2015 edition, March 2015.

[72] E Obert. *Aerodynamic design of transport aircraft*. IOS Press, Netherlands, 2009.

[73] ANDERSON. *Fundamentals of aerodynamics*. McGraw-Hill Education, Columbus, OH, 6 edition, April 2016.

[74] J. Mariens, A. Elham, and M. J. L. van Tooren. Quasi-three-dimensional aerodynamic solver for multidisciplinary design optimization of lifting surfaces. *Journal of Aircraft*, 51(2):547–558, March 2014.

[75] W.P.J. Visser. Generic analysis methods for gas turbine engine performance.

[76] Edward M Greitzer, PA Bonnefoy, E DelaRosaBlanco, CS Dorbian, M Drela, DK Hall, RJ Hansman, JI Hileman, RH Liebeck, J Lovegren, et al. N+ 3 aircraft concept designs and trade studies. volume 2: Appendices— design methodologies for aerodynamics, structures, weight, and thermodynamic cycles. Technical report, 2010.

[77] Jack D Mattingly, William H Heiser, and David T Pratt. *Aircraft engine design, second edition*. American Institute of Aeronautics and Astronautics, Reston ,VA, January 2002.

[78] Airbus. A350 - aircraft characteristics - airport and maintenance planning. Technical report, AIRBUS S.A.S, 2021.

[79] Kalyanmoy Deb. Unveiling innovative design principles by means of multiple conflicting objectives. *Engineering Optimization*, 35(5):445–470, October 2003.

[80] Edmund K. Burke and Graham Kendall, editors. *Search Methodologies*. Springer US, 2014.

[81] Kalyanmoy Deb. *Multi-Objective Optimization using Evolutionary Algorithms*. John Wiley & Sons, LTD, 2001.

[82] Aviv Navon, Aviv Shamsian, Gal Chechik, and Ethan Fetaya. Learning the pareto front with hypernetworks. *arXiv preprint arXiv:2010.04104*, 2020.

[83] Andrew B. Lambe and Joaquim R. R. A. Martins. Extensions to the design structure matrix for the description of multidisciplinary design, analysis, and optimization processes. *Structural and Multidisciplinary Optimization*, 46(2):273–284, January 2012.

A Appendix A: Gantt-chart of the research proposed

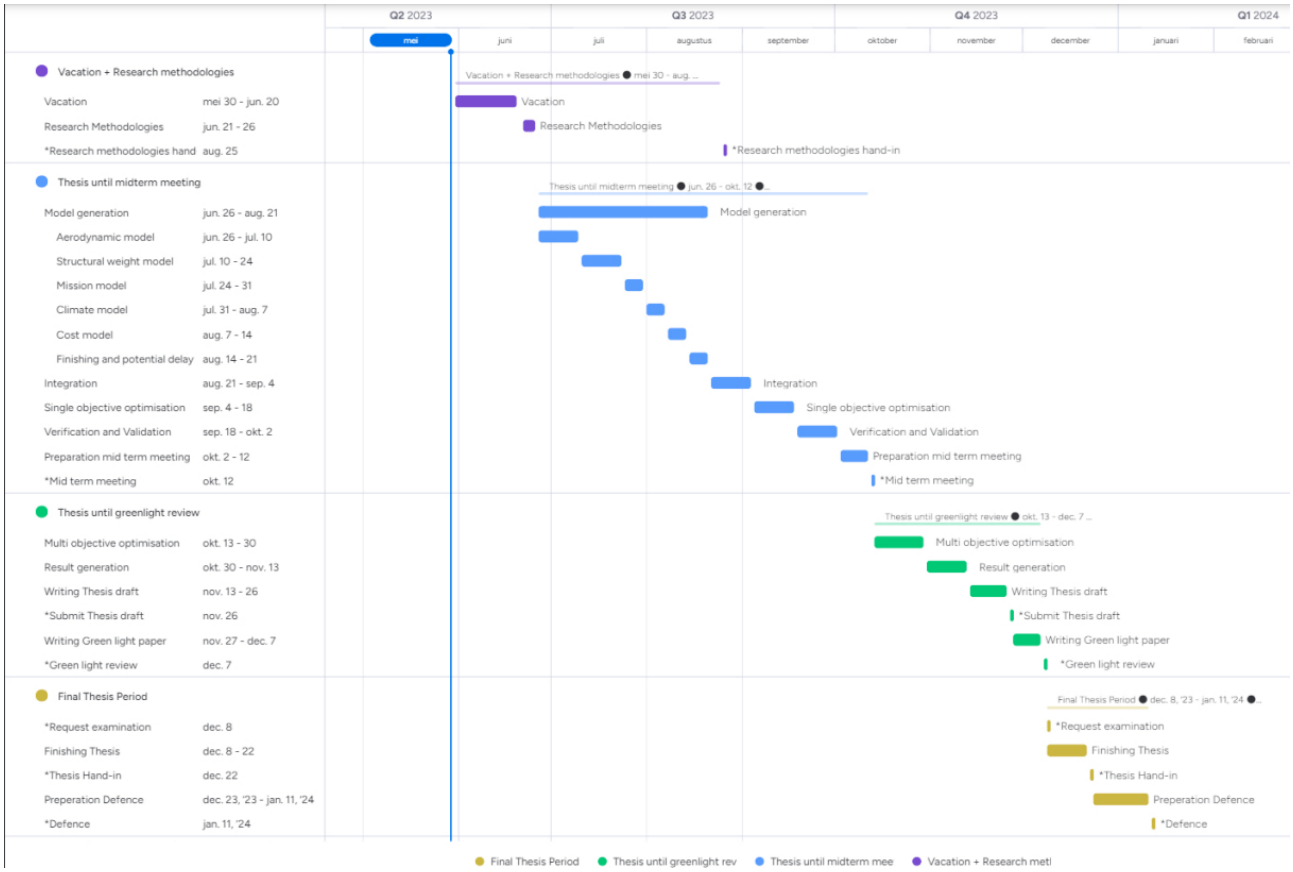

Figure 11: Gantt-chart for the upcoming thesis period

Part III

Supporting work

1

ModeFrontier

The optimisation and sensitivity analysis was performed with ModeFrontier. ModeFRONTIER is a multidisciplinary and multi-objective optimisation software platform developed by ESTECO [1]. This software applies a modular environment in which you graphically build the workflow and connect all the components and is able to perform with several external programs, such as MS Excel, Matlab and Python.

Figure 1.1 The figure presents a simplified workflow used in the research, focusing on two design variables for clarity. Initially, a starting point is set. The normalised design variables are then processed through a calculator node to determine their absolute values. These absolute design variables are subsequently fed into a Python node containing a script that computes the objectives and constraints. Finally, the workflow concludes with an end node connection.

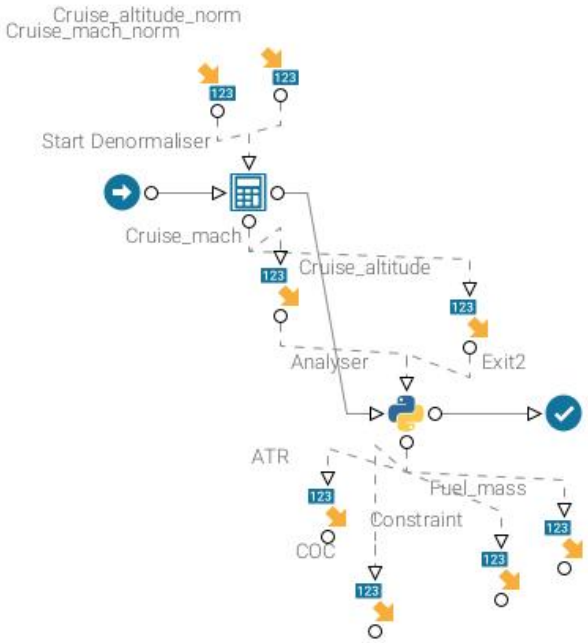

Figure 1.1: Simplified workflow in ModeFrontier

Various functionalities were implemented using the constructed workflow. The scientific paper utilised a sensitivity analysis to reduce the number of design variables and consequently decrease computational time. To conduct the sensitivity analyses, a comprehensive set of results was necessary. The

[1] modeFrontier. Retrieved on May 27th 2024 ,https://engineering.esteco.com/modefrontier/

results were acquired using a design of experiments (DOE) for 1000 designs, employing a space filler algorithm. ModeFrontier offers a variety of algorithms, including Random, Sobol, Constraint satisfaction, and Uniform Latin Hypercube (ULH). The use of ULH was chosen due to its ability to effectively handle a large number of design variables and ensure a uniform distribution across the design space. ULH achieves this by minimising correlation and maximising the distance between points. However, the ”Random” option was truly random and offered a solution that was less evenly distributed. Sobol was constrained to a maximum of 10 design variables, and the constraint satisfaction process focused solely on identifying feasible design points.

Following the execution of the DOE, ModeFrontier offers several chart options, with the basic scatter plot, history plot, and broken constraint plot being the most commonly used. The history plot can be accessed during execution to monitor the progress of convergence. However, the Scatter matrix chart was also of interest for the sensitivity analysis. The correlation between various design variables and the objectives, ATR and COC (total_doc_design), is shown in Figure 1.2. The lower left corner displays the correlation between two variables, highlighting the distinct contrast between ATR and the costs. Moreover, it has already been demonstrated that the pressure ratio of the low pressure compressor has minimal impact on the objectives. Additionally, this demonstrates a weak correlation between the design variables depicted, indicating that they have been carefully selected to allow for independent assessment of each variable’s effect. The central diagonal displays the quantity and nature of designs that are accessible for the particular design variable. This demonstrates a satisfactory even distribution among all the design variables, with the colour green representing a design that is feasible and meets the constraints, yellow indicating an infeasible design, and red indicating a design with an error. Lastly, the scatter plots in the upper right corner display the relationships between variables using colour codes. The names on the horizontal axis represent the x-axis, while the names on the vertical axis represent the y-axis.

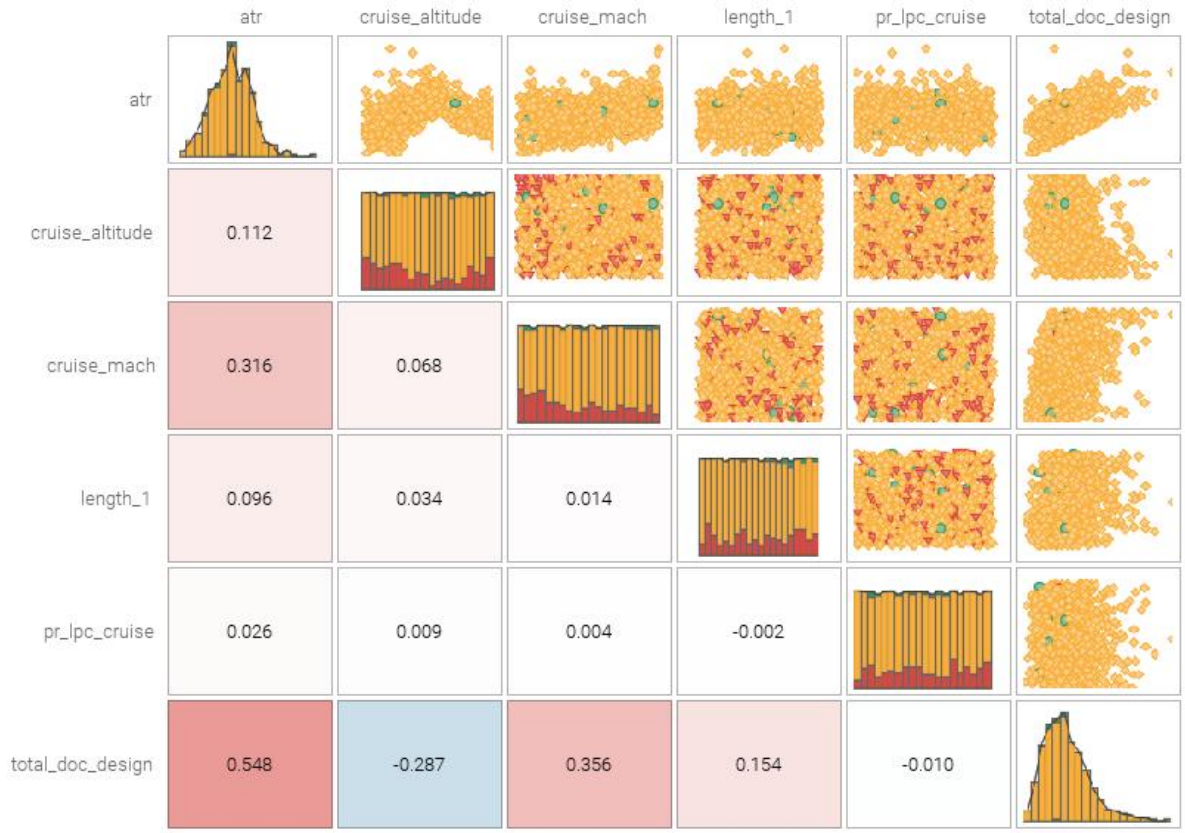

Figure 1.2: Scatter matrix chart in ModeFrontier, in which the yellow bubbles indicate an unfeasible design, red an error design and green an feasible design

The sensitivity analysis was conducted using the dataset obtained from the DOE. The sensitivity anal-

ysis utilised three algorithms: Polynomial Chaos Expansion (PCE), Distributed Random Forest (DRF), and SS-ANOVA. For the sensitivity analysis, all three methods were utilised to evaluate both objectives and identify the constraints that were most violated. Nevertheless, the paper only presents the outcomes of the PCE, as it exhibited the highest level of accuracy. The sensitivity analysis was conducted multiple times after major adjustments to the models. The sensitivity analysis results for all three algorithms are provided in Figure 1.3 for the ATR objective and Figure 1.4 for the cost objective. These analyses excluded the keel and crown heights because previous analyses demonstrated that they had minimal impact. The effects associated with the asterisk were established as constants, as they consistently had the lowest values for both objectives and all algorithms.

The accuracy of the analysis varied significantly depending on the algorithms used. The algorithm's accuracy was assessed using the R-squared metric. Specifically, the SS-ANOVA algorithm achieved an R-squared value of 0.65, the DRF algorithm achieved 0.90, and the PCE algorithm achieved 0.98. These high R-squared values justify the inclusion of the algorithm in the paper. The sensitivity analyses yield the normalised variance values. The variance quantifies the extent to which an adjustment in a particular design variable would lead to a corresponding change in the objective value. Normalised so that the sum of all contributions equals one. Ultimately, both figures demonstrate that altering the operational conditions, specifically the altitude and mach number, has the most substantial impact on the objectives.

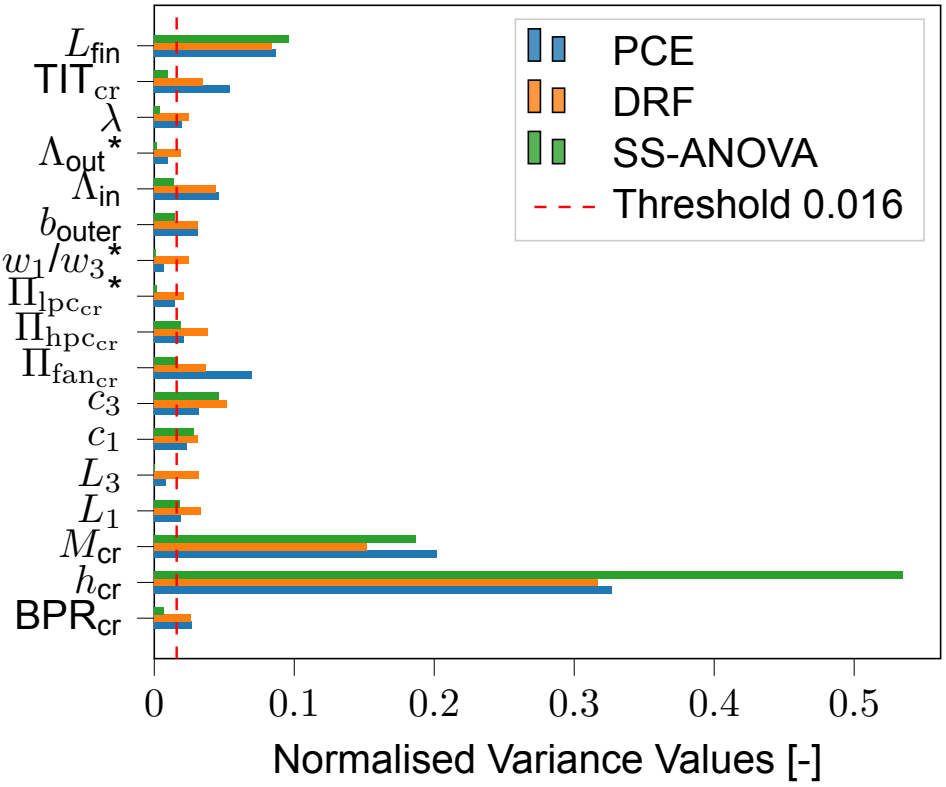

Figure 1.3: Sensitivity analysis of ATR for the three analysis algorithms

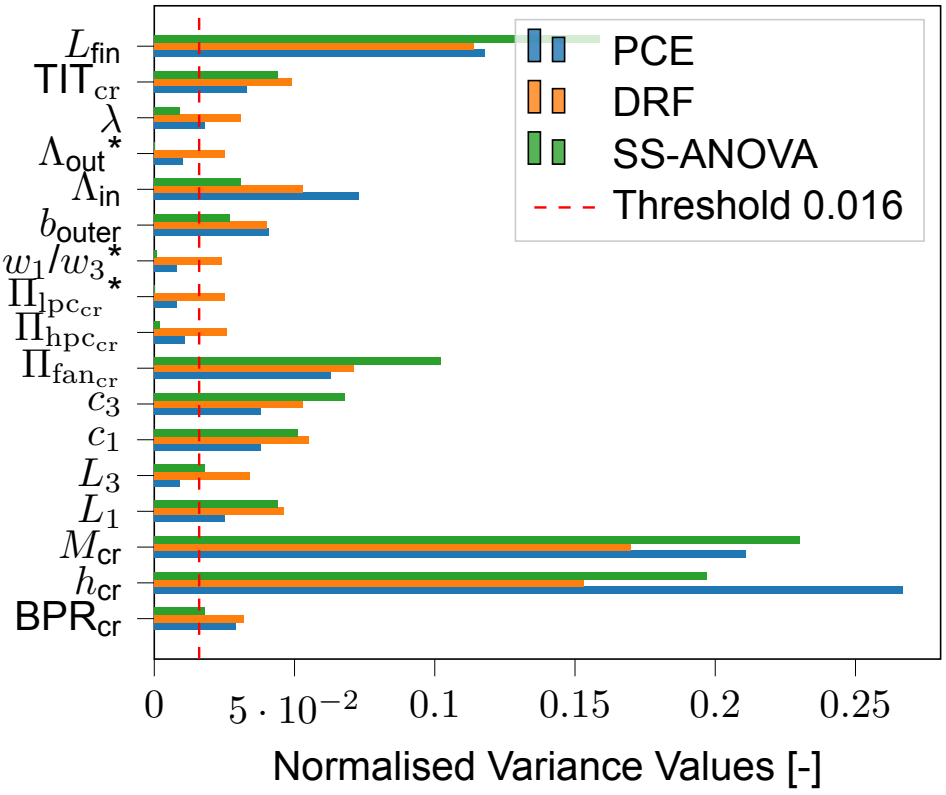

Figure 1.4: Sensitivity analysis of COC for the three analysis algorithms

2

Additional Verification

This chapter describes an additional verification of assumptions applied to the propulsion model and fuel burn model.

2.1. Propulsion model

The turbofan engine in this research was based on the GEnx-1B-70. This is different from previous research on the Flying-V-900, which applied the Trent-XWB-84 similar to the A350-900. However, this engine was bigger and heavier and was not deemed necessary as the take-off thrust of the FV-900 was lower. The take-off thrust of the Trent-XWB-84 is around the 375kN[1], while the maximum take-off thrust following from this research was 301kN for the climate optimised Flying-V . Hence, the GEnx-1B-70 which is normally applied for a smaller B787 with a take-off thrust of 310kN[2] was a better fit.

The weight of the turbofan engine in the propulsion model was computed with TASOPT appendix H by Drela, but several weight options were available [2]. There were two decisions to be made geared or non-geared and advanced materials or old materials used until mid 2000s. A direct drive non-geared turbofan was applied, as this reduces the complexity and corresponds to the GEnx-1B-70. The decision of the material choice was made with by comparison to the GEnx-1B-70, which has a dry weight of 6150kg. Analysis with similar efficiencies, pressure ratios and bypass ratios resulted in a weight for the old materials of 7905kg, while the advanced materials resulted in a weight of 6390kg. Hence, the advanced materials was chosen, which was expected as the GEnx-1B-70 applies compposite materials in the engine. Equation 2.1 estimates the engine dry mass from the bypass ratio, overall pressure ratio and mass flow through the core given in lbs/s. The nacelle and systems weight of the engine that make up the remainder of the engine weight are computed with a method proposed by Torenbeek, which was already implented by Oosterom [8][5].

$$
\begin{aligned}
&W_{\text{engine, lbs}} = a \left(\frac{\dot{m}_{\text{core}}}{100s} \right)^b \left(\frac{\text{OPR}}{40} \right)^c \\
&\text{with:} \\
&a = \left(1.538 \times 10^{1}\right) \text{BPR}^2 + \left(4.011 \times 10^{2}\right) \text{BPR} + 631.5 \\
&b = \left(1.057 \times 10^{-3}\right) \text{BPR}^2 - \left(3.693 \times 10^{-2}\right) \text{BPR} + 1.171 \\
&c = \left(-1.022 \times 10^{-2}\right) \text{BPR} + 0.232
\end{aligned}
\tag{2.1}
$$

[1] EASA. Retrieved on May 27th 2024, https://www.easa.europa.eu

[2] GE Aerospace. Retrieved on May 27th 2024, https://www.geaerospace.com/sites/default/files/datasheet-genx.pdf

2.2. Verification mission analysis

The mission analysis model estimated the fuel required. Nevertheless, it was presumed that the quantity of fuel consumed during the loiter and diversion phase would constitute 5% of the overall fuel fraction. Typically, the Breguet range and endurance equations are used in this case. The choice to utilise a 5% fuel fraction for these stages was made in order to maintain consistency with previous studies conducted on the Flying-V. Hence, it is crucial to examine the extent of disparity between the two methods in order to determine whether these assumptions should continue to be employed in future research. In addition, a more detailed mission analysis was conducted during the climate impact assessment, wherein the fuel consumption was calculated for each individual time interval. Therefore, it is also important to examine whether the fuel consumption derived from the climate analysis matches the fuel consumption obtained from the simple mission analysis.

The fuel consumption for both the design mission and the average reference mission was calculated for the baseline Flying-V and presented in Table 2.1. This suggests that assuming a 5% fuel fraction for the design mission is valid, as it only results in a 200kg increase in fuel mass. This increase could be viewed as an additional safety margin. However, in the reference mission, the fuel mass decreases by 2% while maintaining the same requirements for diversion distance (200nm) and loiter time (30 minutes). This would lead to a decreased ATR_{100} in the climate analysis, as the amount of fuel burned was less than what was necessary. However, it can be argued that this is intended for a typical reference mission, as the majority of missions would not need to deviate or loiter.

The results derived from the detailed mission analysis used to calculate the climate impact indicate a substantially reduced fuel mass. The mass reduction for the design mission is 6%, while for the reference mission it is 11%. Therefore, the standard mission analysis model used has a notable tendency to overestimate, which can be considered as an additional safety reserve.

Table 2.1: Verification of the applied mission model

Mission model	m_{fuel} design mission [10^3kg]	m_{fuel} reference mission [10^3kg]
Model with 5% fraction	88.4	37.5
Model with Breguet	88.2	38.3
Detailed model	82.8	33.3

3

Additional Results

This chapter will provide additional results obtained in the research. The additional results will first consist of some Pie charts for the costs of several designs. Then figures regarding the designs are given.

3.1. Cost

The paper only provides information about the cash operating cost, although the costs actually comprise multiple components. These components include the cost of flight, which is further divided into fuel, oil, and crew expenses, as well as the cost of maintenance, which is divided into aircraft and engine costs. The pie chart illustrates the relative costs. The pie charts are given for the three single objective optimisation results and the two extreme designs, for cost and climate obtained from the multi objective optimisation. Figure 3.1, Figure 3.2 and Figure 3.3 provide information about the proportions of operational costs for the fuel-optimised, climate-optimised, and cost-optimised single objective optimisation (SOO) designs, respectively. The fuel-optimised and cost-optimised designs have nearly identical cash operating cost. Nevertheless, the fuel-optimised option has a reduced impact on fuel and oil expenses, as anticipated. The cost-optimised design, on the other hand, achieves cost reduction by minimising maintenance expenses and increasing flight speed to lower crew costs. The climate-optimised design results in reduced maintenance and fuel and oil costs, primarily due to the significant crew expenses. However, the absolute costs for maintenance, fuel, and oil are greater.

Figure 3.4 and Figure 3.5 provide information about the proportions of operational costs for the climate-optimised, and cost-optimised multi objective optimisation (MOO) designs, respectively. These figures exhibit a similar pattern to the single-objective optimisation, but with lower fuel mass and higher operational empty mass for these optimisations. As a result, fuel and oil costs are relatively lower, while maintenance costs are relatively higher. Additionally, the climate-optimised design had the Mach number set at its minimum limit, which further increased flight time and crew costs compared to the climate-optimised single-objective optimisation design, which flew slightly above the minimum value.

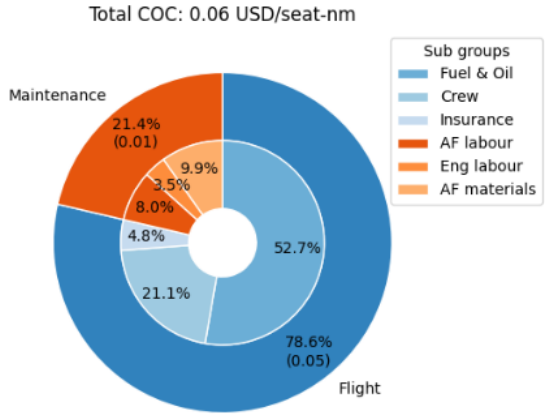

Figure 3.1: Pie chart of the operational costs for the SOO fuel-optimised FV-900

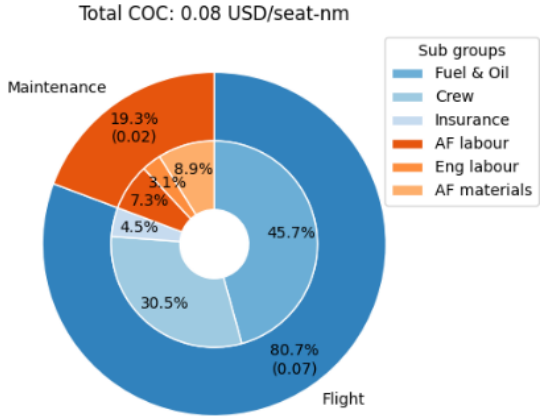

Figure 3.2: Pie chart of the operational costs for the SOO climate-optimised FV-900

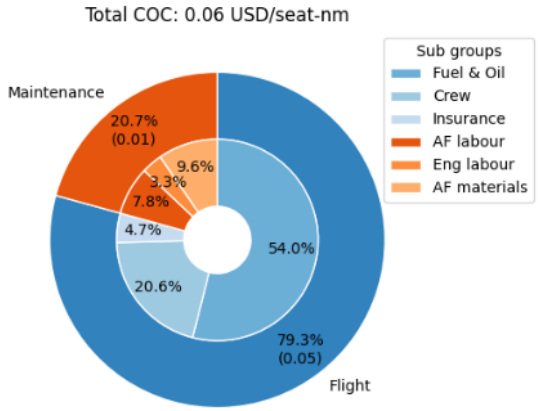

Figure 3.3: Pie chart of the operational costs for the SOO cost-optimised FV-900

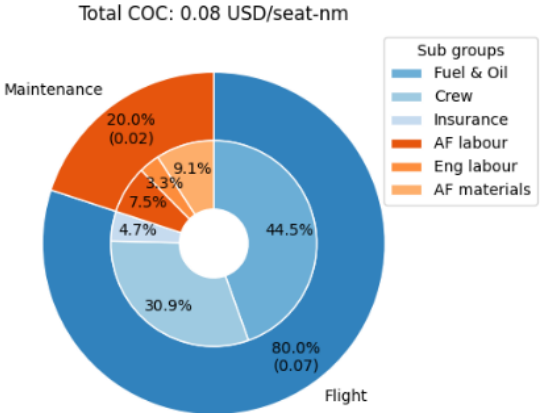

Figure 3.4: Pie chart of the operational costs for the MOO climate-optimised FV-900

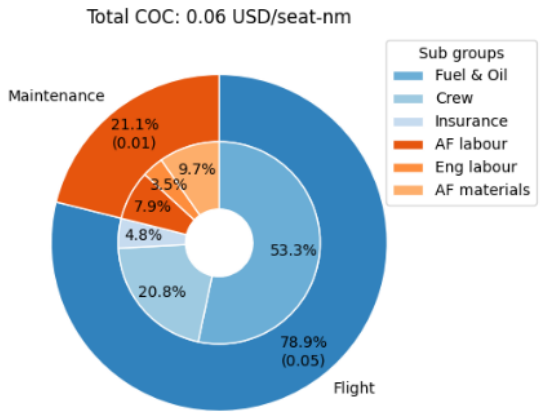

Figure 3.5: Pie chart of the operational costs for the MOO cost-optimised FV-900

3.2. Flying-V designs

Several figures of the design of the optimised FV-900 are made with ParaPy. Most figures contain overlapping designs to investigate the difference between the designs. For all the designs a similar colour convention as in the paper is applied, in which red implicates the climate-optimised design, blue the cost-optimised design and green the fuel-optimised design.

The three Flying-V designs optimised for a single objective can be seen in Figure 3.6 from an isometric perspective. It is evident that the fuel-optimised design has a greater length, while the fin of the climate-optimised design is comparatively shorter. The top view depicted in Figure 3.7 additionally showcases the elongated fuel-optimised FV-900 and its increased sweep angle. Moreover, it demonstrates the transitions between section 1 and section 3, highlighting that the fuel-optimised design has a considerably longer section 1 compared to the climate and cost-optimised design. The complete side view is included in Figure 3.8 in order to observe the side view of the anterior section of the wing. However, since the wing's height remains constant, it does not have any impact and all three views appear identical. The concluding segment of the side perspective was described in the scientific paper. The front view depicted in Figure 3.9 reveals that the inner portion of the wing is approximately the same length for the climate and cost designs, while it is shorter for the fuel design. Nevertheless, the final segment exhibits similarities between the fuel-optimised and cost-optimised designs. The climate design features a shorter outer wing section and a winglet with a another cant angle, although the cant angle was fixed. Indicating a minor error in the process of creating the geometry for the climate-optimised Flying-V.

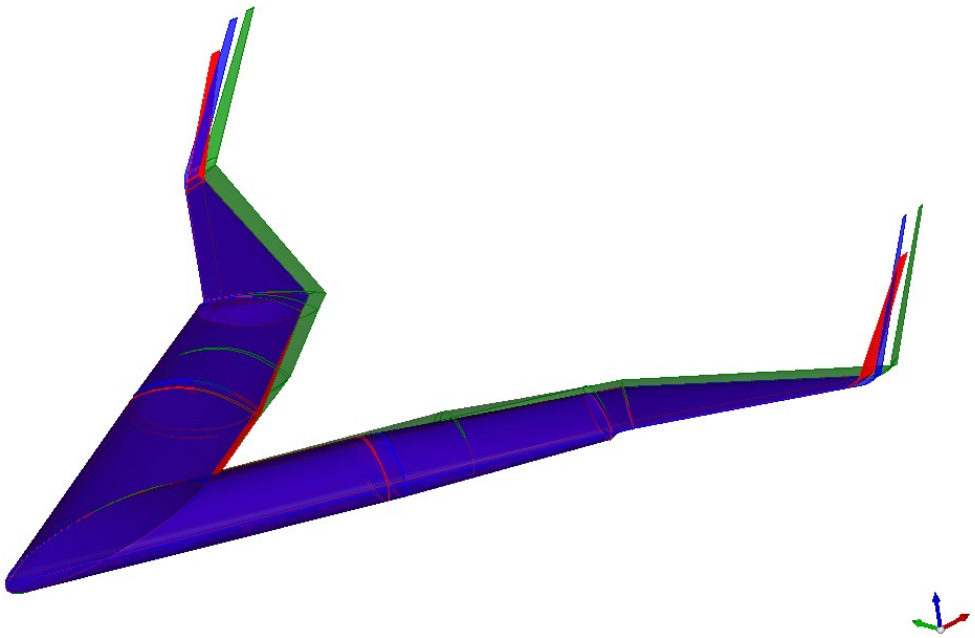

Figure 3.6: Isometric view of fuel-optimal (green), climate-optimal (red) and cost-optimal (blue) FV-900 from the single objective optimisation

The two climate-optimised and the cost-optimised design for the multi objective analysis are shown from multiple perspectives in Figure 3.10, Figure 3.11, Figure 3.12 and Figure 3.13. Both designs are in almost all these perspectives similar to each other, in which the most significant difference could be seen from the top view, which shows a longer root chord for the climate optimised design.

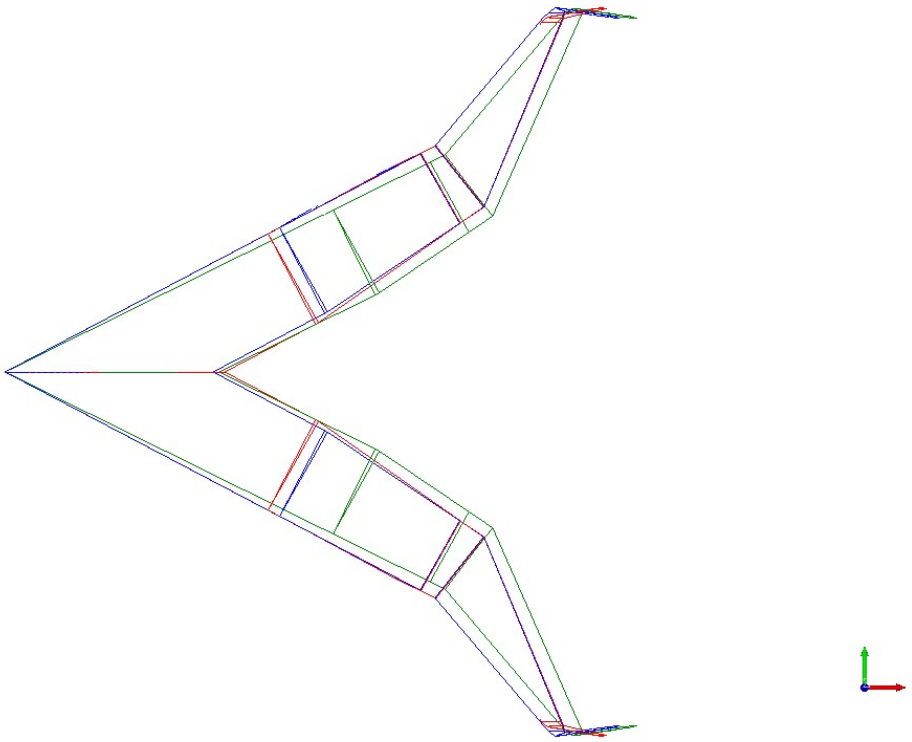

Figure 3.7: Top view of fuel-optimal (green), climate-optimal (red) and cost-optimal (blue) FV-900 from the single objective optimisation

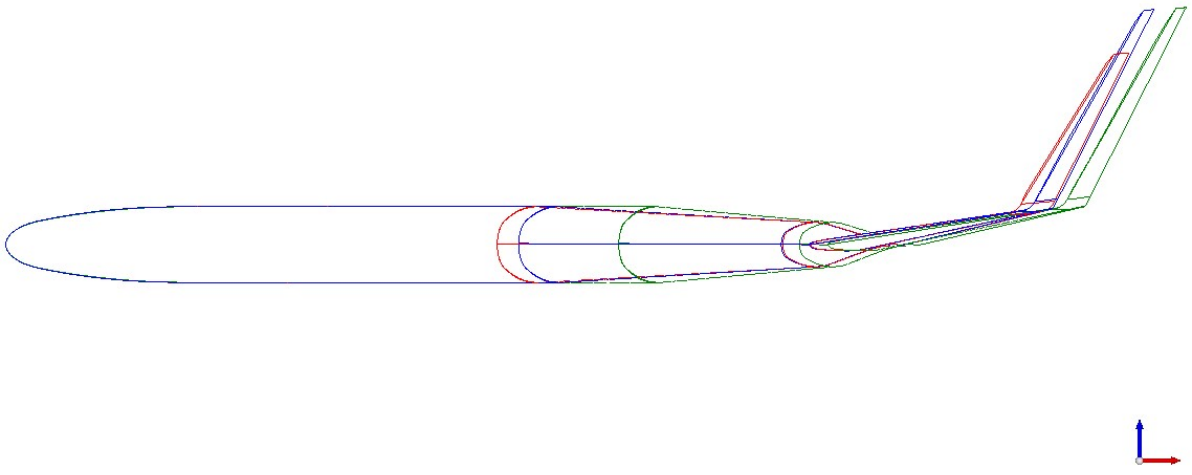

Figure 3.8: Side view of fuel-optimal (green), climate-optimal (red) and cost-optimal (blue) FV-900 from the single objective optimisation

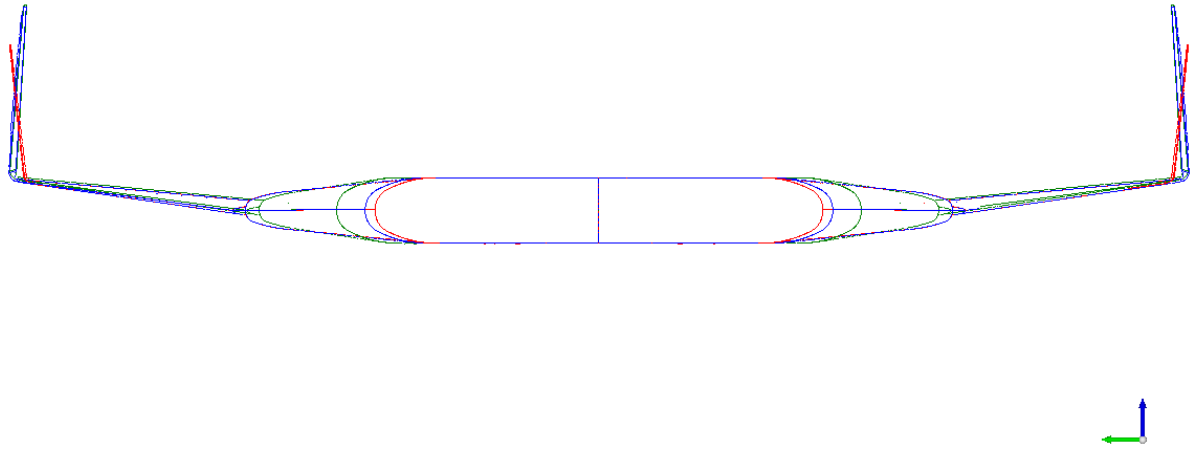

Figure 3.9: Front view of fuel-optimal (green), climate-optimal (red) and cost-optimal (blue) FV-900 from the single objective optimisation

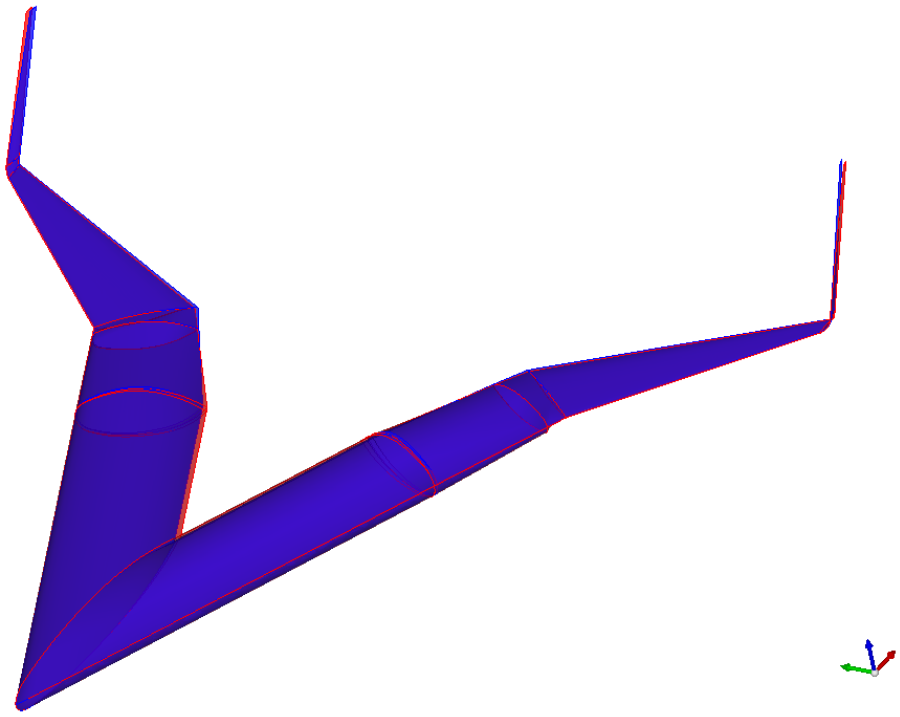

Figure 3.10: Isometric view of climate-optimal (red) and cost-optimal (blue) designs from the multi objective optimisation

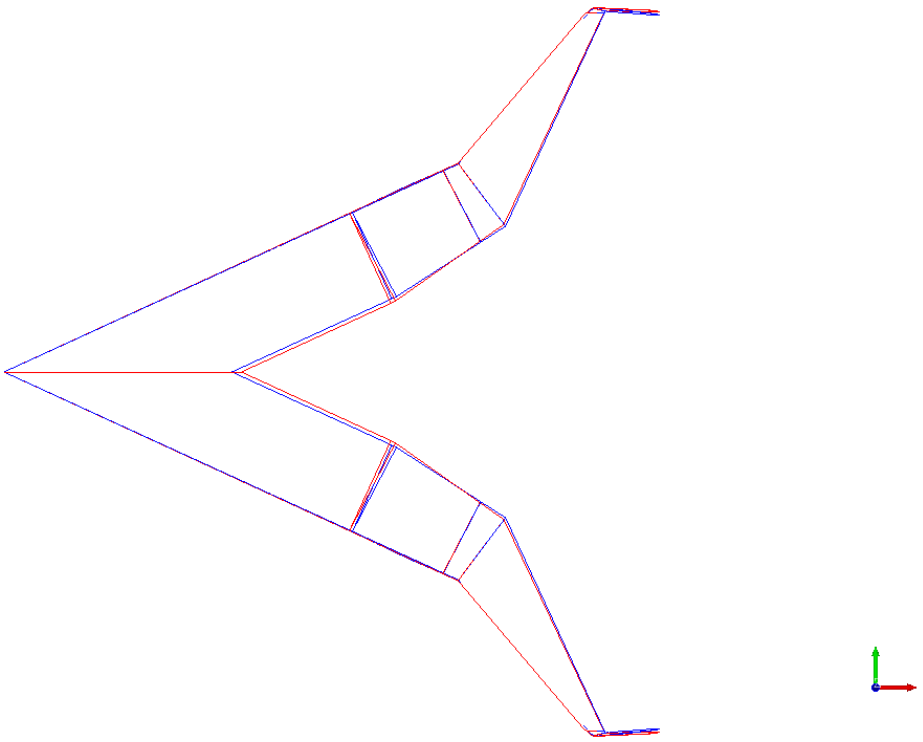

Figure 3.11: Top view of climate-optimal (red) and cost-optimal (blue) designs from the multi objective optimisation

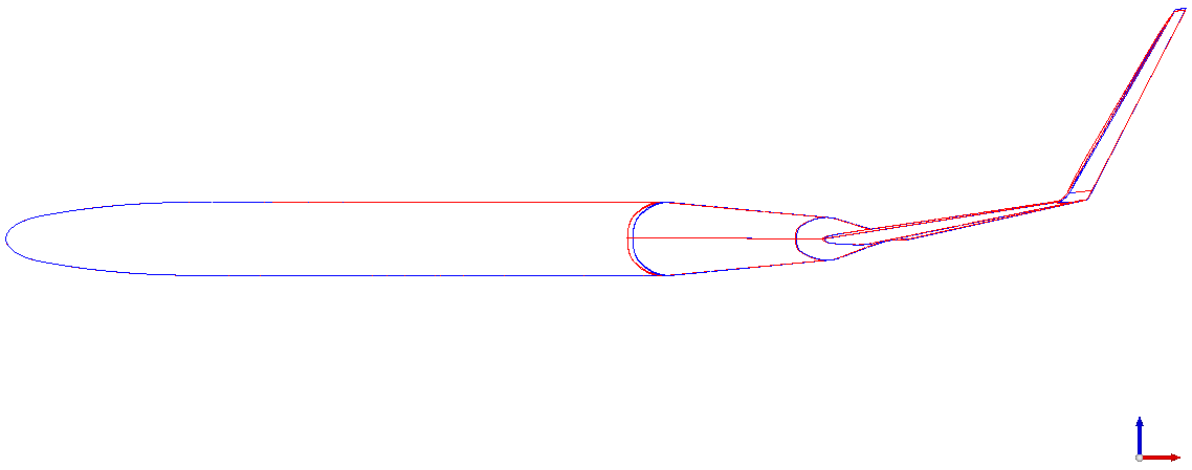

Figure 3.12: Side view of climate-optimal (red) and cost-optimal (blue) designs from the multi objective optimisation

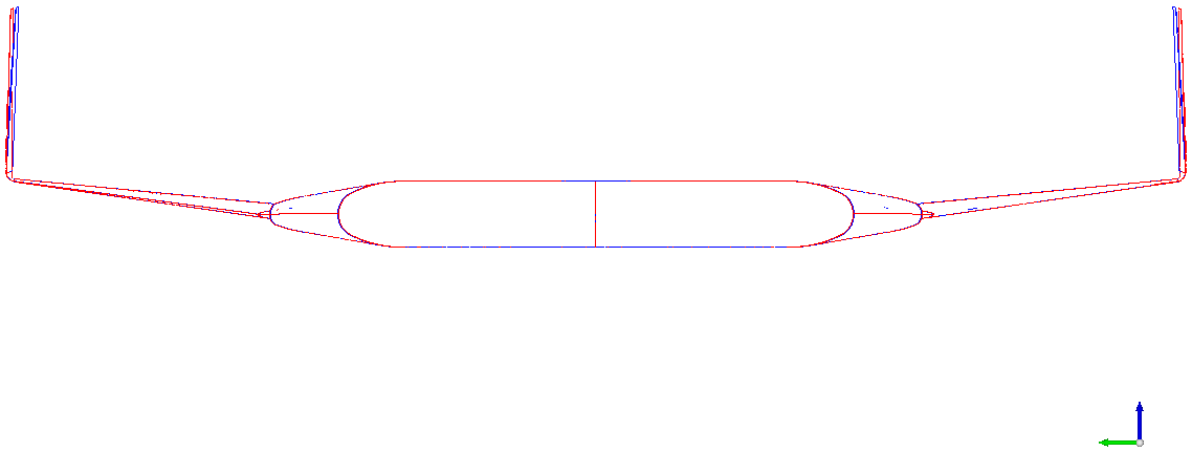

Figure 3.13: Front view of climate-optimal (red) and cost-optimal (blue) designs from the multi objective optimisation

References

[1] J. Benad. “The Flying V A new Aircraft Configuration for Commercial Passenger Transport”. en. In: (2015). DOI: 10.25967/370094. URL: https://publikationen.dglr.de/?tx_dglrpublications_pi1[document_id]=370094.

[2] E.M. Greitzer and P.A. Bonnefoy et al. *N+3 Aircraft Concept Designs and Trade Studies, Final Report Volume 2: Appendices—Design Methodologies for Aerodynamics, Structures, Weight, and Thermodynamic Cycles*. CR 216794/VOL2. NASA, 2010.

[3] D.S. Lee et al. “The contribution of global aviation to anthropogenic climate forcing for 2000 to 2018”. In: *Atmospheric Environment* 244 (Jan. 2021), p. 117834. DOI: 10.1016/j.atmosenv.2020.117834. URL: https://doi.org/10.1016/j.atmosenv.2020.117834.

[4] Sigrun Matthes et al. “Mitigation of Non-CO2 Aviation’s Climate Impact by Changing Cruise Altitudes”. In: *Aerospace* 8.2 (Jan. 2021), p. 36. DOI: 10.3390/aerospace8020036. URL: https://doi.org/10.3390/aerospace8020036.

[5] Wilco Oosterom. *Flying-V Family Design*. 2021. URL: http://resolver.tudelft.nl/uuid:9e8f9a41-8830-405d-8676-c46bf6b07891.

[6] International Civil Aviation Organization. *ICAO Long-Term Traffic Forecasts: Passenger and Cargo*. Tech. rep. ICAO, 2016.

[7] Matthijs Reekers. “Climate Effects of the Flying-V”. MA thesis. Technische universiteit Delft, 2021.

[8] Egbert Torenbeek. *Advanced Aircraft Design*. Wiley, May 2013. DOI: 10.1002/9781118568101. URL: https://doi.org/10.1002/9781118568101.

[9] UNFCCC. “The Paris Agreement”. In: *Paris Climate Change Conference - November 2015*. 2018.